Geological Quarterly, 2020, **64** (2): 422–459
DOI: http://dx.doi.org/10.7306/gq.1532

Diagenesis, sequence stratigraphy and reservoir quality of the Carboniferous deposits of the southeastern Lublin Basin (SE Poland)

Aleksandra KOZŁOWSKA[1, *] and Maria I. WAKSMUNDZKA[1]

[1] Polish Geological Institute – National Research Institute, Rakowiecka 4, 00-975 Warszawa, Poland

Kozłowska, A., Waksmundzka, M.I., 2020. Diagenesis, sequence stratigraphy and reservoir quality of the Carboniferous deposits of the southeastern Lublin Basin (SE Poland). Geological Quarterly, **64** (2): 422–459, doi: 10.7306/gq.1532

Associate Editor: Leszek Marks

This study estimates the reservoir properties of the Carboniferous deposits in the southeastern part of the Lublin Basin based on diagenetic and sequence stratigraphic patterns. Depositional sequences distinguished represent the following environments/processes: shallow clay and carbonate shelves, deltaic, fluvial, and hyperconcentrated flow while parasequences (cyclothems), maximum regression-initial transgression surfaces (T), maximum flooding surfaces (MFS) and also lowstand (LST), transgressive (TST) and highstand (HST) systems tracts have been recognised. Sequences recognized may be linked to the global stratigraphic division of the Carboniferous, thus providing a time framework and environmental context for petrographic and petrophysical examinations. The reservoir properties were found to be clearly controlled by depositional environment, diagenetic history and burial. The best properties were recognized in sandstone lithosomes formed in braided, meandering and anastomosed fluvial channels and hyperconcentrated flows which fill the incised valleys and belong to the LST. They are characterized by good porosity reaching up to 15.1%. The TST and HST deposits are represented chiefly by claystones, mudstones and limestones that formed in a shallow shelf and deltaic environment, being sealing intervals. The diagenetic history of sandstones comprises eo-, meso- and telodiagenetic phases. The major processes acting during the first of these were mechanical compaction, dissolution of mineral grains, formation of predominantly quartz overgrowths around the quartz grains, and crystallization of kaolinite. During mesodiagenesis, cementation with quartz, kaolinite and carbonates continued along with the formation of dickite and fibrous illite; moreover, mineral grains were dissolved and chemical compaction set in. The effects of telodiagenetic processes were feldspar dissolution and precipitation of kaolinite. During diagenesis the maximum temperature affecting the Carboniferous deposits was ~120°C. Compaction and cementation were the main factors responsible for the reduction of porosity by approximately 55 and 38%, respectively. One of the major diagenetic processes was dissolution resulting in the formation of secondary porosity. The Serpukhovian and Bashkirian sandstones from sequence 11 show good reservoir potential, while those from sequences 6, 9, 10, 12–14 only fair potential.

Key words: diagenesis, sequence stratigraphy, reservoir quality, Carboniferous, Lublin Basin.

INTRODUCTION

Previous examinations of reservoir properties of the Carboniferous in the Lublin Basin have been confined to the lithostratigraphic units (Kozłowska et al.,1998; Kozłowska, 2003, 2009) distinguished by Porzycki and Żelichowski (1977 *fide* Porzycki, 1979) and geophysical interpretations (Kaczyński, 1984; Chabiera, 1997a, b; Helcel-Weil and Dzięgielowski, 2003). Investigations carried out by Waksmundzka (2008b) revealed that the boundaries of these units are diachronous and their age and time span is different in various parts of the Lublin Basin, thus reducing their correlative value. However, the use of sequence stratigraphy enables precise correlation where the stratigraphic framework is based on isochronous surfaces (Waksmundzka 2007a, b, 2008a, b, 2010a, b, 2012a, b, 2013, 2014, 2018). It is also extremely helpful for reconstruction of depositional environments and their evolution with time, which has greatly influenced the burial diagenetic evolution pathways of reservoir quality in sandstones (Morad et al., 2000, 2012; Reed et al., 2005).

The present work, estimating the reservoir properties of the Carboniferous strata in the SE part of the Lublin Basin (Fig. 1), is based on diagenetic and sequence stratigraphic analyses. The latter was particularly focused on the potential of sandstone reservoir lithosomes and provided a temporal and palaeoenvironmental context for petrographic and petrophysical examinations. The results enabled reconstruction of the diagenetic succession and its effect on the formation of pore space in the sandstones in relation to facies development and depositional architecture.

* Corresponding author, e-mail: aleksandra.kozlowska@pgi.gov.pl

Received: December 18, 2019; accepted: February 19, 2020; first published online: May 5, 2020

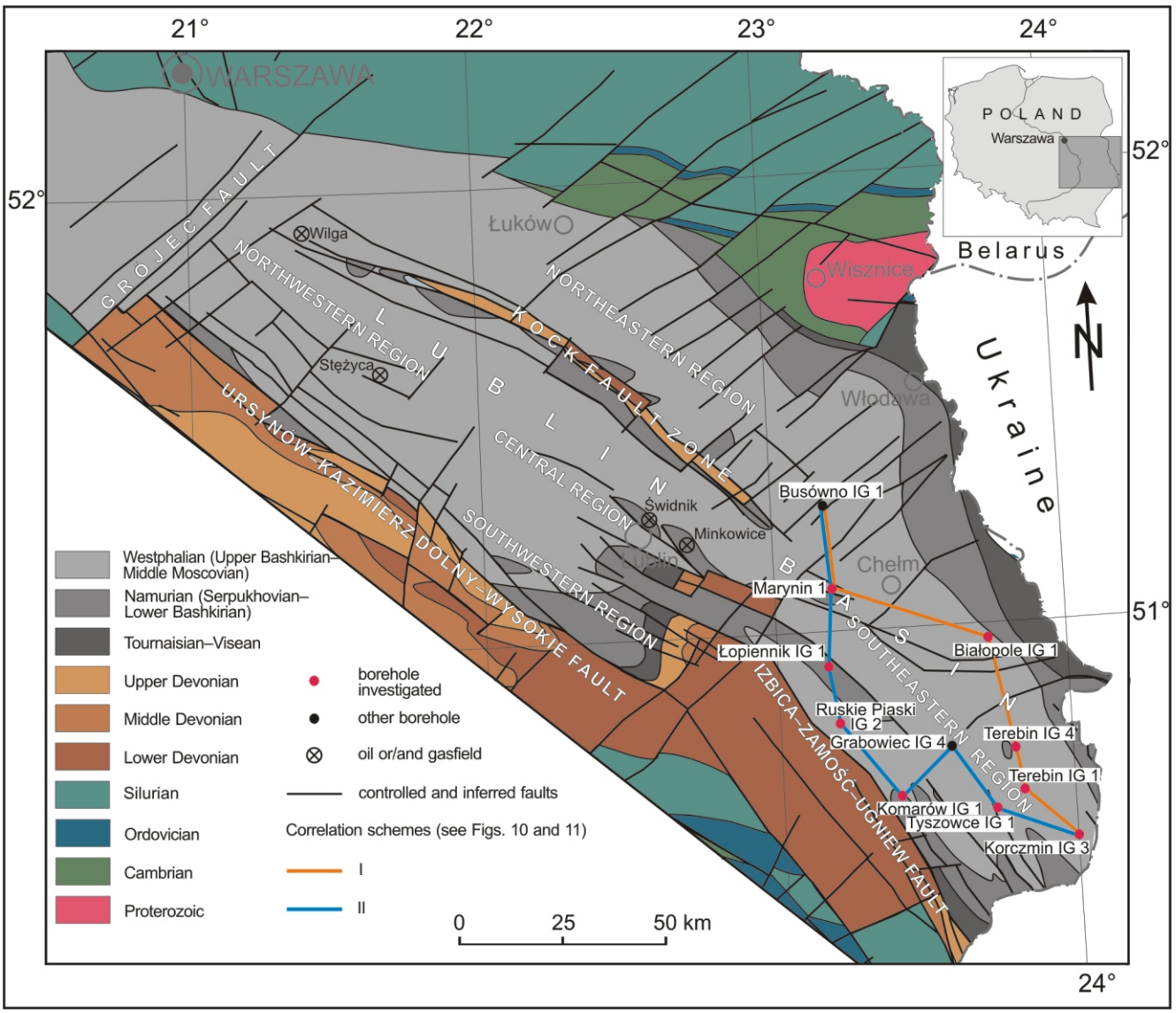

Fig. 1. Geological-structural map of the Lublin Basin (modified after Waksmundzka and Buła, 2017), with location of the boreholes studied

GEOLOGICAL SETTING

The Lublin Basin is located in SE Poland (Fig. 1), its extension in Ukraine being the Lviv–Volyn Coal Basin. The present boundary of the Lublin Basin is defined by the sub-Mesozoic extent of the Carboniferous strata and by major tectonic zones in the NW and SW (Żelichowski, 1969a, 1972). The basin axis runs NW–SE. The NE part of the basin is gently inclined towards the SW, this being associated with the regional dip of the East European craton basement, while the steep inclination of the western edge is controlled by the tectonic boundary (Krzywiec et al., 2017). A NE–SW fault system has been found to occur in the basin along with transverse (Żelichowski,1972; Żelichowski and Porzycki, 1983) and E–W faults (Tomaszczyk and Jarosiński, 2017). In the NW and central part of the basin there runs a major tectonic zone called the Kock Fault. The overall tectonic style of the Lublin Basin is defined by less-intense thin-skinned deformation (Krzywiec et al., 2017; Tomaszczyk and Jarosiński, 2017; Kufrasa et al., 2019) and its present shape is due to tectonic inversion (Narkiewicz et al., 2007; Krzywiec, 2009).

In its SE part the Carboniferous deposits rest, with a stratigraphic gap, on the Devonian and are overlain by either Cretaceous or Jurassic deposits. The Carboniferous thickness is variable – from 515 m (Białopole IG 1 borehole) to 1,430 m (Ruskie Piaski IG 2 borehole), the shallowest occurrence of its top has been found in the east, but it dips notably towards the NW, SW and S. The succession is built of claystones, mudstones, siltstones, sandstones, conglomerates, limestones, *Stigmaria* soils and coals, with occasional volcanic and bauxitic rocks in its lowermost part. According to Musiał and Tabor (1979, 1988) and later Porzycki and Zdanowski (1995) the Carboniferous succession is of upper Visean–Westphalian D? age. However, age determinations of basalts indicate the oldest rocks of the basin to be late Tournaisian (Pańczyk and Nawrocki, 2015). Thus in terms of the global chronostratigraphy the Carboniferous succession is represented by the upper Tournaisian–lower Moscovian (Waksmundzka, 2008b, 2013, 2018). The lithostratigraphy established by Porzycki and Żelichowski (1977 *fide* Porzycki, 1979) comprises the following four formations: Huczwa, Terebin (Korczmin and Komarów members), Dęblin (Bug and Kumów members) and Lublin,

while the youngest, i.e. the Magnuszew Formation, is missing. Both the Dęblin and the Lublin formations are partly or completely eroded away (Fig. 2).

Lowermost in the succession is the tripartite Huczwa Formation with limestones prevailing in the lower and upper parts and more abundant mudstones with sandstone intercalations in the middle. The Terebin Formation is built predominantly of claystones and mudstones and less frequent limestones and sandstones. The Dęblin Formation is distinctive through a higher share of sandstones which constitute the Bug and Kumów members. Higher in the section occur the coal-bearing deposits of the Lublin Formation represented by claystones and mudstones with coal and sandstone intercalations.

The lithofacies development and sequence stratigraphy revealed the clearly tripartite nature of the Carboniferous succession in the Lublin Basin (Waksmundzka, 2013). The lowermost part comprising sequences 1–10 (upper Tournaisian–lower Bashkirian) originated in a mostly marine and distal deltaic depositional regime (excluding the close-to-bottom interval). The middle part corresponding to sequences 11–16 (lower and middle Bashkirian) was formed in a deltaic-fluvial regime, whereas the uppermost part corresponding to sequences 17–22 (middle Bashkirian–lower Moscovian) contains exclusively continental strata laid down in a fluvial environment with mature swamps, lakes and lake deltas on alluvial plains. In the study area there occur only the lower and middle parts of the Carboniferous succession comprising sequences 1–16 (upper Tournaisian–upper Bashkirian), while the uppermost part is absent through erosion.

MATERIALS AND METHODS

The present studies are based on geological data and wireline logs from 8 boreholes located in the SE part of the Lublin Basin (Fig. 1). Two of them (Komarów IG 1 and Tyszowce IG 1) were fully cored, while from others core recovery was incomplete. All boreholes have penetrated the entire Carboniferous succession.

The sedimentological investigations via the use of lithofacies analyses have been focused on individual lithofacies (Reading, 1978; Walker, 1992), lithofacies associations and cyclothems. These were described according to the lithofacies code introduced by Miall (1977, 1978), Rust (1978), Zieliński (1992a, b, 1995) and Gradziński et al. (1995) with later modifications by Waksmundzka (2012b, 2013). Index lithofacies of greatest thicknesses have been distinguished and thickness relationships determined within the associations were also coded. The method devised by Baldwin and Butler (1985) was used, for calculation of the thickness reduction ratio whose value increases with depth, this approach having been tested by Waksmundzka (2013) in previous sedimentological Carboniferous investigations.

Similar to Read and Dean (1976) and Allen (1965, 1970) the cyclothem boundaries were set at the tops of the phytogenic formations (coal, carbonaceous claystone) and in the absence of these lithofacies at levels of rapid changes in grain size. To define the bedforms, processes, sub-environments and depositional environments within the overall palaeoenvironmental architecture (Miall, 1985, 1988) the interpretation required a genetic approach to lithofacies, their associations and cyclothems.

Investigations into the facies development of the Carboniferous succession and its depositional architecture, and the lateral extension of sandstone lithosomes in particular, have been based on litho-facial correlation and sequence stratigraphy. Due to a full core recovery and good biostratigraphic constraints, sequence stratigraphic divisions could be adopted (Waksmundzka, 2018) in examinations of the Carboniferous in the SE part of the basin. The Carboniferous sections were compiled on the assumption that the faunal levels and the corresponding local maxima of the gamma ray curve (Waksmundzka, 2010a, 2013) are isochronous horizons i.e. *Posidonia corrugata* I, *Posidonia corrugata* II and *Dunbarella papyracea* (Musiał and Tabor, 1988). In lithofacies and sequence stratigraphic schemes the assumed reference horizon is the local maximum of the gamma ray curve corresponding to the *Dunbarella papyracea* level found in boreholes (Marynin IG 1, Ruskie Piaski IG 2). For the remaining boreholes with poorer coring representation the reference horizon was assumed to be the bottom of the youngest sequence 12 present in all boreholes. Two correlation schemes have been constructed in which data from three borehole sections i.e. Busówno IG 1, Komarów IG 1 (Waksmundzka, 2007a, 2014) and Grabowiec IG 4 have been included for better reliability (Fig. 1):

I – applicable to the NE part of the study area, and distinctive through smaller Carboniferous thicknesses, with a transition to the zone of larger thicknesses;

II – cutting the study area farther in the SW, and applicable to the transition zone from smaller to larger and locally much larger thicknesses.

In the sections examined, 16 depositional sequences were defined following Michum (1977) and using sequence stratigraphic methods described in detail by Waksmundzka (2010a, 2012b, 2013). The depositional sequences are of type I *sensu* Vail and Todd (1981) as they are bounded by type I subaerial unconformities. Within the sequences, maximum regression surfaces were distinguished, which also proved to be the initial transgression surfaces, together with maximum flooding surfaces and lowstand, transgressive and highstand systems tracts. The systems tracts show a cyclic structure and are built of coarsening-upward, non-gradational and fining-upward cyclothems (Waksmundzka, 2010a, 2012b, 2013) which correspond to parasequences (Van Wagoner, 1985). The sequence stratigraphic division was coupled with the global and West European Carboniferous chronostratigraphic divisions, thus providing a chronostratigraphic framework for detailed diagenetic studies and estimation of reservoir properties in the sandstone lithosomes.

264 thin sections saturated with blue resin to enable distinction of pore spaces were examined using a polarizing *Optiphot 2* microscope manufactured by *Nikon*. In 115 samples, mainly of sandstones, the grain size distribution was defined by counting 300 points with the use of a Prior universal stage (Jaworowski and Juskowiak, 1973). The microlithofacies divisions were based on Dott's classification modified by Pettijohn et al. (1972) with further changes by Jaworowski (1987). Similarly to arenites, wackes were subdivided into sublithic and subarkosic types. To define the types of carbonate cement, 102 uncovered thin sections were stained with Evamy's solution.

40 sandstone samples have been subjected to cathodoluminescence analysis using the *CCL 8200 mk 3* model with cold cathode made by Cambridge Image Technology Ltd.

Fluid inclusions have been examined on 20 double-side-polished thin sections on the Linkam heating and freezing *THMS600* equipment with 1°C accuracy relative to the commonly used SYNFLINC standards.

Samples were scanned using two types of electron microscope – produced by *JSM-35 JEOL* and *LEO 1430*. Both cooperate with the *EDS ISIS* energy dispersive spectrometer manu-

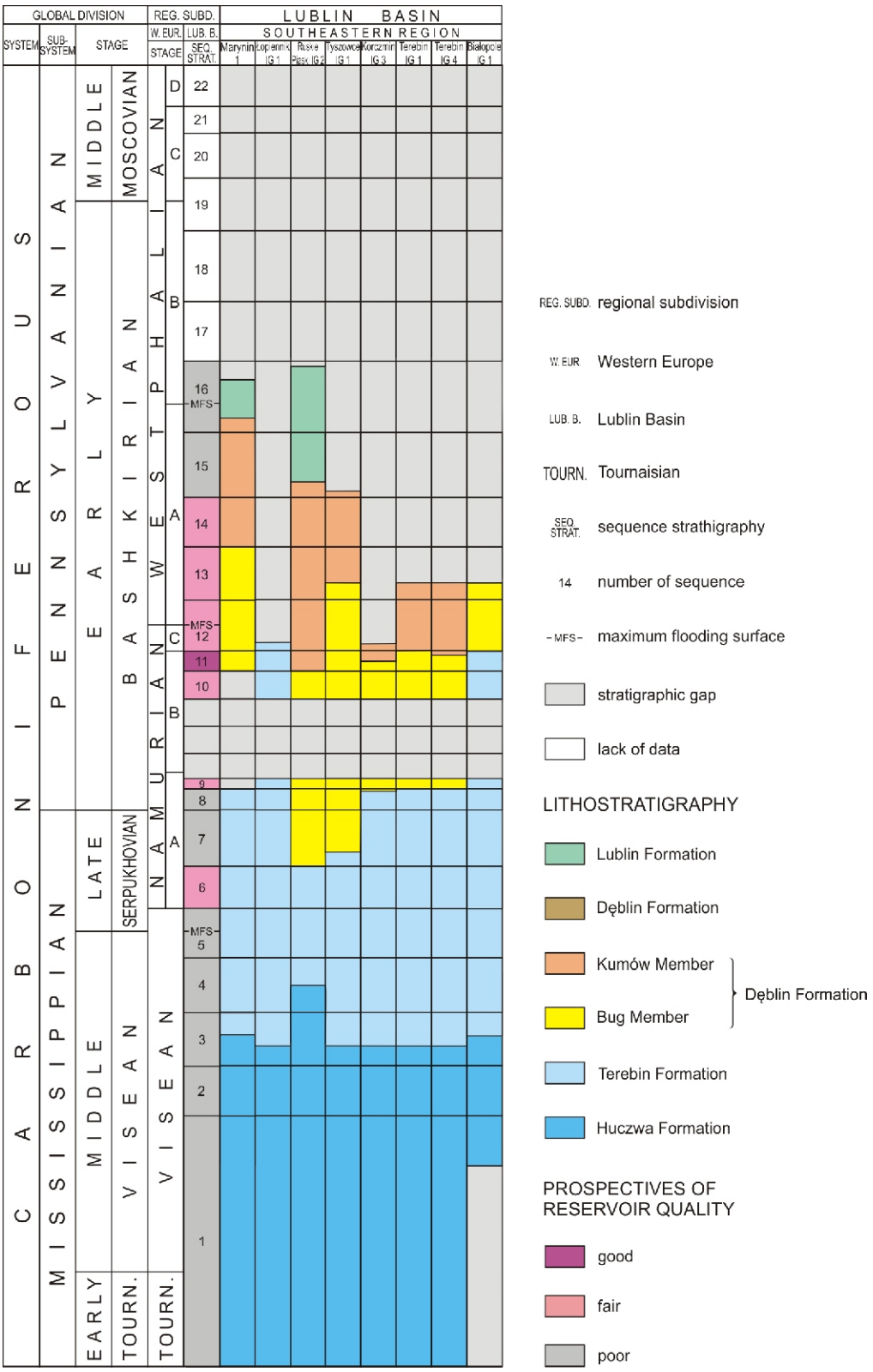

Fig. 2. Chronostratigraphic divisions, lithostratigraphy and sequence stratigraphy of the Carboniferous succession in the southeastern Lublin Basin (modified after Waksmundzka, 2018) with prospective reservoir quality

factured by Oxford Instruments. 42 chip samples dusted with carbon and then with gold were analysed. Examinations of 27 polished uncovered thin sections yielded backscattered electron images (BEI). The chemical composition of 39 carbonate samples was also defined using scanning electron microscopy (SEM) with an energy dispersive X-ray analyser. All quantitative results have been recalculated to molecular composition.

The *X'Pert PW 3020X-ray* diffractometer manufactured by Philips with a Cu K radiation and semiconductor detector was used for X-ray examinations. The position of peaks and their comparison with the JCPDS standards (Joint Committee on Powder Diffraction Standards) enabled definition of the phase composition. Clay minerals <0.2 μm in size separated from sandstones according to the method described by Moore and Reynolds (1989) were identified. Air-dried oriented samples have been glycolized and heated in the angular range of 0–30°2 and 19–34°2 .

Infra-red examinations were conducted in a single-beam *FT-IR FTS135* spectrometer within the range from 400 to 4000 cm^{-1}, focusing on the 3000–4000 cm^{-1} range (interval of stretching vibrations for the OH group). Samples were prepared by the pellet method.

Isotopic values of oxygen and carbon in carbonate minerals were obtained for 33 sandstone samples. Examinations were conducted on gaseous CO_2 from carbonate samples in accordance with standard procedures for the reaction of phosphoric acid with pure carbonates (McCrea, 1950) and carbonate mixtures (Al-Aasm et al., 1990). The measurements were completed using a modified *M11305* spectrometer (Hałas, 1979; Durakiewicz and Hałas, 1994) with an accuracy of ±0.08 %. The ^{13}C results obtained are shown on the PDB scale and the ^{18}O values on the PDB and SMOW scales.

Effective porosity, permeability and pore space parameters were determined for 40 sandstone samples. A helium pycnometer has been used for porosity coefficient measurements and the permeability coefficient has been calculated from the Darcy equation (Pirson, 1950) considering the correction for gas compressibility. Examinations of pore space (bulk density, porosimeter porosity, size of the average capillary, specific surface, number of pores >1 μm, threshold diameter and hysteresis) were conducted with the use of a mercury porosimeter.

The final estimation of the reservoir potential was based on a comprehensive review of results yielded by sedimentological, sequence stratigraphic, petrographic and petrophysical examinations. These permitted the distinction of 3 types of reservoir potential of sandstone lithosomes for conventional hydrocarbons, considering such parameters as thickness, lateral extent, seal and petrophysical features (Table 1). A thickness equal or exceeding 10 m, the presence of a seal, effective porosity >5% (after Jenyon, 1990) and permeability exceeding 1 mD (following the classification by Levorsen, 1967) are considered prerequisite for reservoir potential.

Table 1

Adopted criteria of prospective reservoir quality of the Carboniferous succession in the southeastern Lublin Basin

Prospectives of reservoir quality	Parameter			
	Thickness =/>10 m	Lateral continuation	Seal	Petrophysic Porosity >5% Permeability >1 mD
Good	+	+	+	+
Fair	+	–	+/+?	+
Poor	–	–	–	–

+ presence; +? supposed presence; – absence

RESULTS

LITHOFACIES, THEIR ASSOCIATIONS AND CYCLICITY

In the Carboniferous core sections a number of lithofacies were distinguished, the characteristics of which are given in Tables 2 and 3 along with interpretation of bedforms, processes, depositional subenvironments and environments in which they originated. The most typical lithofacies are illustrated in Figures 3 and 4. A distinctive feature of the Lublin Carboniferous succession is its depositional cyclicity, understood as a multiple repetition of lithological assemblages with a defined succession of features which constitute a cyclic depositional unit (Gradziński et al., 1986). On the basis of the classification by Waksmundzka (1998, 2010a, 2012b, 2013) fining-upward, coarsening-upward and non-gradational cyclothems have been identified. The lithofacies occurring within the fining-upward cyclothems have been grouped into associations which has enabled the identification of depositional environments and subenvironments (Tables 2 and 4). A single lithofacies assemblage can correspond to a fining-upward cyclothem, but usually the latter embraces two lithofacies associations. As for the remaining lithofacies (Table 3) occurring in the intervals with coarsening-upward and non-gradational cyclothems, a division of lithofacies associations proved unnecessary.

FINING-UPWARD CYCLOTHEMS

Fining-upward cyclothems occur in all the borehole sections examined. Three major types have been recognised: I, IIa, and IIb (Table 5). Moderately frequent single-part cyclothems of type I are distinctive by the presence of a single lower coarse-grained part and the lack of an upper fine-grained part (Fig. 5). The upwards fining of grains is connected with the grading of conglomerates and coarse-grained sandstone into medium- and fine-grained sandstones. In type I cyclothems, the high-energy lithofacies Gm, Sm, Ss, Sh2, Sl are predominant. The thickness of these cyclothems ranges from 2 to 5.8 m.

The most frequent is the other type of fining-upward IIa cyclothem, which is bipartite (Figs. 5–7). The grading is of conglomerates and coarse-grained sandstones through to medium- and fine-grained sandstones and then into mudstones. Several kinds of lithofacies successions have been identified. In the lower coarse-grained parts, high-energy lithofacies i.e. Gs, Ss, Sm, Sh2, and Sl are prevalent, while lower-energy lithofacies are less frequent. In the upper, fine-grained parts there occur lithofacies Fm or Fh, deposited from suspension. The IIa cyclothems can reach up to 10 m thick and their lower and upper parts up to 6.9 and 3.4 m, respectively.

Less frequent are type IIb fining-upward cyclothems (Figs. 5 and 6). The grading is of fine-grained sandstones passing into mudstones and/or into clayey *Stigmaria* soils. Predominant in the lower part, with thicknesses only up to 0.9 m, are low-energy lithofacies i.e. Sr, Sf and Sh1. The upper fine-grained parts show a moderate thickness reaching up to 9.1 m and contain either lithofacies Fm, Fh, deposited from suspension, or lithofacies Fn, FSw, formed at a very low flow energy. At the top of some IIb cyclothems, muddy and clayey *Stigmaria* soils R occur.

Table 2

Characteristics of the lithofacies present within fining-upward cyclothems, and interpretation their depositional environments

Litofacies	Structure	Colour	Flora	Range of thickness [m]	Depositional process	Hyperconcentrated flow	Braided river	Meandering river	Anastomosing fluvial system
C Coal/carbonaceous claystone	massive	black	very common unlabelled	0.01–0.7	deposition of plant remains coalification				■
R *Stigmaria* soil	nodular	grey, dark grey, black	stigmaria appendixes plant chaff	0.2–7	lack of flow, deposition from clayey or muddy suspension, deposition of plant remains, pedogenic			■	■
Fm Massive claystone and mudstone	massive	dark grey, grey, black	plant chaff	0.1–11	lack of flow, deposition from clayey or muddy suspension		■	■	■
Fh Horizontal laminated claystone and mudstone	horizontal lamination	dark grey, grey	plant chaff	0.1–2.9			■	■	■
Fn Lenticular laminated siltstone	lenticular lamination	dark grey, grey	plant chaff	0.1–1.7	rhythmic bedload transport in ripples (lower part of lower flow regime) and lack of flow – deposition from muddy and silty suspension				■
FSw Wavy laminated sandy siltstone	wavy lamination	dark grey, grey	plant chaff	0.1–0.7				■	■
FSd Disturbed sandy siltstone	disturbed	dark grey	plant chaff	0.1–2	unstable density stratification shear fractures			■	■
Fd Disturbed mudstone		grey, dark grey	plant chaff	0.2–2				■	■
Sd Disturbed sandstone		grey, light grey	plant chaff	0.1–1.2	disturbation connected with large plant fragments and organic matter, unstable density stratification				■
Sh Sh2 Horizontal stratified sandstone (Fig. 3C)	horizontal stratification	light grey	plant chaff	0.1–1.8	deposition in upper plane bed (upper flow regime)		■	■	■
Sh Sh1 Horizontal laminated sandstone (Fig. 3D)	horizontal lamination	light grey, grey	plant chaff	0.1–0.7	deposition in lower plane bed from sandy suspension			■	■
Sf Flaser laminated sandstone	flaser lamination	light grey, grey	plant chaff	0.1–4.8	rhythmic bedload transport in ripples (lower part of lower flow regime) and lack of flow – deposition from muddy and silty suspension			■	■
Sr Ripple cross-laminated sandstone (Fig. 3E)	ripple cross-lamination	light grey, grey	carbonaceous matter	0.1–3.2	rhythmic bedload transport in ripples (lower part of lower flow regime)		■	■	■
Sx Large-scale cross-stratified sandstone	cross-stratification	light grey	carbonaceous matter	0.4	bedload transport in transverse bars or megaripples (lower or upper part of lower flow regime)	■			
Sp Planar cross-stratified sandstone (Fig. 3A)	planar cross-stratification (tabular and wedge-shaped)	light grey	carbonaceous matter	0.1–0.8	bedload transport in transverse bars (lower part of lower flow regime)			■	
Gp Planar cross-stratified conglomerate			carbonaceous matter	0.4				■	
St Trough cross-stratified sandstone (Fig. 3I)	trough cross-stratification	light grey, grey	plant chaff	0.1–0.6	rhythmic bedload transport in megaripples (upper part of lower flow regime)		■	■	■
Sl Low-angle cross-stratified sandstone (Fig. 3F)	low-angle cross-stratification	light grey	lack	0.1–2	bedload transport in washed-out megaripples and transverse bars (transition from lower to upper flow regime)		■	■	■
Sm Massive sandstone (Fig. 3G)	massive	light grey, grey, grey-brown, brown	plant chaff	2.5–6	hyperconcentrated flow	■			
				0.1–1.2	deposition in upper plane bed (upper flow regime)		■	■	■
GSm Massive sandy conglomerate		grey, grey-beige	lack	0.9–1.2			■		
Gm Massive conglomerate		light grey	lack	0.5			■		
Se Erosional scours sandstone (Fig. 3B)		grey, grey-red	large plant fragments	0.04–0.15	development of erosional surfaces with cobbles deposition in upper plane bed (upper flow regime)		■		
Ss Scour-fill sandstone		light grey, grey-brown	large plant fragments	0.2–2	erosion of large scour and their filling in upper plane bed (upper flow regime)	■		■	■
Gs Scour-fill conglomerate (Fig. 3H)		light grey	large plant fragments	0.3–1.2					■

Table 3

Characteristics of the lithofacies occurred within coarsening-upward and non-gradational cyclothems, and interpretation of their depositional environments

Litofacies	Structure	Colour	Flora	Fauna	Range of thickness [m]	Depositional process	Shallow shelf		Subaquatic part of inner-shelf delta			Delta plain					
							Shallow clay shelf	Shallow carbonate shelf	Prodelta	Delta front	Mouth bar	Lake bottom	Outer lake delta	Peat swamp	Overgrown lake	Overgrown plain	Distributary channel
C Coal/carbonaceous claystone (Fig. 4D)	massive	black	very common unlabelec	lack	0.01–0.7	deposition of plant remains coalification								■			
R *Stigmaria* soil (Fig. 4A)	nodular	grey, cark grey black beige grey-green	stigmaria appendixes plant chaff	lack	0.07–5.3	lack of flow, deposition from clayey or muddy suspension, deposition of plant remains, pedogenic									■	■	
Sm Massive sandstone	massive	light grey, grey, grey-brown, brown	plant chaff	lack	0.1–0.6	deposition in upper plane bed (upper flow regime)											■
Sl Low-angle cross-stratified sandstone	low-angle cross-stratification	light grey, grey	plant chaff/lack	lack	0.1–2	bedload transport in washed-out megaripples and transverse bars (transition from lower to upper flow regime)											■
St Trough cross-stratified sandstone	trough cross-stratification	light grey, grey	plant chaff/lack	lack	0.1–0.6	rhythmic bedload transport in megaripples (upper part of lower flow regime)											■
Sr Ripple cross-laminated sandstone	ripple cross-lamination	light grey, grey	plant chaff	lack	0.1–3.2	rhythmic bedload transport in ripples (lower part of lower flow regime)											■
Sf Flaser laminated sandstone	flaser lamination	grey, light grey	plant chaff	lack	0.1–4.8	rhythmic bedload transport in ripples (lower part of lower flow regime) and lack of flow – deposition from muddy and silty suspension					■						
Sh1 Horizontal laminated sandstone	horizontal lamination	light grey, grey	plant chaff	lack	0.1–0.7	deposition in lower plane bed from sandy suspension					■						
Sd Disturbed sandstone	disturbed	light grey	plant chaff	lack	0.2–1.1	roots – *stigmaria* disturbances unstable density stratification bioturbations					■						
FSd Disturbed sandy siltstone (Fig. 4E)	disturbed	dark grey, grey	plant chaff	lack	0.1–1.4	unstable density stratification bioturbations roots – *stigmaria* disturbances shear fractures				■							
Fd Disturbed mudstone	disturbed	grey, cark grey	plant chaff	lack	0.2–2					■							
FSw Wavy laminated sandy siltstone (Fig. 4H)	wavy lamination	cark grey, grey	plant chaff	lack	0.1–3	rhythmic bedload transport in current and wave ripples and lack of flow – deposition from muddy and silty suspension				■							
Fw Wavy laminated siltstone	wavy lamination	cark grey, light grey, grey-green, brown	plant chaff	lack	0.3–1.1					■							
Fn Lenticular laminated siltstone	enticular lamination	dark grey, grey	plant chaff	lack	0.1–1.7					■							
Fh Horizontal laminated claystone and mudstone: Fh2 Horizontal laminated mudstone (Fig. 4G)	horizontal lamination	cark grey, black, grey	plant chaff	lack	0.1–5.3	lack of flow – deposition from clayey or muddy suspension			■	■		■	■				
Fh Horizontal laminated claystone and mudstone: Fh1 Horizontal laminated claystone		dark grey	lack/p ant chaff	marine	0.2–8.9		■		■								
Fm Massive claystone and mudstone: Fm5 Grey massive mudstone (Fig. 4I)	massive	light grey, grey-green, beige green, green-rec	lack/p ant chaff	lack	0.2–2.5							■	■				
Fm Massive claystone and mudstone: Fm4 Black massive mudstone		dark grey, black	very common plant chaff, large plant fragments	lack	0.1–3.6							■	■				
Fm Massive claystone and mudstone: Fm3 Dark grey massive mudstone (Fig. 4C)		dark grey, black grey	plant chaff	marine/ lack	0.2–8.7		■		■	■							
Fm Massive claystone and mudstone: Fm2 Grey massive claystone		dark grey, black, grey, light grey	plant chaff	lack/ fresh-water	0.2–3.5							■	■				
Fm Massive claystone and mudstone: Fm1 Black massive claystone (Fig. 4B)		black, dark grey	lack	marine/ lack	0.2–17		■		■								
M Marl	massive	black, dark grey	lack	marine	0.1–4	lack of flow – deposition from clayey suspension deposition of limy marine fauna remains		■									
L Limestone (Fig. 4F)	massive, nodular	cark grey, grey be ge	lack	marine	0.1–61.5	deposition of limy marine fauna remains		■									

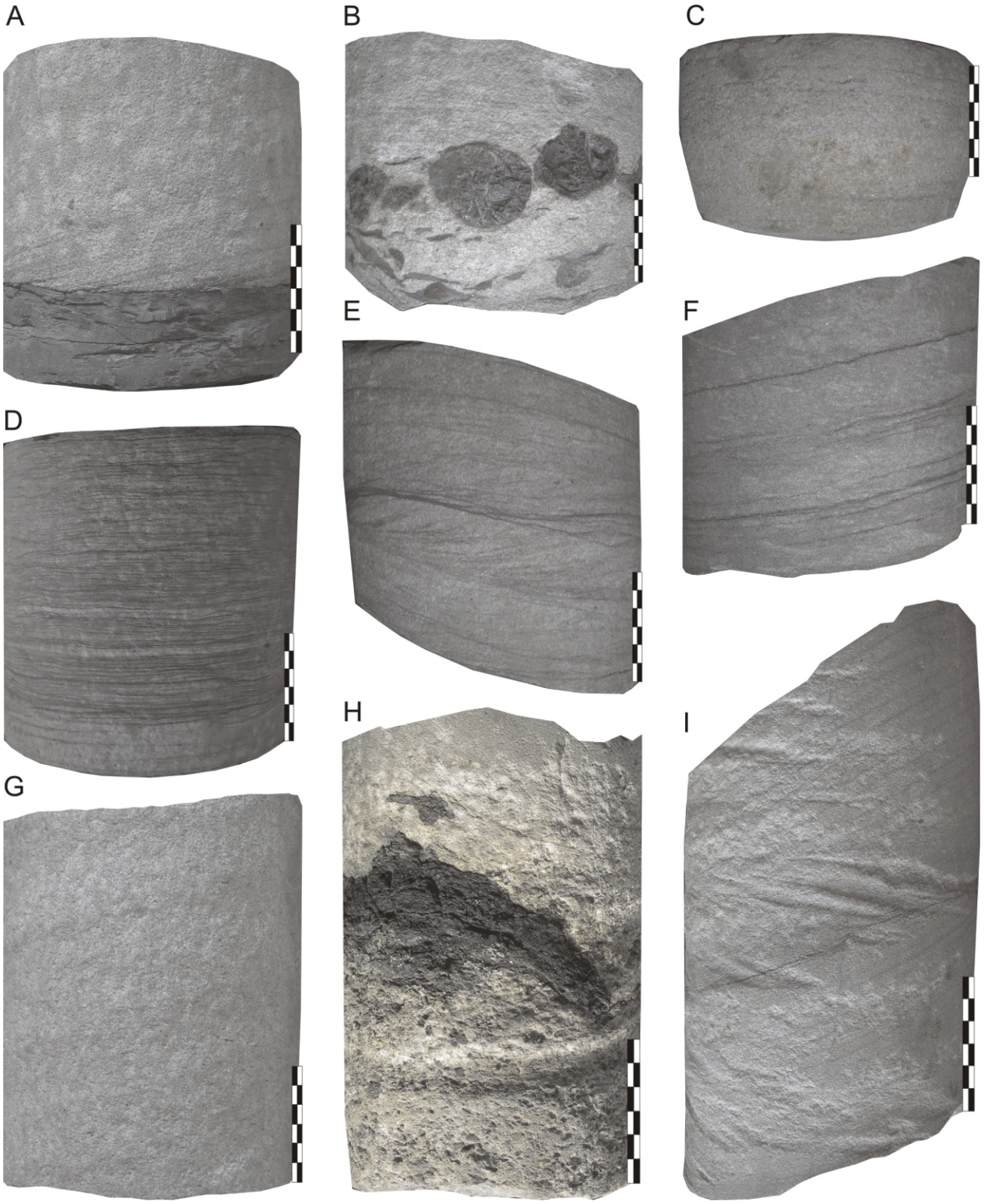

Fig. 3. Examples of coarse-grained lithofacies

A – lithofacies Sp: medium-grained planar cross-stratified sandstone, at the bottom lithofacies Fh: horizontal laminated mudstone; Terebin IG 1 borehole; depth 738.64–738.77 m; LST of sequence 10; Bashkirian; **B** – lithofacies Se: medium-grained sandstone in erosional scours with clasts of grey claystone and brown siderite nodules; Terebin IG 1 borehole; depth 737.04–737.12 m; LST of sequence 10; Bashkirian; **C**– lithofacies Sh2: coarse-grained horizontally stratified sandstone; Tyszowce IG 1 borehole; depth 892.80–892.87 m; LST of sequence 13; Bashkirian; **D** – lithofacies Sh1: fine-grained horizontally laminated sandstone with lamination accentuated by abundant fine plant detritus; Terebin IG 1 borehole; depth 803.91–804.04 m; LST of sequence 8; Bashkirian; **E** – lithofacies Sr: fine-grained ripple cross-laminated sandstone; Tyszowce IG 1 borehole; depth 1,027.13–1,027.26 m; LST of sequence 11; Bashkirian; **F** – lithofacies Sl: fine-grained low-angle cross-stratified sandstone; Tyszowce IG 1 borehole; depth 1,036.08–1,036.22 m; LST of sequence 11; Bashkirian; **G** – lithofacies Sm: fine-grained massive sandstone; Terebin IG 1 borehole; depth 775.29–775.45 m; LST of sequence 9; Bashkirian; **H** – lithofacies Gs: conglomerate with scour-and-fill structures with clasts of grey claystone and black carbonaceous matter; Korczmin IG 3 borehole; depth 778.00–778.23 m; LST of sequence 7; Serpukhovian; **I** – lithofacies St: fine-grained trough cross-stratified sandstone; Tyszowce IG 1 borehole; depth 906.28–906.50 m; LST of sequence 12; Bashkirian; units on scale bar = 1 cm

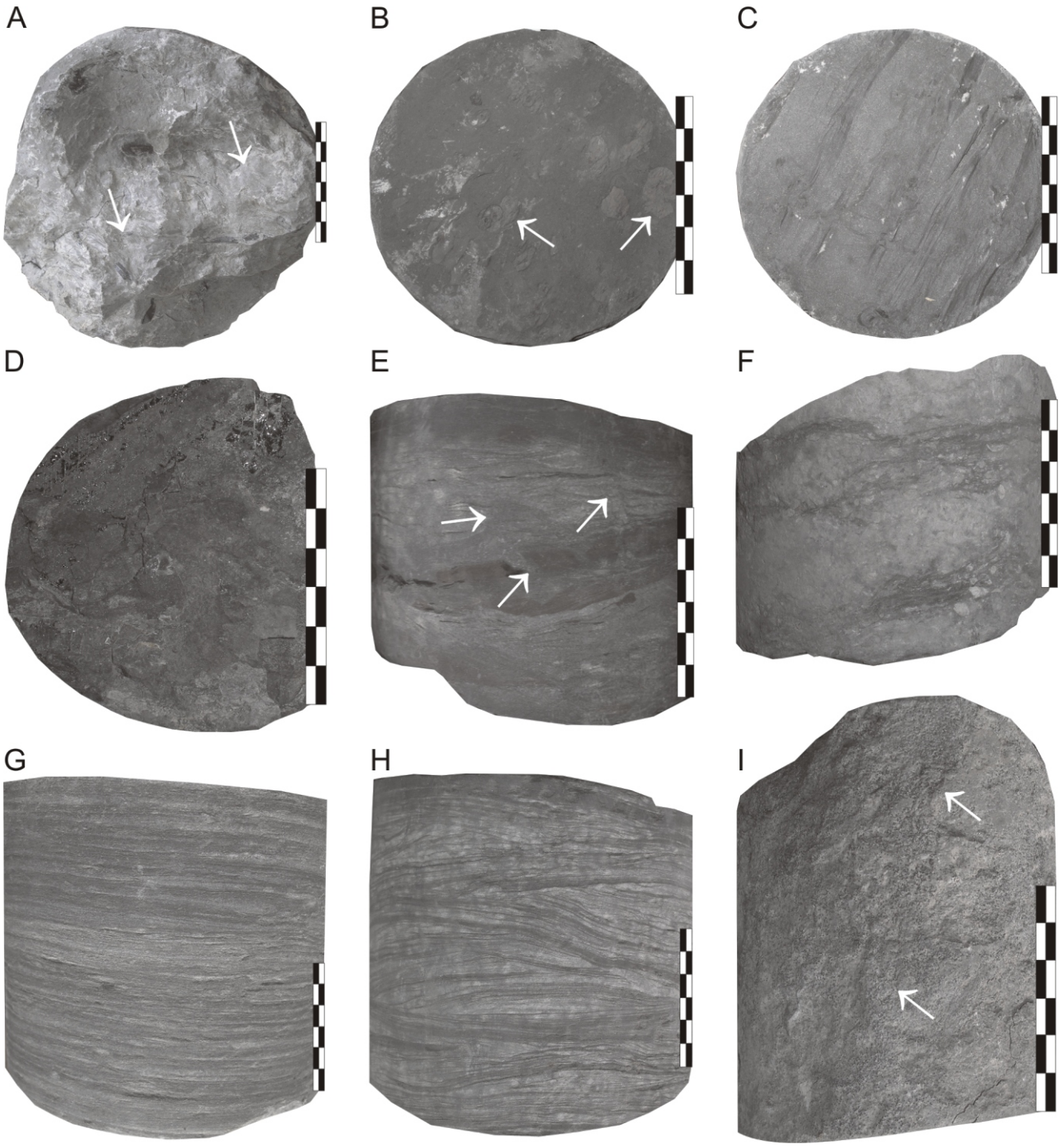

Fig. 4. Examples of fine-grained and phytogenic lithofacies

A – lithofacies R: clayey *Stigmaria* soil; slickenside-related compaction (arrows) and black plant detritus are observable; Terebin IG 1 borehole; depth 560.75 m; TST of sequence 11; Bashkirian; **B** – lithofacies Fm1: black massive claystone with goniatites (arrows); Marynin 1 borehole; depth 992.3 m; MFS of sequence 7; Serpukhovian; **C** – lithofacies Fm3: dark grey massive mudstone with black plant detritus; Marynin 1 borehole; depth 1,007.6 m; HST of sequence 6; Serpukhovian; **D** – lithofacies C: coal; Marynin 1 borehole; depth 1,135.4 m; T of sequence 6; Serpukhovian; **E** – lithofacies FSd: sandy siltstone disturbed by plant roots (arrows) with brown siderite nodules; Ruskie Piaski IG 2 borehole; depth 1,441.0-1,441.1 m; HST of sequence 13; Bashkirian; **F** – lithofacies L: limestone with white faunal detritus; Marynin 1 borehole; depth 1,063.20-1,063.27 m; TST of sequence 6; Serpukhovian; **G** – lithofacies Fh2: horizontally laminated mudstone; Ruskie Piaski IG 2 borehole; depth 1,347.73-1,347.84 m; TST of sequence 14; Bashkirian; **H** – lithofacies FSw: wavy laminated sandy siltstone; Terebin IG 1 borehole; depth 835.57-835.68 m; HST of sequence 7; Serpukhovian; **I** – lithofacies Fm5: grey massive mudstone with common spherulites of siderite in the place of plant roots (arrows); Ruskie Piaski IG 2 borehole; depth 1,749.68-1,749.78 m; LST of sequence 8; Bashkirian; units on scale bar = 1 cm

Table 4

Lithofacies associations developed in braided and meanderind rivers, anastomosing fluvial systems, as well as hyperconcentrated flow deposits with reference to sequence stratigraphy and chronostratigraphy

Borehole	Lithofacies association	Sequence stratigraphy	Chronostratigraphy
Hyperconcentrated flow			
Tyszowce IG 1	Sm 920.1–927.7 m	11	Bashkirian
	Sm (Ss) 1085.2–1094.6 m	9	
Braided river			
Tyszowce IG 1	Sh2 (Sl) 750.9–752.05 m	15	Bashkirian
	Sl (Sm) 752.05–754.05 m		
	Sl (Sm, Sh2) 1074.4–1077.4 m	10	
	Sl, Sh2, Sr 1077.4–1082.2 m		
	Sm, Sr (Gm) 1082.2–1085.2 m		
Korczmin IG 3	Sm (Sx, Fm) 775.5–778.6 m	7	Serpukhovian
	Gs (Sh2) 1352.8–1354.1 m	1	Tournaisian
	GSm 1354.8–1355.2 m	1	
Meandering river			
Tyszowce IG 1	St, Fm (Sh2) 750.1–750.9 m	15	Bashkirian
	Fm (Sp, Sl) 890.5–893.1 m	12	
	Fh (FSw, Sf, Sh1) 895.3–901.5 m		
	Fm (R) 1227.2–1231.2 m	7	Serpukhovian
	Sm (Sl, Sr, St) 1231.2–1238.3 m		
Marynin IG 1	Fm 1314.0–1317.0 m	3	Visean
	Sm, Sx (Ss, Sl) 1317.0–1321.7 m		
Terebin IG 1	Sx, Sf (Sr, Sh2) 502.2–522.1 m	13	Bashkirian
Anastomosing fluvial system			
Tyszowce IG 1	Fm (R) 734.8–747.9 m	15	Bashkirian
	Sh2 (Sr) 747.9–750.1 m		
	Fm, Fh (Sf) 768.9–787.1 m	14	
	Fn (Sf, Sx) 787.1–798.8 m		
	Fh, Fm (FSw, Sf) 798.8–806.6 m		
	C (Sm, St) 887.8–890.5 m	13	
	Fm, Fh (R) 909.7–920.1 m	12	
	Fm (R, C) 1010.3–1024.2 m	11	
	St, Sx (Sr) 1024.2–1029.8 m		
	Fh (Fm) 1062.5–1071.7 m	10	
	Sm (Sl, Ss) 1071.7–1074.4 m		
	Fm 1565.8–1572.1 m	4	Visean
	Sh2 (Sf) 1572.1–1574.8 m		
Marynin 1	C (Fm) 1304.0–1311.24 m	3	
	Sr (Sx) 1311.24–1314.0 m		
	Fm (R) 1353.0–1360.2 m	2	
	Sh1 (Sm, Sr) 1360.2–1362.0 m		
Terebin IG 1	C (Fh, Fm) 522.1–523.7 m	12	Bashkirian
	Sm (Ss) 523.7–525.5 m		
Korczmin IG 3	Sr (R, Fm) 449.8–455.6 m	12	
	Fm (R, Fh) 553.5–588.8 m	11	
	Sr 588.8–595.6 m		
	Fm, Fh 628.7–640.1 m	10	
	Sl (Sm) 640.1–646.7 m		
	Fm (R) 767.9–773.6 m	7	Serpukhovian
	Sh2 (Sm) 773.6–775.5 m		
	Fm (Sl) 1349.8–1351.4 m	2	Visean

Table 5

Characteristics of typical fining-upward cyclothems type I, IIa and IIb

Cyclothem type		Lithofacies succesion		Thickness [approx. m]		
		lower part	upper part	lower part	upper part	total
I		Gm Sm+Sl Sr Ss Sm+Sl+Sh2 Sl+Sr+Sh2+St Sh2	absent	2–5.8	absent	2–5.8
II	a	Gs Ss Sm+Sr+Sl Ss Sm+Sx Se+Sl+Sm Sh2 Sl Sm+Sp+Sl+Sf Sh1 Sr+St St+Sx+Sr	Fh Fh Fh Fh Fm R Fm+R+C	1.8–6.9	0.7–3.4	4.3–10
	b	Sr+Sf+Sm+Sh1 Sd+Sh1	Fm+Fh+FSw+Fn Fh+FSw+Fd+Fm R	0.2–0.9	0.1–9.1	0.3–10

COARSENING-UPWARD AND NON-GRADATIONAL CYCLOTHEMS

On the basis of lithofacies succession and degree of completeness, coarsening-upward cyclothems of type Ic, IIc, IId have been identified and shown to be the less complete non-gradational cyclothems of type IIIc and IIId (Figs. 8 and 9; Table 3). The completeness of cyclothems has been analysed within the succession of genetically related clayey and clastic lithofacies with a notable increase in grain size (parts: 1, 2, 3) manifested by the grading of claystone into mudstones, sandy siltstones and finally sandstones.

In the sections examined, there are numerous type Ic coarsening-upward cyclothems within which parts composed of characteristic lithofacies occur from the bottom upwards:

part 0: limestones and dolomites L, marls M;
part 1: claystones Fm1, Fh1, mudstones Fm3;
part 2: mudstones Fh2, Fn and sandy siltstones FSw, FSd;
part 3: fine-grained sandstones Sh1, Sf, Sd;
part 4: claystones Fm2, mudstones Fm4, Fm5, Fh2, Fn and sandy siltstones FSw, FSd, *Stigmaria* soil R and coals C.

Type Ic is represented by complete coarsening-upward cyclothems with the 0 1 2 3 4 succession from the base upwards. Certain lithofacies are devoid of limestones and dolomites L, marls M (part 0) and/or *Stigmaria* soils R and coals C (part 4). The present thickness of the type Ic cyclothems is 1–34 m.

Distinctive among the coarsening-upward cyclothems is the incomplete IIc type lacking lithofacies of parts 2 or 3, which include the following successions: 0 1 2, 1 2 4 or 1 3 4. Usually part 0 does not occur within type IIc and occasionally even part 4 is missing. The thickness of these cyclothems can attain 47 m.

Within the non-gradational IIIc type cyclothems, there occur 0 1 4 part. There is no growth of mineral grains, as they comprise only claystones or mudstones in their lower parts and soils and phytogenic formations at higher levels. The present thickness of these cyclothems is 0.7–12.6 m.

A complete coarsening-upward type Id cyclothem as reported from other parts of the Lublin Basin (Waksmundzka, 2013) was not found in the sections examined. However, rarely occurring type IId cyclothems showing a 1 4 succession (Fig. 9) have been described (Waksmundzka, 2013). Their present thickness attains 1.8 m. Claystones grade upwards into mudstones. The following parts built of characteristic lithofacies occur from the bottom upwards:

part 1: claystones Fm2 grading into mudstones Fm4, Fm5, Fh2, and sandy siltstones FSw;
part 4: clayey and muddy *Stigmaria* soil R.

Among the type IIId non-gradational cyclothems, member 1 is represented exclusively by mudstones and the succession of parts is 1 4. Its thickness attains 9 m.

INTERPRETATION

DEPOSITIONAL ENVIRONMENTS AND PROCESSES

FINING-UPWARD CYCLOTHEMS

In the Carboniferous section of the SE part of the Lublin Basin fining-upward cyclothems occur with features indicative of their fluvial provenance (Figs. 5–7; Tables 2 and 4). Below, the environments are described in which fining-upward cyclothems originated, from highest to lowest energy.

Hyperconcentrated flows. Associations formed in this environment and known from the Tyszowce IG 1 borehole are distinctive by an erosional surface at the bottom overlain by high-energy sandstones Ss with abundant carbonaceous, clayey and muddy clasts. Higher in the section there occur thick intervals of massive sandstone Sm. As a rule the associations are monolithofacies with occasional thin intervals of Sx, Sl, Sh2 lithofacies (Fig. 6). The prevailing massive structure points to rapid deposition (Arnott and Hand, 1989) under conditions of hyperconcentrated flow developed in incised fluvial valleys (Svendsen et al., 2003) where a strong sediment overload (20–50% according to Pierson and Costa, 1987) hindered bottom transport. The hyperconcentrated flow moved along the entire width of the valley undercutting its slopes, which collapsed and supplied large amounts of sandy material (comp. Martinsen, 1994). Such processes can be active in the early phases of incised valley infill (Martinsen, 1994) and conglomerates lying at their bottom are termed “lowstand basal conglomerates” (for example Plint, 1988). Within this association the fining upward pattern has been noted along with a transition from coarse- and medium-grained to fine-grained sandstones which subsequently grade into mudstones which, in turn, are classified into a higher association. This type of succession has been included into the type IIa fining-upward cyclothem. The lower

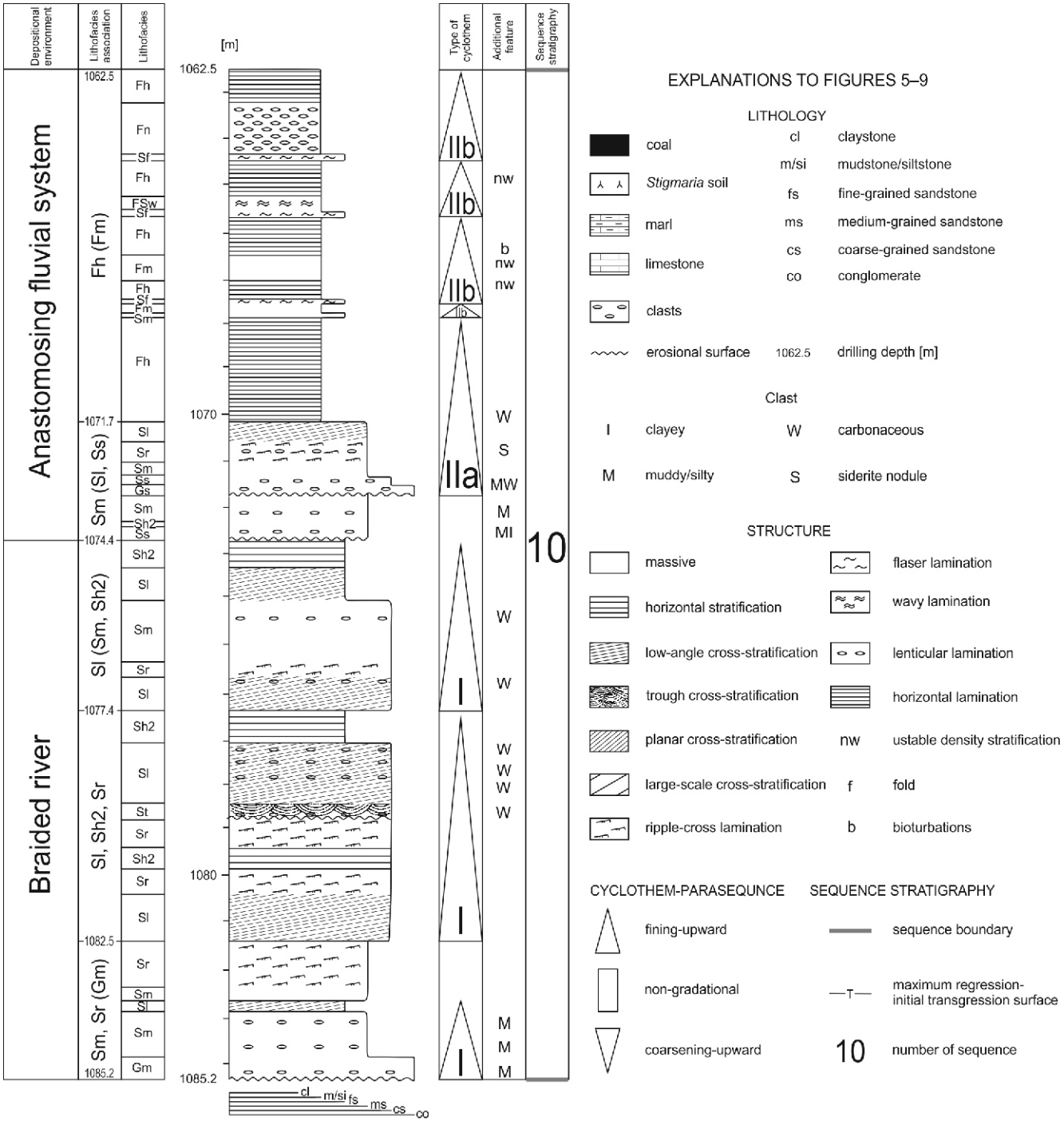

Fig. 5. Lithofacies associations and fining-upward cyclothems deposited from braided river and anastomosing fluvial system environments, Tyszowce IG 1 borehole, LST of sequence 10, Bashkirian

part of this cyclothem consists of high-energy lithofacies i.e. Ss, Sm and Sx deposited during hyperconcentrated flow, while the upper one comprises Fh lithofacies deposited from suspension after the waning of the flow. Also present are single-part cyclothems type I with a fining-upward pattern involving transition from coarse- to fine-grained sandstones, resulting from slowing of the hyperconcentrated flow.

Braided rivers. From the Tyszowce IG 1 and Korczmin IG 3 boreholes, 8 lithofacies associations have been described, characterized by a clear predominance of high-energy sandstone lithofacies Sh2, Sl, Sm, Gm and the lack or minor share (9–21%) of fine-grained lithofacies such as Fm and Fh (Fig. 5). Blakey and Gubitosa (1984) reported a <5% share of mud/clay in braided river deposits, while Rust (1978) found this proportion, though including fine-grained sandstones, to be 10–15%. Most probably these associations originated in sand-bed braided channels (cf. Moody-Stuart, 1966; Miall, 1996) with rapid bed aggradation. Reductions in current velocity resulted in the formation of the low-energy Sr lithofacies and subsequently the deposition of Fm and Fh lithofacies from standing

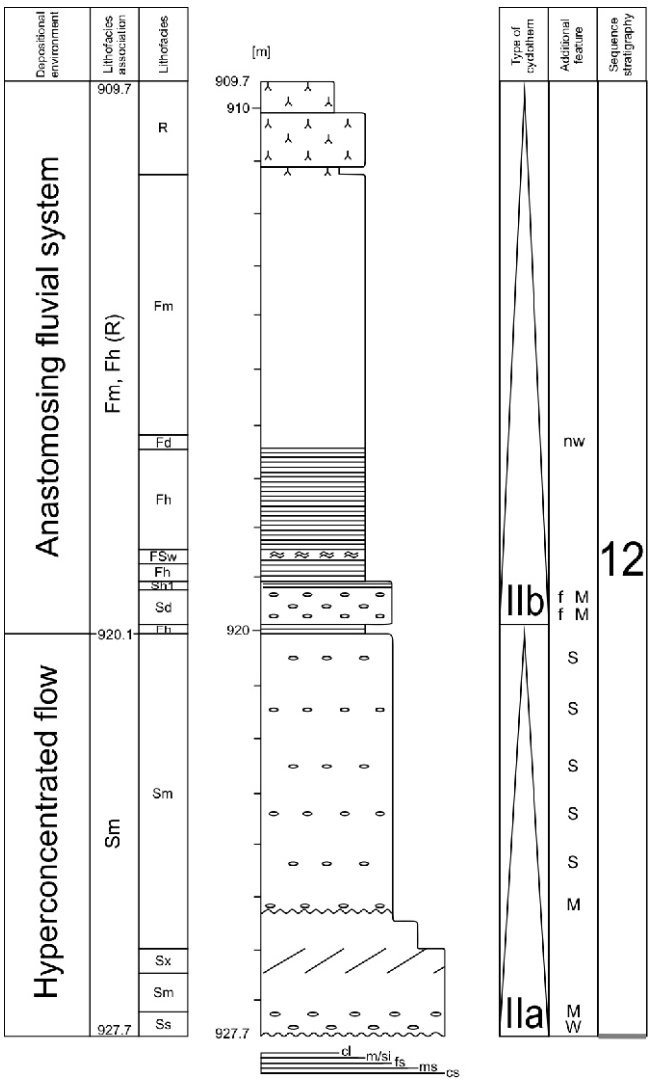

Fig. 6. Lithofacies associations and fining-upward cyclothems deposited from hyperconcentrated flow and anastomosing fluvial system environments, Tyszowce IG 1 borehole, LST of sequence 12, Bashkirian

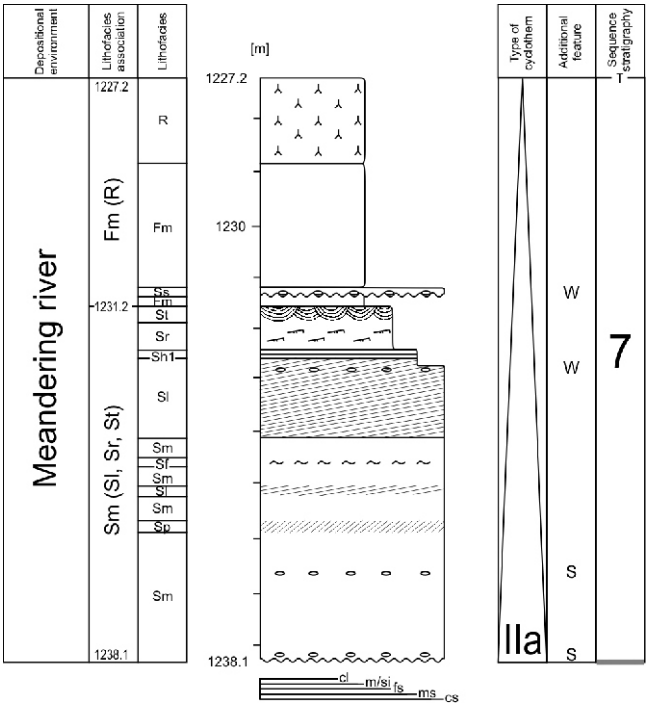

Fig. 7. Lithofacies associations and fining-upward cyclothems deposited from a meandering river environment, Tyszowce IG 1 borehole, LST of sequence 7, Serpukhovian

water on braidplains The absence of these lithofacies suggests highstand deposition and the lack of low-energy conditions.

In this lithofacies association the normal grading is expressed by the gradual transition from conglomerates to medium-grained sandstones or coarse- to fine-grained sandstones. These are type I fining-upward cyclothems containing solely high-energy coarse-grained deposits accompanied by lower-energy lithofacies. The origin of fining-upward cyclothems is related to the decreasing velocity and sediment-bearing capacity of the flow, and the filling of sand-bed braided channels.

The second type of the IIa fining-upward cyclothem contains high-energy lithofacies mainly in its lower part while lower-energy ones occur higher in the succession. Such cyclothems originate due to the filling and hence disuse of channels, as well as to clayey-muddy deposition from suspension on braidplains following the fall of high-water. Fining-upwards cyclothems from deposits of similar provenance have been reported by numerous authors e.g., Gradziński (1973), Rust (1978), Cant and Walker (1978), Rust and Gibling (1990), and Zieliński (1997).

Meandering rivers. 8 lithofacies associations have been recognized in the Tyszowce IG 1, Marynin 1 and Terebin IG1 boreholes with fine-grained and phytogenic lithofacies, at 50–70%, prevailing over sandstones. The fining upwards and transition from coarse-grained sandstones, through medium- to fine-grained are indicative of deposition in a meandering river environment (Fig. 7; cf. Allen, 1963, 1970; Miall, 1977; Bridge and Gordon, 1985). In the sandstone associations, the high-energy lithofacies Sh2, Sl, Sm occur moderately frequently suggesting rapid aggradation, as opposed to typical meandering rivers in which erosion and deposition alternate. Less numerous are lower-energy lithofacies Sl, St, Sp, Sr.

At the top the sandstone associations gradually pass into low-energy lithofacies Fm and phytogenic *Stigmaria* soils R. These lithofacies are typical of the floodplain of sand-bed meandering rivers. They sedimented by suspension in standing water, and were subsequently vegetated. Soil-forming processes have contributed to their development.

Within the deposits of meandering rivers there occur type IIa fining-upward cyclothems where sandstones lithofacies grade into fine-grained and phytogenic ones. The formation of cyclothems is related to autocyclic processes such as the drop in flow velocity and sediment-carrying capacity and the lateral migration of meanders, as well as to allocyclic events such as a decrease of flow velocity and resultant filling of channels due to base sea level (BSL) rise. Type IIb cyclothems have been encountered in fine-grained associations deposited on floodplains. Their lower parts are built of sandstones comprising low-energy sandstone lithofacies typical of waning flow in crevasse splays. The upper parts comprise claystone and mudstone lithofacies typical of a floodplain where deposition took place mainly in lakes in which *Stigmaria* soils R formed after overgrowing with vegetation. Fining-upward cyclothems have been described also from meandering rivers by many au-

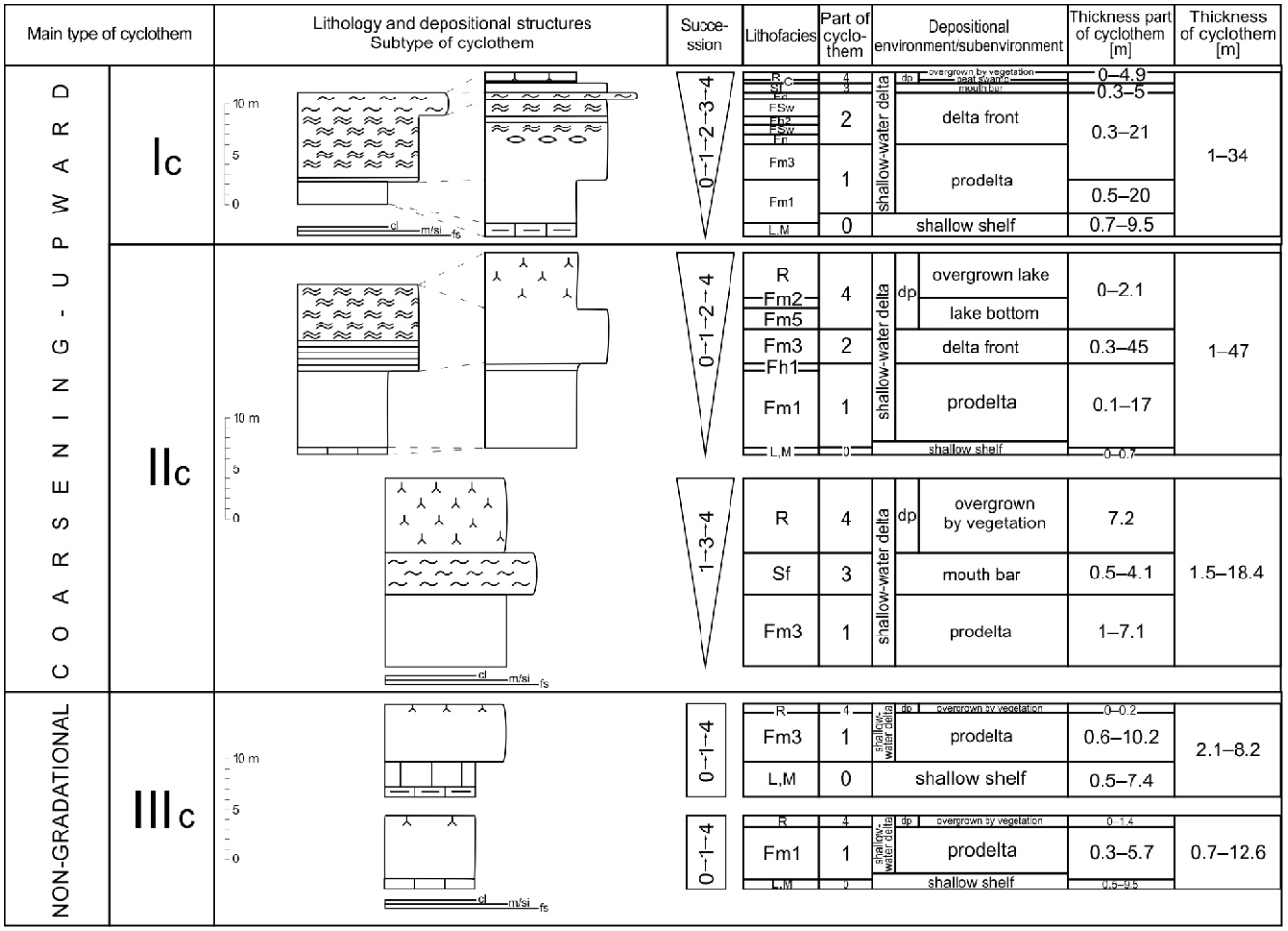

Fig. 8. Schematic example of coarsening-upward cyclothems types Ic and IIc and non-gradational cyclothems types IIIc with their depositional environments, Tyszowce IG 1, dp – delta plain

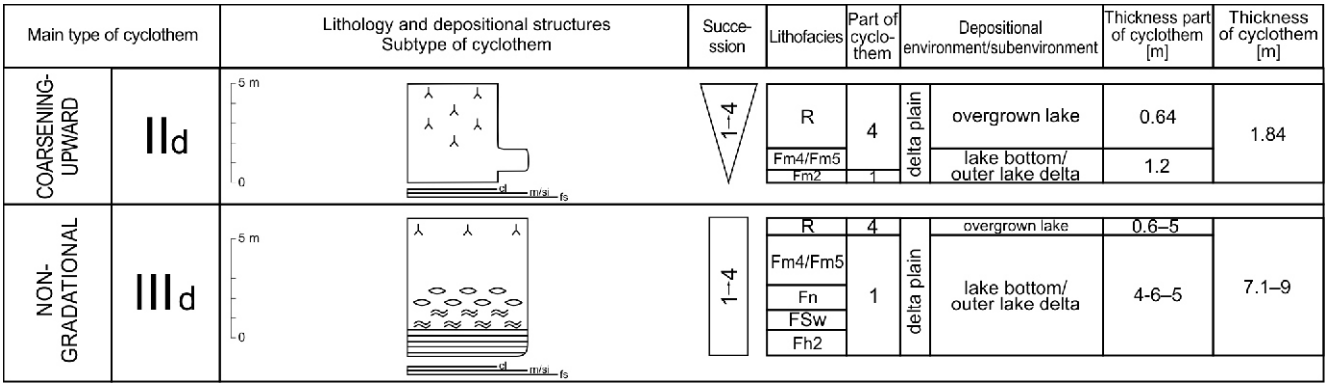

Fig. 9. Schematic examples of coarsening-upward cyclothems types IId and non-gradational cyclothems types IIId with their depositional environments, Tyszowce IG 1

thors e.g., Allen (1964), Jackson II (1978), Radomski and Gradziński (1981), Nemec (1984).

Anastomosing fluvial system. The most abundant lithofacies associations of this kind are recognized in the Tyszowce IG 1, Marynin 1, Terebin IG 1 and Korczmin IG 3 boreholes. Some contain only sandstone lithofacies Sr, Sx formed in variable hydrodynamic conditions with predominant low energy flow. Such conditions could have occurred in shallow low-energy channels with aggradational sedimentation. The variations of energy from high to low and the periodic lack of flow favoured the formation of associations containing lithofacies Sh2, Sr, Sf, Sh1, Sm. Their deposition occurred in channels of varying energy with and dominated by bed aggradation. The other sandstone associations with prevailing lithofacies Sm, Sl, Ss, Sh2 originated in high-energy channels with very strong bed aggradation. However, river channels ac-

tive in the anastomosed fluvial system showed exceptionally high aggradation rates (Figs. 5 and 6). Similar features of channel deposits of the anastomosing fluvial system have been described from the Canadian Carboniferous by Rust (1984) and Nadon (1994). Also, thickness relationships between sandstone associations and the overlying low-energy associations containing solely fine-grained lithofacies Fm, Fh and phytogenic R and C are indicative of such an environment. Their thickness makes up 74–97% of the total thickness of both associations.

The anastomosing fluvial system is characterized by the presence of two or more interconnected channels of different patterns and a flood plain situated between them (cf. Smith, 1983; Gradziński et al., 2000, 2003; Makaske, 2001). On the proximal floodplain, crevasse splays are formed (Sm, Sf), whereas at a distance from the channels there are lakes accumulating clay and mud (Fm, Fh) along with peat marshes accumulating organic matter (C). *Stigmaria* soils R occupy overgrown areas.

These anastomosing fluvial successions comprise type IIa fining-upward cyclothems built of a lower sandstone partly laid down in the channel and of an upper fine-grained part deposited on a flood plain. This kind of cyclothem reflects the filling and waning of channels caused by avulsion and BSL rise as well as deposition on a flooded floodplain overgrown by vegetation favouring the development of marshes. Type IIb cyclothems have also been described resulting from crevasse splays.

COARSENING-UPWARD AND NON-GRADATIONAL CYCLOTHEMS

A specific feature of the Carboniferous succession from the SE part of the Lublin Basin, enabling the reconstruction of depositional environments and sub-environments, is the frequent occurrence of coarsening-upward and genetically related non-gradational cyclothems (Figs. 8 and 9). Such cyclothems may be typical of delta as well as fluvial deposits (Scruton, 1960; Fisher et al., 1969; Elliot, 1974, 1975, 1976a, b, 1978; Coleman and Wright, 1975). This permitted their identification within the Lublin Carboniferous succession and, considering earlier models, the reconstruction of deltas in which they formed (Figs. 10 and 11). The progradation of delta lobes when sediments of the individual subenvironments invade both each other and the prodelta, coupled with increasingly coarsening-upward patterns arranged in cyclothems, are autocyclic phenomena (Elliot, 1975, 1976b). In a reversed complete type Ic cyclothem the successive parts indicate a shallow shelf environment and such deltaic sub-environments as prodelta, slope, mouth bar and delta plain (Fig. 8). Fm1 and Fh1 claystones found within part 0 were deposited in at least two environments. Those containing a goniatite fauna and distinctively very high radioactivity levels recorded as maxima on gamma-ray logs have been recognized as typical of a clayey shallow shelf situated in the delta foreland (comp. Collinson, 1988; Hampson, 1995; Hampson et al., 1999). In the central part of the basin (Waksmundzka, 2010a) as well as in the study area these lithofacies are most typical of the *Posidonia corrugata* I, *Posidonia corrugata* II and *Dunbarella papyracea* faunal levels (Musiał and Tabor, 1988). Most probably, the remaining claystones devoid of fauna and exhibiting lower radioactivity are related to the most distal delta part, the prodelta.

Occasionally, within the 0 part there are L limestones or M marls formed also in the delta foreland on a ramp-type shallow carbonate shelf, the model of which has been designed by Flügel (2004). For the Lublin Carboniferous this environment has been described in detail by Skompski (1988, 1995a, b) and Waksmundzka (1998, 2010a, 2013).

Allocyclic factors such as BSL variations have a modifying effect on the formation of various types of coarsening-upward and non-gradational cyclothems and their stratigraphic successions. According to Waksmundzka (2013) base level rise is responsible for the origination of distal variations of type IIc coarsening-upward and type IIIc non-gradational cyclothems in a retrograding delta system and its foreland. Occasionally they are seen to contain MFS. However, at a high BSL, the prograding delta lobes entered a shallow shelf where thin carbonates or clays had been deposited. As a result, a proximal variety of type Ic coarsening-upward cyclothems was formed, equivalent to the British Yoredale cyclothems (Leeder and Strudwick, 1987; Tucker, 1991).

The typical lithofacies succession within the type IId coarsening-upward and type IIId non-gradational cyclothems indicates that they were laid down on a delta plain (Fig. 9). Part 1 contains sediments deposited in lakes or lake deltas, while the *Stigmaria* soils of part 4 formed in lakes overgrown by vegetation with contribution from soil-forming processes.

The distinctive lithofacies development of the Carboniferous in the SE part of the Lublin Basin and the presence of coarsening-upward cyclothems suggests that they may have formed within a fluvial-dominated shallow-marine delta with a delta plain of type D (deltaic system model no. 8) according to the classification by Postma (1990, 1995). The best recent example of this delta type is the Mississippi delta (Coleman, 1988). According to the delta classification by Porębski and Steel (2003), considering the relationship between the position on the shelf and the BSL state, the Lublin Carboniferous deltas have been classified into the group of inner-shelf deltas in which progradational and aggradational growth takes place during a high BSL (Waksmundzka, 2010a, 2013). The papers cited above include visualization of the development and variability of the deltaic environments and sub-environments in the Carboniferous of the Lublin Basin, dependent on the BSL.

SEQUENCE STRATIGRAPHY

SEQUENCES 1–3

LST: The lower unconformity of sequence 1 is equivalent to the Carboniferous base (Figs. 10 and 11). In the majority of higher successions, thin sandstones occur that formed in strongly aggradational high-energy fluvial channels. These are overlain by thick mudstones deposited on floodplains (Korczmin IG 3, Tyszowce IG 1, Łopiennik IG 1). These channels likely functioned within an anastomosing fluvial system and their filling and waning was controlled by BSL rise. At the base of sequence 1 there occasionally occur *Stigmaria* soils deposited on floodplains (Terebin IG1) whereas prodelta or shallow clayey shelf sediments have been recognized in Terebin IG 4 and Ruskie Piaski IG 2. All the above indicates that marine deposition set in as early as in LS time. By contrast, in the Marynin 1 borehole, thin volcanic rocks occur.

The lower unconformity of sequence 2 runs below thin sandstones formed in channels of the anastomosing fluvial system (Korczmin IG 3, Tyszowce IG 1, Łopiennik IG 1, Marynin 1). But only in the vicinity of the Marynin 1 section does the lower boundary of sequence 3 run below thin sandstones deposited by meandering rivers. Above this floodplain mudstones occur, followed by thin channel sandstones and claystones laid down on the floodplain of an anastomosing fluvial system. In the other

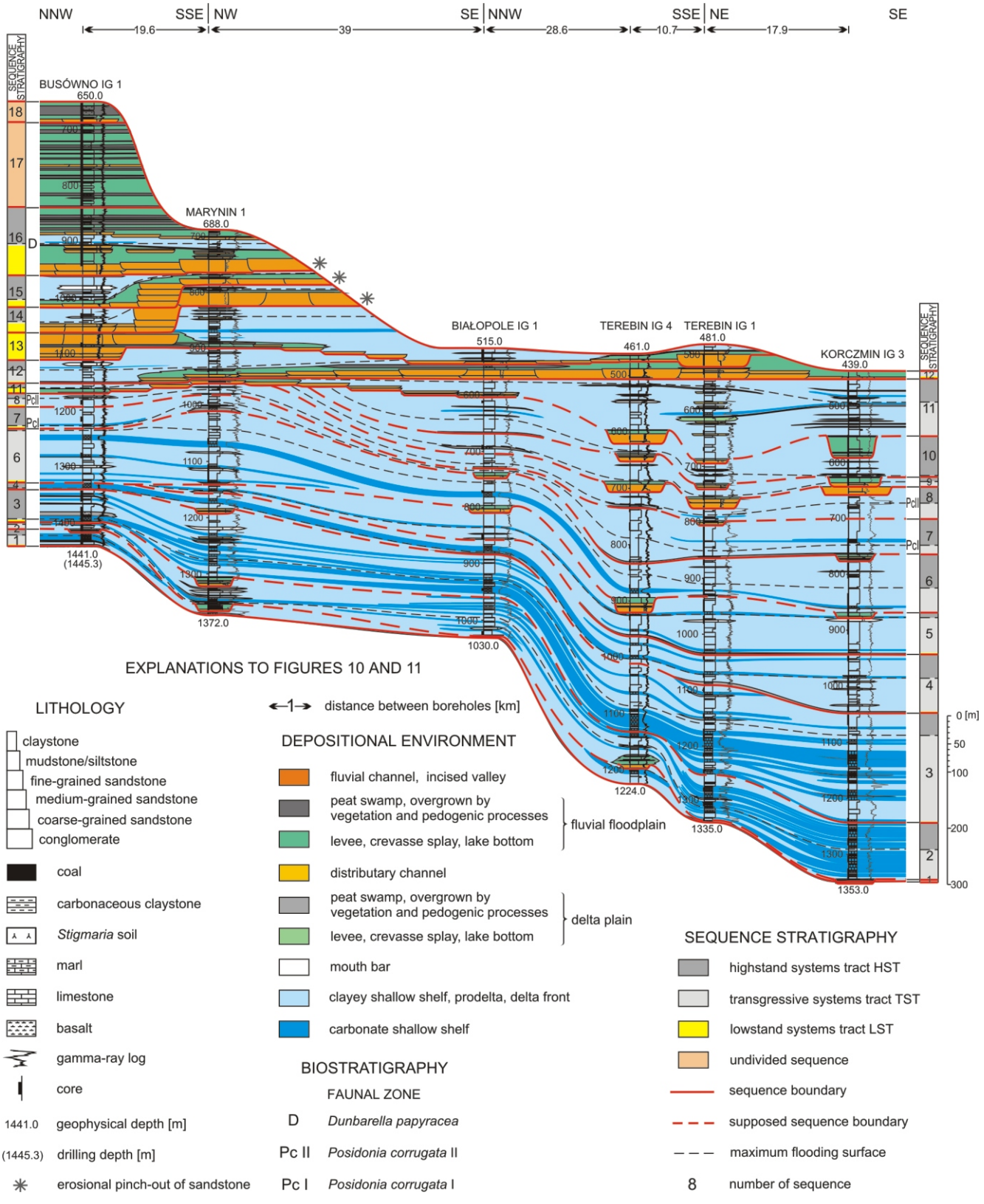

Fig. 10. Correlation scheme I – lithofacies and sequence stratigraphy of the Carboniferous succession of the NE part of the southeastern Lublin Basin

For details see online verision

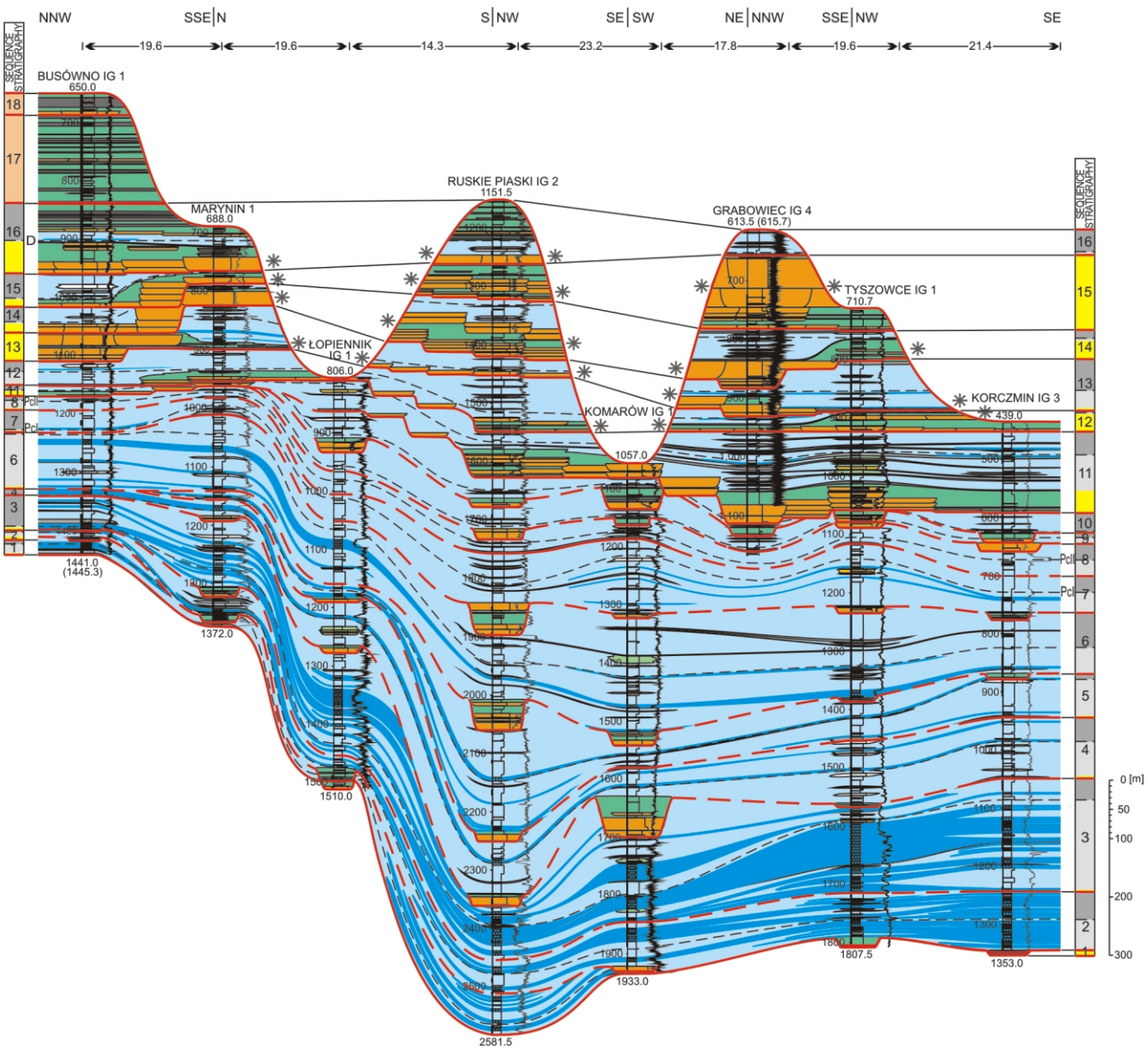

Fig. 11. Correlation scheme II – lithofacies and sequence stratigraphy of the Carboniferous succession of the SW part of the southeastern Lublin Basin

For details see online verision

sections the LST sequence 3 is represented by thin *Stigmaria* soils formed on a delta plain (Korczmin IG 3, Terebin IG 4, Tyszowce IG 1). Thus, only in the northern part of the study area the formation of sequence 3 was preceded by strong erosion resulting in the origination of river channels, while in the remaining area erosion was not so strong or was lacking completely and the shelf was exposed subaerially.

Within the LST sequences 1–3 channel sandstone lithosomes are rare and have a small thickness of low hydrocarbon potential.

TST: Within sequence 1 these deposits are represented by claystones and mudstones laid down on an inner-shelf delta and shallow clayey shelf, intercalated with limestones and marls indicative of a carbonate ramp on a shallow shelf (Terebin IG 4 and Ruskie Piaski IG 2).

Formations of TST sequences 2 and 3 are separated from the LST by the T surface manifested at the base of the first delta or shallow shelf carbonate deposits. The claystones and mudstones of an inner-shelf delta and shallow clayey shelf intercalate with numerous very thick carbonate ramp limestones. Rare thin sandstones were formed in delta mouth bars (e.g., Terebin IG 4), distributary channels (e.g., Tyszowce IG 1, Ruskie Piaski IG 2) and *Stigmaria* soil levels (e.g., Korczmin IG 3, Tyszowce IG 1) which mark minor BSL fluctuations resulting in the appearance of short-lived continental deposition.

MFS surfaces of sequences 1–3 run within the gamma ray log maxima or their conformity correlatives, in claystones originated in a clayey shallow shelf.

HST: HST deposits of sequence 1, encountered only in the Terebin IG 4 and Ruskie Piaski IG 2 boreholes, are developed similarly to its TST. HST sequences 2 and 3, however, present in every borehole section examined, are analogous to TST sediments of these sequences, the only difference being a lesser thickness and rarer presence of carbonate banks.

Sequences 1–3 show a distinct thickness predominance of deposits of a carbonate ramp on a shallow shelf, shallow clayey shelf and distal parts of an inner-shelf delta; their depositional regime can be defined as a marine-deltaic one. Sequences of similar qualities have been described by Smith Jr. and Read (1999, 2001) from the Upper Mississippian of the Illinois Basin, USA.

SEQUENCES 4–10

LST: Some of the lower unconformities run at the base of the *Stigmaria* soils deposited on delta plains (Figs. 10 and 11), while others are connected with strong fluvial erosion, which led to the formation of incised valleys of sequences 4–6 in the SW corner of the study area. Subsequently these were filled with fluvial sediments which in the Tyszowce IG 1 borehole originated in an anastomosing fluvial system. Farther to the east the incised valleys are absent and deposition took place on delta plains or close to mouth bars.

No sediments accumulated during LS sequence 7 in the north and north-east, but farther to the south deposition took place in meandering rivers (Tyszowce IG 1) and braided rivers grading vertically into the anastomosing fluvial system (Korczmin IG 3). LST sequence 8 includes thin *Stigmaria* soils and coals of a delta plain and sandstones of distributary delta channels or mouth bars. Only in the vicinity of the Terebin IG 1 borehole does an incised valley appear, filled with deposits of hyperconcentrated flows. Higher, there are thick floodplain deposits of an anastomosing fluvial system. Excepting the NE part of the basin, LST sequences 9 and 10 are mostly represented by alluvia filling incised valleys. In the vicinity of the Terebin IG 1, Tyszowce IG 1 and Korczmin IG 3 boreholes, the valleys are filled with hyperconcentrated flow deposits of braided and anostomosed system channels. These are overlain by mudstones and fluvial floodplain sandstones.

Within the LST there are commonly channel sandstone lithosomes with promising thicknesses attaining 12–33 m but of limited and discontinuous lateral extent. These have been encountered in sequences 4–7 and 9–10 in the following boreholes: Ruskie Piaski IG 2, Komarów IG 1, Terebin IG 1, Terebin IG 4, Korczmin IG 3, Tyszowce IG 1 and Łopiennik IG 1.

TST: These deposits comprise mainly claystones and mudstones deposited on a clayey shallow shelf, prodelta and inner-shelf delta slopes. Separate thin limestones of a carbonate ramp formed on a shallow shelf are also occasionally encountered. The TST also includes thin sandstones of mouth bars and distributary channels along with *Stigmaria* soils and coal that formed on delta plains. MFSs run at the bases of some limestones or within the gamma ray logs maxima.

HST: The development and provenance of HST deposits are similar to those of the TST. Typically their thickness is reduced by erosion active during the successive LS.

TST together with HST successions represented by claystones and mudstones have large thicknesses reaching up to 20–200 m and provide good sealing for sandstones of LST sequences 4–7 and 9–10.

A distinct predominance of large thicknesses in inner-shelf delta deposits suggests a deltaic depositional regime for sequences 4–10. Similarly developed sequences are reported from the Carboniferous of England by Davies and McLean (1996) and Tucker (2003) as well as from the Pennsylvanian of Kansas, USA by Maynard and Leeder (1992).

SEQUENCES 11–16

LST: These successions are typically developed as very thick fluvial channel sandstones, claystones, mudstones, *Stigmaria* soils and coals laid down on flood plains (Figs. 10 and 11). They fill valleys which were incised over the entire study area during the successive low BSL with contribution from strong fluvial erosion. LST sequence 11, recognized in the Tyszowce IG 1 borehole, was formed via hyperconcentrated flows in meandering and anastomosing river systems whereas deposits from the vicinity of Korczmin IG 3 represent an anastomosing fluvial system only. During LST sequences 12–15 meandering rivers were predominantly active (Tyszowce IG 1, Terebin IG 1) together with anastomosing fluvial systems (Tyszowce IG 1, Korczmin IG 3, Terebin IG 1), and less commonly braided rivers (Tyszowce IG 1).

Within the LST, channel sandstone lithosomes of promising thicknesses between 15–40 m are common, showing a continuous lateral extent at a km scale and present in sequences 11–16 of all the sections examined. An example of variation in the present-day thickness of LST sequence 11 sandstones and inferred direction of incised valley axes is illustrated in Figure 12A.

TST: Sequences 11–16 comprise mainly claystones and mudstones deposited in clayey shallow shelf areas, and the prodelta and slope of inner-shelf deltas. There are sporadic thin carbonate units representative of carbonate ramps on a shallow shelf and occasionally sandstones of mouth bars and distributary delta channels as well as *Stigmaria* soils and delta plain coals. As compared with TST sequences 4–10, they have larger thicknesses and are much more frequent. MFS run within the gamma ray log maxima, or distal deltaic or clayey shallow shelf lithofacies.

HST: The development and provenance of these successions are similar to those of the TST. Usually their thickness was reduced by erosion active during the successive LS and by post-Carboniferous erosion.

Sequence 11 of TST and HST together has a large thickness attaining 40–100 m (excepting the Komarów IG 1 borehole) which can provide good sealing (Fig. 12B) for the potential sandstone reservoir lithosomes present in the LST of this sequence (Fig. 12A). In the remaining sequences 12–16, TST and HST deposits are characterized by smaller thicknesses (ten to several tens of m) possibly contributing to local sealing. However, the proximity of the Carboniferous top being a major erosional surface coupled with the wedging out of lithosomes under the Mesozoic overburden reduce the sealing quality.

The abundance of very thick fluvial deposits adjacent to an inner-shelf delta suggests a fluvial-deltaic depositional regime for sequences 11–16. Sequences analogous in their lithofacies development and thickness relationships between systems tracts have been described from the Pennsylvanian in England (Martinsen at al., 1995), Germany (Süss et al., 2001), Ukraine (Izart et al., 2003a, b) and Russia (Briand et al., 1998).

CORRELATION OF SEQUENCE STRATIGRAPHY WITH THE CHRONOSTRATIGRAPHIC SCHEME

The sequence stratigraphic scheme established for the sections examined (Figs. 10 and 11) has been correlated to the West European (Ramsbottom, 1977, 1978) and global Carboniferous chronostratigraphic divisions (Davydov et al., 2012; Fig. 2). This correlation is based on the model established by Waksmundzka (2010a, 2013, 2018) where three maximum flooding surfaces with reliable biostratigraphic dating based on goniatite and conodont faunas (Musiał and Tabor, 1988; Skompski, 1996, 1998) have been taken into account.

The age of sequence 1 has been determined via the dating of basalts from the NE part of the Lublin Basin which were found to be of upper Tournaisian age (Pańczyk and Nawrocki, 2015). Thus, according to the present state of art, the estimated age of

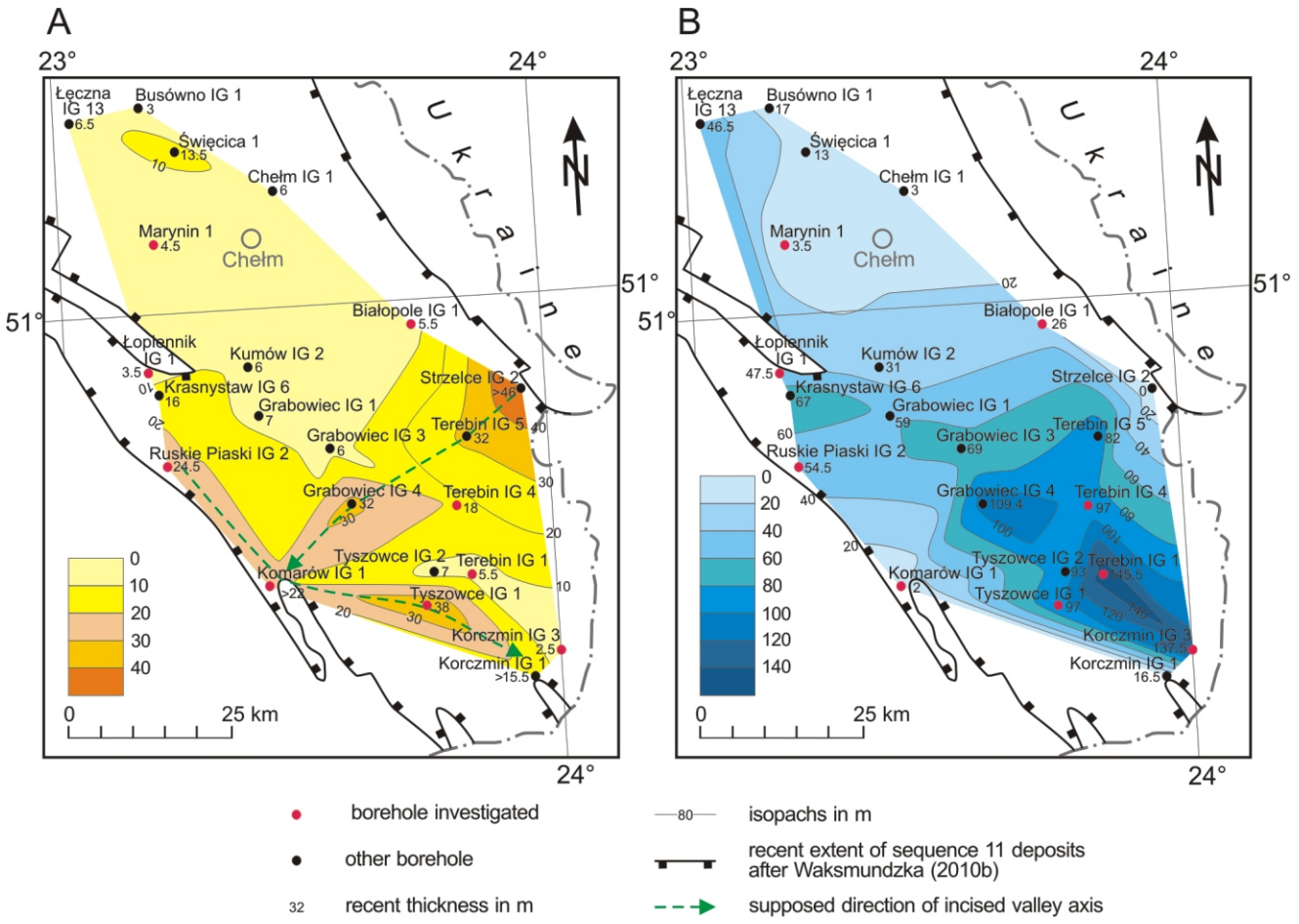

Fig. 12A – variation in recent thickness of the potential sandstone reservoir lithosomes of LST sequence 11 and inferred direction of incised valley axes; B – variation in present total thickness of TST and HST sequence 11 deposits which can provide good sealing for the potential sandstone reservoir lithosomes present in the LST of this sequence

Data regarding of other boreholes is from Waksmundzka (2005, 2010b, 2012c)

sequence 1 and sequences 2 to the lower part of sequence 5 can be inferred as upper Tournaisian–middle Visean and upper Visean respectively. Sequences 5–7 have been ascribed to the Serpukhovian and sequences 8–16 to the Bashkirian (Fig. 2).

Similarly to other parts of the Lublin Basin, a stratigraphic gap corresponding to the Lower Bashkirian has been noted in the sections examined (Waksmundzka, 1998, 2010a).

At its top the Carboniferous shows varying degrees of erosional reduction, being greatest in the vicinity of the Komarów IG 1, Korczmin IG 3 and Łopiennik IG 1 boreholes. This is less pronounced in the Białopole IG 1, Terebin IG 1, and Terebin IG 4 boreholes. In these boreholes the Carboniferous comprises sequences from 1 to 11–13, equivalent to the inferred upper Tournaisian–lower Bashkirian. In the remaining boreholes the succession is more complete, although partly reduced as it includes sequences from 1 to 16 thus reaching up to the upper Bashkirian.

PETROGRAPHY

The Carboniferous succession examined is built chiefly of clastic, with subordinate carbonate, components.

The sandstones are represented by locally numerous fine- to coarse grained subarkosic, quartz and sublithic arenites as well as wackes – most often very fine-grained and fine-grained, subarkosic, quartz and sublithic, less frequently lithic or arkosic (Figs. 13–15). The sandstones show either a random or an oriented texture accentuated by arrangement of organic matter, siderite and mica flakes. At the top of the Carboniferous in boreholes Korczmin IG 3, Łopiennik IG 1 and Marynin 1 there occur volcanoclastic sandstones, from fine- to coarse-grained sublithic or lithic arenites and wackes.

Usually siltstones and sandy siltstones have an oriented texture accentuated by a parallel arrangement of clay minerals and mica flakes commonly accompanied by organic matter and siderite. The mineral composition of the siltstones is identical with that of the sandstones. The groundmass is built of clay minerals (kaolinite, illite, chlorites, mixed-layered minerals illite/smectite, with the amount of illite averaging 90%) and silica.

In the claystones and silty and sandy claystones the texture is either haphazard or oriented, accentuated by the arrangement of organic matter, clay minerals, mica flakes, siderite and bioclasts. Claystones are composed mainly of clay minerals, silt-size grains of quartz and locally calcititic micrite. The most abundant clay minerals are kaolinite and illite accompanied by varying amounts of chlorite and mixed layered minerals illite/smectite, the amount of illite averaging 90%. Locally there occur quartz grains, mica flakes, bioclasts (brachiopod and foraminifer fragments), siderite spherulites and pyrite.

The conglomerates are represented by polymictic paraconglomerates known only from the Korczmin IG 3 bore-

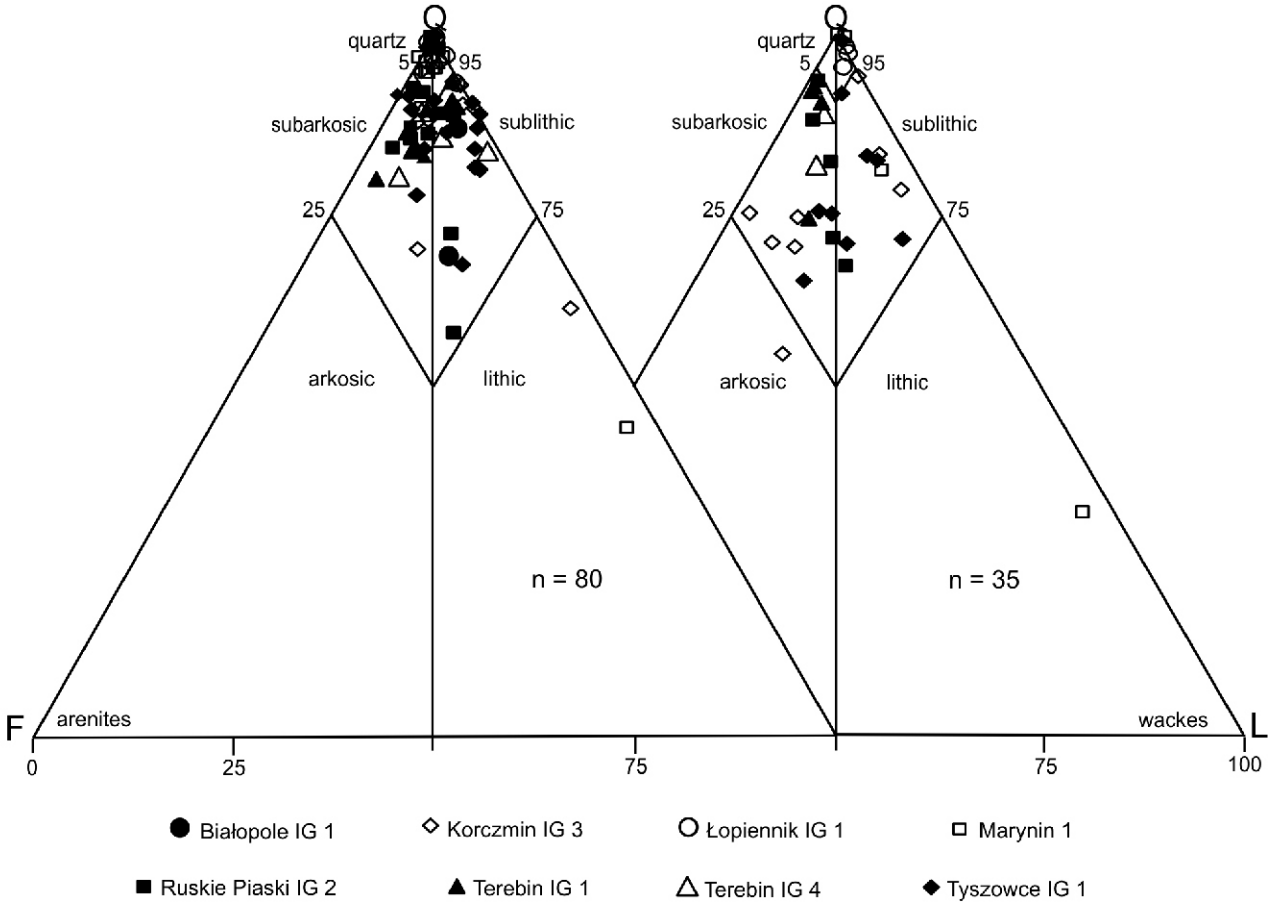

Fig. 13. Carboniferous sandstones according to classification triangles of Pettijohn et al. (1972)

Q – quartz, F – feldspar, L – lithoclasts

hole (sequence 7). The space between clasts of acid volcanic and sideritic rocks and mono- and polymictic quartz is filled with matrix which is a mixture of sand and cement of quartz, kaolinite and scarce ankerite.

The organodetrital limestones (grainstones, less often packstones and wackestones) are recrystallized to varying degrees (Dunham *fide* Jaworowski, 1987), and built of bioclasts, the amount of which can reach up to 80 vol.%, cemented by calcite or locally dolomite. Among the bioclasts fragments of foraminifers, echinoderms, bryozoans, algae, corals and molluscs have been identified, often pyritized and their voids filled with kaolinite or chalcedony. Terrigenous admixtures are rare and usually represented by clay minerals, organic matter, iron hydroxides and quartz fragments.

FRAMEWORK COMPOSITION OF THE SANDSTONES

The major mineral component of the framework composition of the sandstones is quartz averaging ~50–60 vol.% of the rock. Monocrystalline quartz grains prevail over polycrystalline grains which usually constitute 5–20 vol.% of the total quartz grains. Fragments of quartzite, quartzitic schist and chert have been classified within the polycrystalline quartz group (Pettijohn et al., 1972). The amounts of feldspars are variable – 5 vol.% on average, the maximum value exceeding 10 vol.%. K-feldspars prevail over plagioclases. K-feldspars subjected to cathodoluminescence analysis show a blue colour (Fig. 14A), sporadically yellow-brown and yellow-green. Plagioclase luminesces green. Most frequent are feldspar grains affected by dissolution (Fig. 14B), transformation or replacement by secondary minerals. Also variable is the content of micas, mainly muscovite and biotite, as well as chlorite which is often a transformation product of biotite. In arenites it usually comprises up to 5 vol.% but reaches 20 vol.% in wackes. Very often the mica flakes are bent due to mechanical compaction. The heavy mineral assemblages consists of zircon, apatite, titanite and rutile.

A significant component of the mineral framework are lithoclasts, the content of which is usually 5 vol.% though with a maximum of 42.7 vol.%. These are represented by magmatic rocks with volcanic prevailing over plutonic rocks. Acid rock clasts and fragments of volcanic glass have been noted. Among the plutonic rocks granitoids are predominant. Clasts of metamorphic rocks are common, mainly of quartz-mica schist. Locally present are fragments of sedimentary rocks, chiefly claystones, siltstones, sandstones and sideritic rocks.

Most often the detrital material is semi-rounded and well sorted. In arenites point contacts predominate, concave-convex and straight ones being scarce. In wackes, solely point contacts occur, or these are lacking completely.

The pore spaces between the detrital grains are fully or partly filled with matrix and/or cement. Usually the matrix comprises clay minerals, commonly mixed with quartz silt, while the cement consists of diagenetic minerals among which the most abundant are quartz, clay minerals and carbonates.

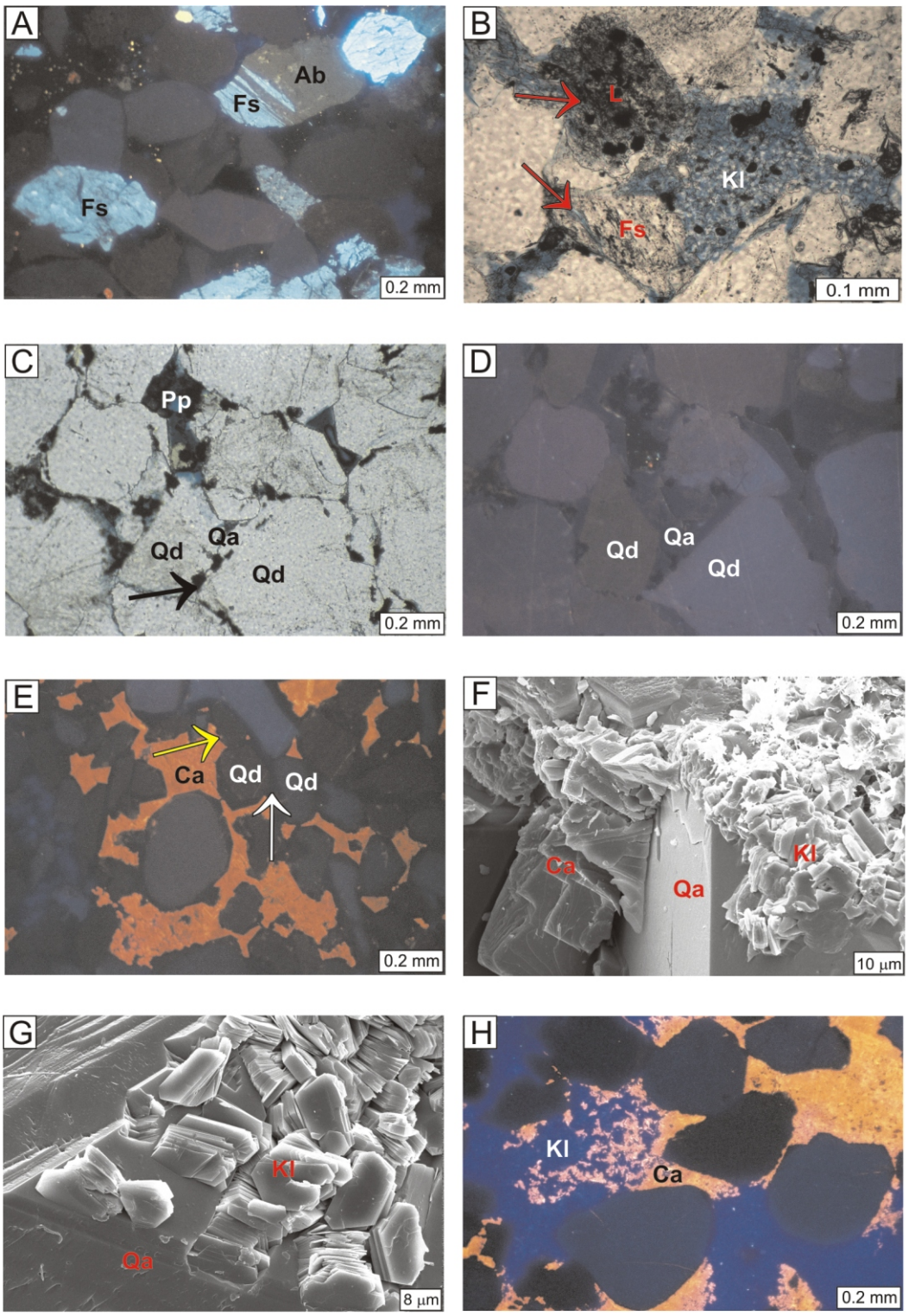

Fig. 14. Photographs of sandstones taken using a polarizing microscope (PL), cathodoluminescence (CL) and scanning electron microscope (SEI, BEI)

A – fragment of subarkosic arenite, CL image, blue luminescence of potassium feldspars (Fs), some altered to albite (Ab) with brown luminescence, Terebin IG 4 borehole, depth 501.0 m, LST of sequence 12, Bashkirian; **B** – secondary porosity (arrowed) in dissolved grains of potassium feldspar (Fs) and lithoclast (L) and microporosity in kaolinite (Kl) in subarkosic arenite, sample impregnated with blue resin, PL – plane polarized light, Terebin IG 1 borehole, depth 518.0 m, LST of sequence 13, Bashkirian; **C** – siderite crystals (arrowed) at the contact between quartz grain (Qd) and quartz overgrowths (Qa) in sublithic arenite, primary porosity (Pp), sample impregnated with blue resin, PL – plane polarized light, Tyszowce IG 1 borehole, depth 1,060.6 m, LST of sequence 10, Bashkirian; **D** – sample shown in Figure C, CL image, dark blue luminescence of authigenic quartz (Qa) and brown and blue of quartz grains (Qd); **E** – fragment of quartz arenite, CL image, no luminescence of authigenic quartz (white arrow) and brown and blue of quartz grains (Qd), red luminescence of calcite (Ca) cement replacing authigenic quartz (yellow arrow), Tyszowce IG 1 borehole, depth 1,597.8 m, TST of sequence 3, Visean; **F** – authigenic quartz crystal (Qa), booklet kaolinite (Kl) and calcite (Ca) in pore space of subarkosic arenite, Tyszowce IG 1 borehole, depth 926.0 m, SEI image, LST of sequence 11, Bashkirian; **G** – booklet kaolinite (Kl) overgrown by authigenic quartz (Qa) in pore space of sublithic arenite, Tyszowce IG 1 borehole, depth 1,026.7 m, SEI image, LST of sequence 11, Bashkirian; **H** – fragment of quartz arenite, CL image, dark blue luminescence of kaolinite (Kl) engulfed by calcite (Ca) of yellow-orange luminescence, Marynin 1 borehole, depth 1,359.1, LST of sequence 2, Visean

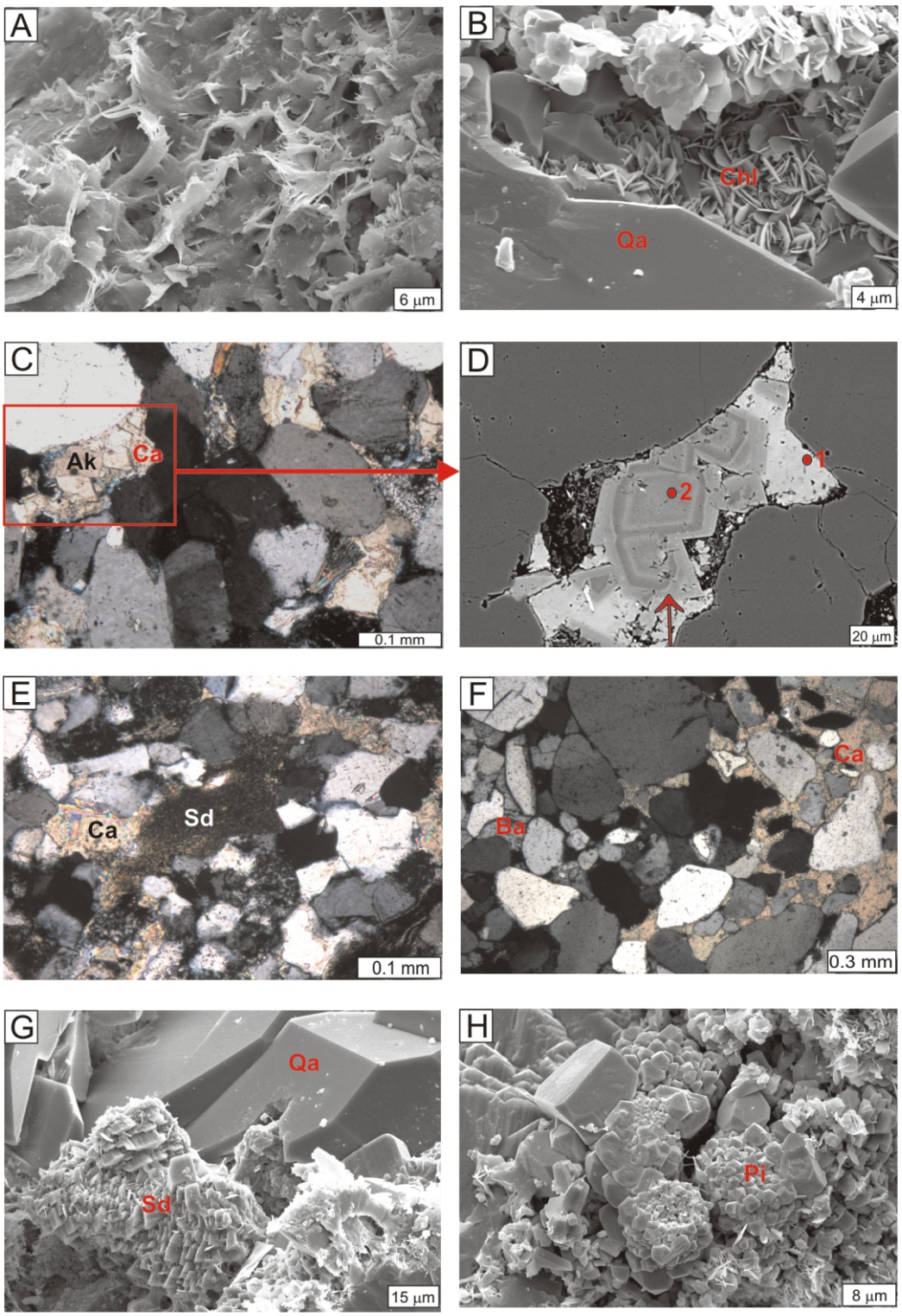

Fig. 15. Photographs of sandstones taken using a polarizing microscope (PL) and scanning electron microscope (SEI, BEI)

A – fibrous illite growing on flaky illite in subarkosic arenite pore space, Terebin IG 1 borehole, depth 530.0 m, SEI image, LST of sequence 12, Bashkirian; **B** – fragment of chlorite rim (Chl) on quartz grain, overgrown by authigenic quartz (Qa) in sublithic arenite, Terebin IG 4 borehole, depth 501.0 m, SEI image, LST of sequence 12, Bashkirian; **C** – rhombohedra of ankerite (Ak) engulfed by calcite cement (Ca) in subarkosic arenite, Terebin IG 4 borehole, depth 490.8 m, PL – crossed polars, LST of sequence 12, Bashkirian; **D** – fragment of sample shown in Figure C, BEI image, zoned rhombohedra of ankerite, calcite replacing ankerite (arrowed), 1, 2 – points of chemical analyses (Table 6); **E** – calcite (Ca) and siderite (Sd) cements in sublithic arenite, Tyszowce IG 1 borehole, depth 780.9 m, PL – crossed polars, LST of sequence 14, Bashkirian; **F** – calcite (Ca) and barite (Ba) cements in quartz arenite, Tyszowce IG 1 borehole, depth 1,758.0 m, PL – crossed polars, LST of sequence 2, Visean; **G** – siderite (Sd) and authigenic quartz (Qa) in subarkosic arenite pore space, Tyszowce IG 1 borehole, depth 1,060.0 m, SEI image, LST of sequence 10, Bashkirian; **H** – pyrite (Pi) framboids in subarkosic arenite pore space, Terebin IG 1 borehole, depth 503.5 m, SEI image, LST of sequence 13, Bashkirian

SANDSTONE CEMENTS

Quartz cement occurs as syntaxial overgrowths around the quartz grains, partly or locally completely (Fig. 14C–F) filling the pore spaces. The quartz cement content is usually 1–10 vol.% and 23 vol% at the maximum. Locally the amount of quartz cement increases with depth (Ruskie Piaski IG 2, Tyszowce IG 1). On the basis of the cathodoluminescence analysis of sandstones one generation of authigenic quartz overgrowths could be identified characterized by dark brown, dark blue or absent luminescence (Fig. 14D, E) clearly opposed to quartz grains luminescing in blue-violet, brown, green or red. Locally in the overgrowths two or more shades of brown are noted, which indicates that the cementation with quartz was an unstable process. In places the boundary between detrital quartz and overgrowths is marked by the presence of inclusions or early siderite (Fig. 14C). Authigenic quartz also fills grain fractures suggesting that silicification was preceded by mechanical compaction. In the sandstones, replacement by carbonates (Fig. 14E) and sporadically by barite has been observed. As indicated by the presence of small one-phase inclusions (Goldstein and Reynolds, 1994) the minimum temperature of the formation of authigenic quartz is estimated to be <50°C. In the rare two-phase inclusions the homogenization temperature were found to range between 83.9 and 179.0°C, these values being in agreement with earlier results obtained by Kozłowska and Jarmolowicz-Szulc (2009).

Among the clay minerals the kaolinite subgroup predominates over illite, subordinate chlorite and mixed-layered illite/smectite. The kaolinite subgroup is represented chiefly by kaolinite and less frequently dickite. As shown by infrared examinations (Kozłowska, 2011) kaolinite and dickite intergrowths are common, the kaolinite content being 20–80%. Typically, the kaolinite subgroup content is ~3 vol.% but can reach up to 17 vol.%. The size of authigenic kaolinite and dickite crystals usually falls within the 1–20 μm range. Commonly these show a characteristic booklet structure (Fig. 14F, G). As earlier observed by Kozłowska (2004, 2009, 2011) kaolinite is most frequently vermicular, while dickite shows a blocky structure. The presence of both morphological kaolinite types has been recognized in sandstones throughout the Carboniferous succession. In the CL image the kaolinite subgroup minerals luminesce in dark blue (Fig. 14H). On sites where feldspar grains and mica flakes have been dissolved, transformed kaolinite enters pore spaces. This mineral also forms intergrowths with authigenic quartz. Moreover, it is replaced by ankerite and Fe-calcite and transformed into fibrous illite. Dickite crystals often form intergrowths with kaolinite or occur individually.

In the sandstones, acicular and fibrous illite overgrows illite laths (Fig. 15A), authigenic quartz, carbonates and kaolinite forming within the pore spaces. Present in all borehole profiles, illite is most abundant in sandstones of Ruskie Piaski IG 2, Tyszowce IG 1, Marynin 1, Terebin IG 1 and Terebin IG 4. K-Ar age determinations of diagenetic illite ranging from 286.5 ±3.4 to 257.7 ±2.6 Ma indicate that its crystallization in the SE part of the Lublin Basin began in Permian times (Kozłowska, 2009, 2011).

Chlorites, mainly ferruginous, form rims on quartz grains (Fig. 15B) and fill pore spaces in sandstones from the Terebin IG 1, Terebin IG 4 and Tyszowce IG 1 boreholes.

X-ray examinations revealed the presence of mixed-layered illite/smectite, the illite content exceeding 85%, in the Ruskie Piaski IG 2 and Tyszowce IG 1 boreholes (Kozłowska, 2009, 2011).

The carbonate minerals are represented by: Fe-calcite, Fe-dolomite, ankerite, sideroplesite, siderite and rhodochrosite. Their amount in sandstones reaches 48 vol.%. Usually Fe-calcite forms pore-filling cement, but occasionally also the basic infill of inter- and intra-granular pore spaces (Figs. 14E, F, H and 15C–F). Moreover, it replaces feldspar grains, lithoclasts and quartz as well as cements: quartz (Fig. 14E), kaolinite (Fig. 14H), siderite and ankerite. The chemical composition of calcite is as follows: 88.9–99.2 mol% of $CaCO_3$, 0.3–6.6 mol% of $FeCO_3$, 0–2.0 mol% of $MgCO_3$ and 0–8.6 mol% of $MnCO_3$ (Table 6 and Fig. 16). Depending on the amount of iron and manganese contents it luminesces red, red-orange, orange-yellow or yellow (Fig. 14E, H). Fluid inclusion examinations yielded homogenization temperatures of 75.3–119°C which are in agreement with earlier results obtained for the Carboniferous Lublin Basin (Kozłowska, 2005, 2009; Kozłowska and Jarmołowicz-Szulc, 2009). Isotopic results for Fe-calcite are given in Table 6. The ^{18}O values fall within the –17.65 to –3.48‰PDB range, averaging 13.23‰PDB while the ^{13}C values vary from –19.45 to +1.22‰PDB and average 6.12‰PDB (Fig. 17). The ^{13}C values suggests that calcite was formed in the thermal zone of decarboxylation of organic matter or locally in the zone of microbiological methanogenesis (Morad, 1998).

Fe-dolomite and ankerite commonly occur as isolated euhedral rhombohedral crystals (Fig. 15C, D) or as a massive spar cement. The crystals' composition is: 10.4–26.5 mol% of $FeCO_3$, 17.3–31.2 mol% of $MgCO_3$, 53.5–59.8 mol% of $CaCO_3$ and 0.1–2.2 mol% of $MnCO_3$ (Table 6 and Fig. 16). Most are ankerites with only sporadically Fe-dolomites. Some crystals have a zonal structure due to variable iron/magnesium proportions during crystallization (Fig. 15D). Because of a considerable Fe^{+2} content, the ankerite shows no luminescence on the CL images. Parts of the crystals show a wide undulatory extinction which can indicate the presence of saddle dolomite (ankerite; Radke and Mathis, 1980; Spötl and Pitman, 1998). Ankerite replaces feldspars, quartz and lithoclasts and some components of the cement such as authigenic quartz, siderite and kaolinite. In turn, this mineral itself is replaced by Fe-calcite (Fig. 15D) and was locally subjected to dissolution. Earlier studies of fluid inclusions in ankerite yielded homogenization temperatures ranging from 74 to 117°C (Kozłowska, 2005; Kozłowska and Jarmołowicz-Szulc, 2009) which corresponds to its minimum crystallization temperature. For two samples ^{18}O and ^{13}C values have been found to be –12.30‰PDB and –11.78‰PDB and –1.48‰PDB and –0.14‰PDB, respectively (Table 6 and Fig. 17). They fall in the range of results obtained from earlier measurements: ^{18}O from – 16.22 to – 6.90‰PDB and ^{13}C from – 8.35 to –0.09‰PDB (Kozłowska, 2005, 2009). The ^{13}C values indicate that ankerite formed in the zone of microbiological methanogenesis and locally in the zone of thermal decarboxilation of organic matter (Kozłowska, 2005, 2009).

Sideroplesite and siderite belong to the isomorphic siderite-magnesite series containing 75–100 mol% $FeCO_3$. The minerals analysed have 76.6–96.2 mol% of $FeCO_3$, 1.3–18.5 mol% of $MgCO_3$, 1.5–9.3 mol% of $CaCO_3$ and 0.6–4.3 mol% of $MnCO_3$ (Table 6 and Fig. 16). These minerals occur either as very fine grains or aggregates (Fig. 15E) or spherulites, either separate or aggregated. Locally sideroplesite and siderite envelope detrital grains and in places even separate quartz grains from the authigenic quartz overgrowths (Fig. 14C), or else fill the original pore space (Fig. 15G). These minerals replace feldspars, lithoclasts, micas, but are themselves replaced by ankerite and Fe-calcite. Sideroplesite and siderite belong to early generation minerals. Late generation sideroplesite, common in sandstones of the NW part of the Lublin Basin (Kozłowska 1997, 2001, 2004) and locally in the central part (Kozłowska, 2007), has not been observed. The ^{18}O values fall within –14.48 to –4.30‰PDB averaging –10.35‰PDB, while the ^{13}C values range from –7.55 to + 1.85‰PDB, and average

Table 6

Chemical compositions from microprobe analyses, carbon and oxygen isotopic data and homogenization temperature of the carbonates

Borehole	Depth [m]	Point of analysis	$CaCO_3$ %mol.	$MgCO_3$ %mol.	$FeCO_3$ %mol.	$MnCO_3$ %mol.	^{13}C ‰PDB	^{18}O ‰PDB	Homogenization temperature	Carbonate type
Białopole IG 1	849.5						–1.48	–12.30		ankerite
	1018.2	1	94.2	0.4	1.6	3.8				Mn/Fe-calcite
		2	92.9	1.2	2.4	3.5				Mn/Fe-calcite
Korczmin IG 3	455.1	1	5.4	1.3	89.0	4.3				siderite
		2	96.7	0.7	1.8	0.8	–7.27	–16.57		Fe-calcite
	592.1	1	55.7	23.3	20.2	0.8				ankerite
		2	4.0	6.1	88.3	1.6				sideroplesite
	903.7	1	59.6	17.3	22.1	1.0				ankeryt
		2	97.4	0.1	1.7	0.8	–2.35	–14.82		Fe-calcite
		3	2.3	18.5	76.6	2.6	–1.27	–14.48		sideroplesite
	1350.8						–19.45	–9.78		calcite
	1353.0	1	91.0	2.0	6.6	0.4				Fe-calcite
		2	88.9	1.4	1.1	8.6				Mn-calcite
		3	92.4	0.7	6.0	0.9				Fe-calcite
		4	91.9	0.9	3.0	4.2				Mn/Fe-calcite
		5	5.1	0.0	2.4	92.5				rhodochrosite
Łopiennik IG 1	1494.6	1	96.2	0.0	1.4	2.4	–8.87	–13.44		Mn/Fe-calcite
		2	2.5	0.8	94.7	2.0	–7.55	–11.45		siderite
Marynin 1	733.8						+1.85	–4,30		siderite
	1311.0						–1.72	–9.55		siderite
	1313.7						–5.89	–13.52		calcite
							+0.47	–7.65		siderite
	1322.4	1	1.8	1.1	94.1	3.0	–1.83	–9.96		siderite
		2	94.4	0.9	3.1	1.6	–5.69	–13.75		Fe-calcite
	1337.5	1	97.2	0.4	1.3	1.1	–7.15	–13.85		Fe-calcite
		2	6.4	2.0	88.8	2.8	–1.37	–10.16		siderite
	1339.3						–6.86	–14.11		calcite
	1350.1		94.7	0.2	0.9	4.2	–0.56	–11.33		Mn/Fe-calcite
	1359.1						–8.31	–13.68	117.0	calcite
	1361.2	1	5.3	4.4	87.1	3.2	–5.29	–11.07		siderite
		2	971	0.0	1.9	1.0	–6.12	–12.26		Fe-calcite
	1363.4						–3.34	–10.46	119.0	calcite
Ruskie Piaski IG 2	1209.2	1	1.5	1.7	96.2	0.6	–4.67	–9.70		siderite
		2	4.7	7.5	87.0	0.8				sideroplesite
	1317.0		97.3	1.5	1.2	0.0	+0.24	–6.46		Fe-calcite
	1560.5						–5.19	–8.99		siderite
	1851.5						–10.06	–16.95		calcite
	2374.5								75.3; 75.3; 80.0	calcite
	2382.7		96.2	1.3	1.5	1.0	–0.81	–15.16		Fe-calcite
	2390.7						–2.28	–14.82		calcite
							–3.61	–12.37		siderite
Terebin IG 1	643.0						–6.13	–16.02		calcite
							–2.13	–13.53		siderite
	805.0		95.7	0.0	2.1	2.2	–7.64	–17.65		Fe-calcite
	945.0	1	5.2	9.7	82.1	3.0	–2.76	–11.52		sideroplesite
		2	5.7	5.4	87.6	1.3				sideroplesite
Terebin IG 4	490.8	1	99;2	0.0	0.8	0.0	–16.39	–3.48		Fe-calcite
		2	56.2	31.2	10.4	2.2				ankerite
	652.3	1	9.3	2.0	85.1	3.6				siderite
		2	97.6	0.0	2.2	0.2				Fe-calcite

Tab. 6 cont.

Borehole	Depth [m]	Point of analysis	$CaCO_3$ %mol.	$MgCO_3$ %mol.	$FeCO_3$ %mol.	$MnCO_3$ %mol.	^{13}C ‰PDB	^{18}O ‰PDB	Homogenization temperature	Carbonate type
Tyszowce IG 1	780.9	1	5.7	4.0	86.8	3.5	–4.14	–9.75		sideroplesite
		2	95.6	0.0	1.4	3.0	–7.99	–10.93		Mn/Fe-calcite
	846.0						–14.95	–8.66		calcite
	898.3						–4.13	–17.49		calcite
							–3.08	–12.08		siderite
	921.4		4.7	2.4	91.4	1.5				siderite
	926.0		96.4	0.4	1.6	1.6				Fe-calcite
	991.4						–7.78	–17.15		calcite
							–1.40	–13.71		siderite
	1574.4						–4.71	–16.39		calcite
							–1.59	–13.69		siderite
	1597.8						–2.36	–16.12		calcite
	1670.0	1	59.8	20.2	18.6	1.4	–0.14	–11.78		ankerite
		2	53.5	19.9	26.5	0.1				ankerite
	1758.0		98.1	1.6	0.3	0.0	+1.22	–12.66		calcite

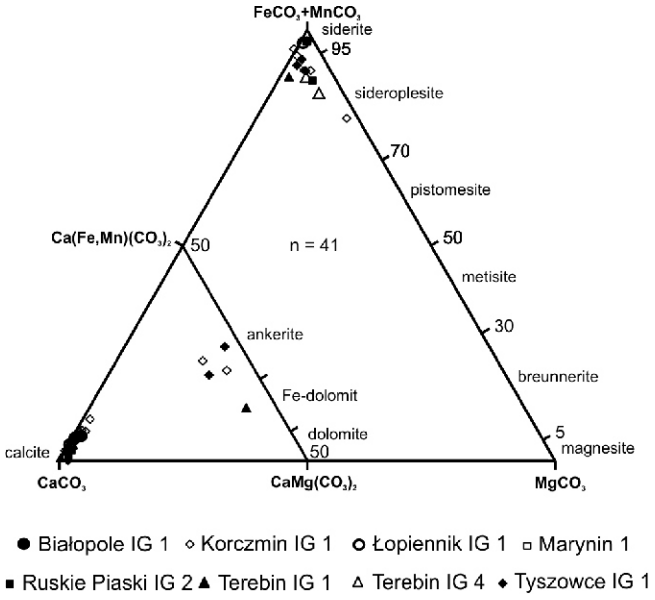

Fig. 16. Triangle diagram of the carbonates, chemical composition at mol%

n – analysis number

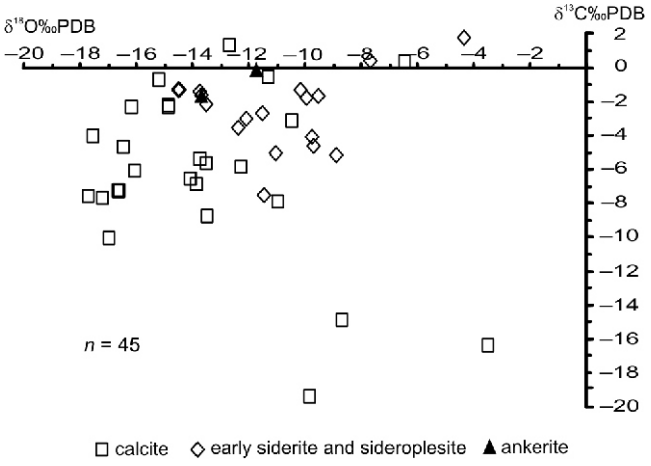

Fig. 17. ^{18}O‰PDB *versus* ^{13}C‰PDB plot of the carbonate cements

–2.36‰PDB (Table 6 and Fig.17). The latter suggest that sideroplesite and siderite originated in the zone of microbiological methanogenesis (Morad, 1998).

Rhodochrosite has been identified in a sandstone sample from the depth of 1353.0 m in the Korczmin IG 3 borehole. Its chemical composition is as follows: 92.5 mol% of $MnCO_3$, 5.1 mol% of $CaCO_3$ and 2.4 mol% of $FeCO_3$ (Table 6). This mineral fills the fissures in quartz grains and partly also the pore space between the grains. In CL images it shows no luminescence.

Other subordinate diagenetic minerals are barite, celestine, pyrite, phosphates and glauconite. The average content of each of these is ~1 vol.%. Barite fills the intergranular spaces in the sandstone (Fig. 15F) and locally replaces detrital grains and carbonate cements and kaolinite. Most often it is met in the top parts of Carboniferous profiles. Chemical analysis revealed the presence of strontium in its composition. Pyrite occurs as separate crystals and grains, commonly enveloped by early-generation siderite. Individual pyrite framboids are common (Fig. 15H). Phosphates form very fine aggregates and luminesce in milky-pink in CL image. Green oval glauconite grains are present between those of the mineral framework. Locally it is replaced by Fe-calcite.

ORGANIC MATTER

The organic matter most common in the Carboniferous succession is humic in nature. The content of macerals of the vitrinite group is ~70% of the total organic matter in the rock (Grotek, 2005, 2008). The thermal maturity corresponds to the main phase of oil generation with reflectivity varying from 0.57 to 1.20% R_o (Grotek, 2005, 2008). The lowest R_o values reported from the SE part of the Lublin Basin suggest that a palaeotemperature of ~80°C affected the Carboniferous strata. The R_o values increase towards the south-west indicating a maximum palaeotemperature of ~120°C.

POROSITY AND PERMEABILITY

Laboratory tests performed on sandstones revealed that their effective porosity varies from 0.6 to 15.1% (Table 7) and decreases with depth. For the Bashkirian, Serpukhovian and Tournaisian–Visean these values are 4.8–15.1 (averaging 9.5%), 0.6–11.6 (averaging 5.9%) and 1.2–6.5 (averaging 4%) respectively. According to Jenyon (1990) such results permit classification of the majority of the examined rocks to deposits of good porosity. Values exceeding 10% have been found in the following boreholes: Korczmin IG 3 – sequences 6, 9, 10; Terebin IG 1 – sequences 7, 9, 12, 13; Terebin IG 4 – sequence 12; Tyszowce IG 1 – sequences 10, 14.

Porosity determined in thin sections attains 13 vol.% and is ~5 vol.% on average. The sandstones are characterized by both primary and secondary porosity, the former being prevalent. As a result of mechanical compaction and cementation, porosity has been strongly reduced. However, its partial preservation is due to the presence of early orthochemical cement at the time of incomplete filling of intergranular space (Fig. 14C).

Table 7

Petrophysical features of selected Carboniferous sandstone samples

Borehole	Sequence stratigraphy	Depth [m]	Grain density [g/cm^3]	Effective porosity [%]	Bulk density [g/cm^3]	Porosimeter density [g/cm^3]	Porosimeter porosity [%]	Average capillary [um]	Specific surface [m^2/g]	Pores >1 um [%]	Threshold diameter [um]	Hysteresis [%]	Permeability [mD]
Korczmin IG 3	11	455.10	2.65	5.22	2.6	2.47	4.97	0.09	0.94	9	0.4	61	n.p.
	11	486.60	2.65	9.08	2.58	2.36	8.49	0.26	0.55	56	3	64	0.10
	10	643.90	2.64	13.8	2.53	2.21	12.43	0.3	0.67	71	25	47	15.08
	9	645.60	2.64	13.92	2.59	2.25	13.26	0.4	0.55	74	30	49	14.79
	6	777.60	2.63	11.46	2.56	2.29	10.71	0.57	0.33	76	40	33	45.24
	5	903.70	2.69	6.27	2.62	2.46	5.86	0.05	1.78	14	0.3	64	n.p.
	4	987.10	2.71	1.21	2.72	2.69	1.22	0.04	0.47	30	0.06	70	n.p.
	1	1350.80	2.7	1.21	2.73	2.69	1.25	0.05	0.36	33	0.2	63	i.d.
Łopiennik IG 1	1	1494.60	2.69	6.46	2.69	2.51	6.46	0.06	1.65	11	0.8	54	i.d.
	1	1509.60	2.66	7.59	2.64	2.45	7.44	0.05	2.68	8	0.6	55	i.d.
	1	1511.40	2.67	7.26	2.59	6.42	6.72	0.03	3.21	11	1	64	i.d.
Ruskie Piaski IG 2	16	1172.50	2.72	5.75	2.71	2.56	5.69	0.05	1.81	16	0.4	55	i.d.
	15	1317.00	2.67	4.82	2.64	2.52	4.68	0.09	0.86	17	1	48	i.d.
	7	1851.50	2.67	0.61	2.65	2.64	0.6	0.09	0.1	56	0.1	26	0.10
	6	2036.00	2.63	3.42	2.61	2.52	3.35	0.05	1.11	20	0.3	54	i.d.
	6	2350.30	2.67	4.65	2.65	2.53	4.56	0.05	1.58	15	1	47	i.d.
	3	2363.50	2.69	3.04	2.67	2.59	2.98	0.04	1.15	24	0.4	49	i.d.
	3	2374.50	2.64	3.58	2.6	2.51	3.44	0.07	0.82	24	1	48	i.d.
	3	2382.70	2.7	1.64	2.68	2.63	1.61	0.06	0.42	33	0.4	36	i.d.
	3	2390.50	2.68	3.17	2.65	2.56	3.08	0.04	1.31	11	0.2	48	0.10
Terebin IG 1	13	503.50	2.64	10.24	2.6	2.35	9.85	0.13	1.34	29	2	56	1.16
	12	530.00	2.65	15.08	2.59	2.22	14.23	0.18	1.4	59	80	44	i.d.
	9	740.50	2.63	13.26	2.55	2.24	12.28	0.33	0.67	71	5	46	i.d.
	8	776.00	2.66	9.26	2.66	2.41	9.26	0.1	1.6	17	2	55	i.d.
	7	805.00	2.67	3.48	2.6	2.52	3.25	0.05	1.05	20	0.2	46	i.d.
	6	870.00	2.64	11.65	2.56	2.28	10.79	0.3	0.63	62	4	63	1.80
Terebin IG 4	12	496.00	2.68	13.59	2.64	2.29	13.07	0.24	0.94	57	10	65	1.21
	12	505.50	2.72	11.85	2.68	2.38	11.39	0.06	3.24	8	1	70	i.d.
Tyszowce IG 1	14	780.90	2.67	5.56	2.64	2.5	5.4	0.07	1.3	14	0.4	58	i.d.
	14	804.30	2.71	11.34	2.67	2.4	10.9	0.1	1.65	14	0.7	55	i.d.
	12	889.10	2.62	7.73	2.63	2.42	7.81	0.17	0.75	26	3	85	1.10
	11	926.00	2.65	7.41	2.63	2.44	7.26	0.11	1.11	12	1	59	i.d.
	11	1026.70	2.65	8.74	2.6	2.38	8.32	0.12	1.16	33	2	59	0.27
	11	1052.30	2.62	6.42	2.58	2.42	6.17	0.11	0.92	31	3	64	0.10
	10	1060.60	2.65	10.09	2.62	2.36	9.8	0.16	1.03	62	30	44	14.81
	9	1081.20	2.67	8,00	2.7	2.47	8.25	0.07	1.8	15	2	65	0.10
	8	1170.20	2.65	8.7	2.61	2.39	8.37	0.1	1.4	9	1	45	i.d.
	3	1597.80	2.66	3.38	2.56	2.48	3.07	0.08	0.59	41	i.d.	40	0.10
	3	1602.20	2.64	5.69	2.6	2.49	5.47	0.11	0.78	11	0.6	62	0.31
	2	1758.00	2.84	1.95	2.79	2.74	1.86	0.09	0.31	27	1	40	i.d

n.p. – no permeability, i.d. – indeterminate

The early cements forming rims are: chlorite, siderite, sideroplesite and quartz. The secondary porosity resulted due to the dissolution of feldspars (Fig. 14B) and subordinately lithoclasts (Fig. 14B), while the dissolution of cements (Fe-calcite and ankerite) was of minor significance. Microporosity among crystallites of authigenic clay minerals, mainly kaolinite, is common (Fig. 14B).

Measurements of porosimetric porosity, the amount of pores >1 μm, threshold diameter and hysteresis (Table 7) indicate that the best reservoir parameters are in the Bashkirian and Serpukhovian sandstones from those borehole sections with good effective porosity. These parameters deteriorate downwards and are poorest in the Tournaisian–Visean. In the Bashkirian sandstones the dynamic porosity is ~10%. The content of pores >1 μm varies from 9 to 74% and averages ~50% in the boreholes Korczmin IG 3 and Terebin IG 1 and only ~30% in Terebin IG 4 and Tyszowce IG 1. The threshold diameter falls into the 0.4–80 μm range but usually does not exceed 10 μm. The average hysteresis value is ~60%. For the Tournaisian–Visean and Serpukhovian sandstones the respective parameters are: dynamic porosity – ~7% and 2%, average content of pores >1 μm – ~30% and 20%, threshold diameter - ~2 μm and <1μm and hysteresis – ~45% and 50%.

In the Ruskie Piaski IG 2 borehole, examined only in some sections because of poor core recovery, there are sandstones with low filtration parameters characterized by: dynamic porosity – ~4%, average content of pores >1μm – ~20%, threshold diameter – <1 μm and hysteresis ~45%. Likewise, from the Łopiennik IG 1 borehole only Tournaisian-Visean sandstones (sequence 1) with poor filtration parameters have been examined.

The permeability of the sandstones ranges from 0 to 45.24 mD (Table 7). The value of this parameter is controlled by porosity and depth of occurrence (Kozłowska, 2003). According to Levorsen's classification (1967) most of these sandstones belong to the group of poor <1 mD or fair 1–10 mD permeability. Individual sandstone samples with good permeability from 10 to 100 mD have been reported from the Bashkirian and Serpukhovian from the boreholes Korczmin IG 3 – sequences 6, 9, 10 and Tyszowce IG 1 – sequence 10.

DISCUSSION

DIAGENETIC HISTORY

Figure 18 summarizes the paragenetic sequence of the Carboniferous sandstones of the SE part of the Lublin Basin. Eo-, meso- and telodiagenetic phases have been distinguished. The temperature of 50°C has been assumed as the boundary between eo- and mesodiagenesis in the sandstones studied (Kozłowska, 2004).

From the beginning of the diagenetic process, mechanical compaction set in. The slightly acidic pore waters caused the decomposition of unstable detrital minerals containing iron which under oxidizing conditions precipitated as hematite or iron oxides. Usually, enrichment in iron occurs at temperatures of ~50°C (Mücke,1994).

Locally the enrichment of pore water with phosphorus resulted in the crystallization of authigenic apatite crystals. Possible sources of phosphorus include dissolved K-feldspars (London, 1992).

The decrease of oxygen content in the pore water caused a change from oxidizing to reducing conditions in the sediment. Gradually, with the decomposition of some mineral components

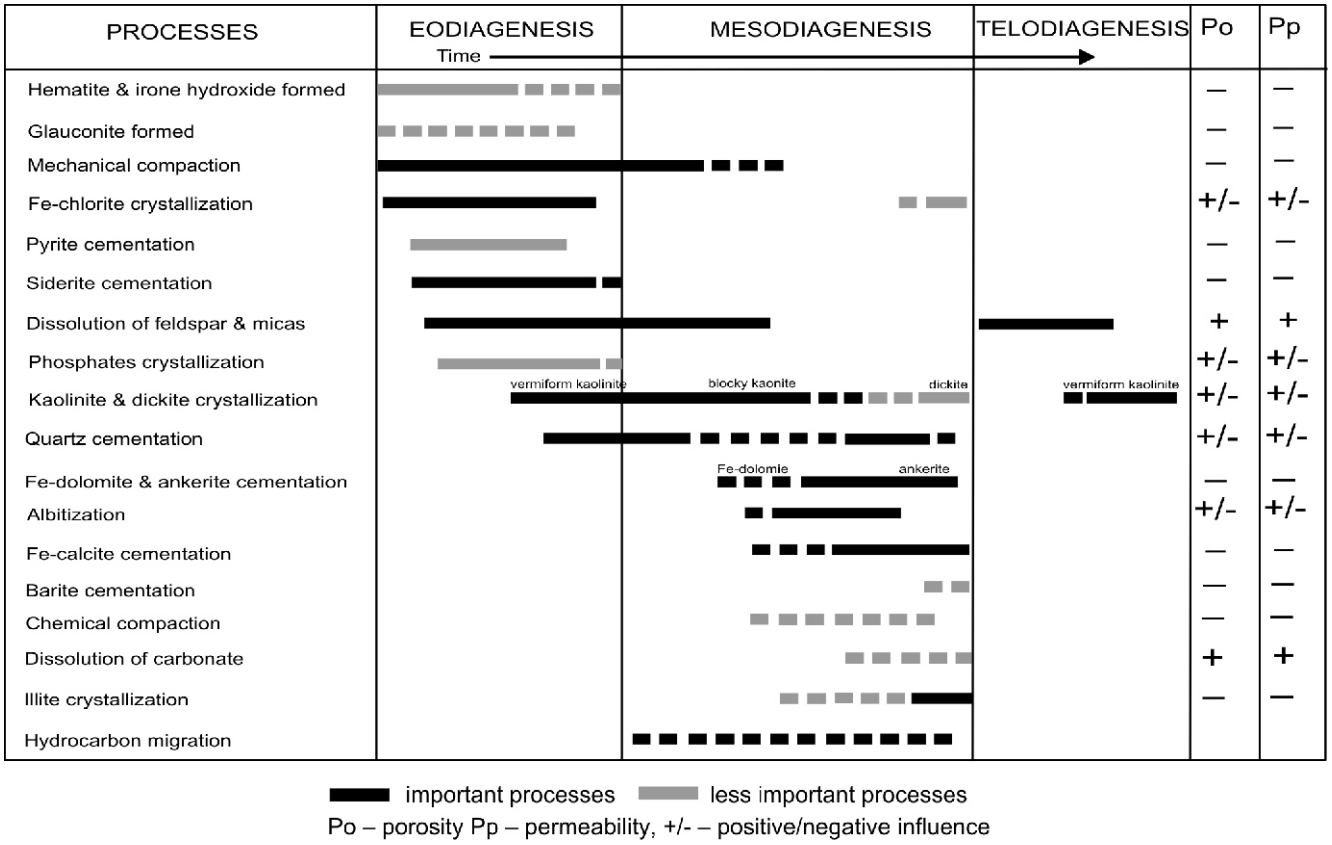

Fig. 18. Synoptic paragenetic sequence of the Carboniferous sandstones

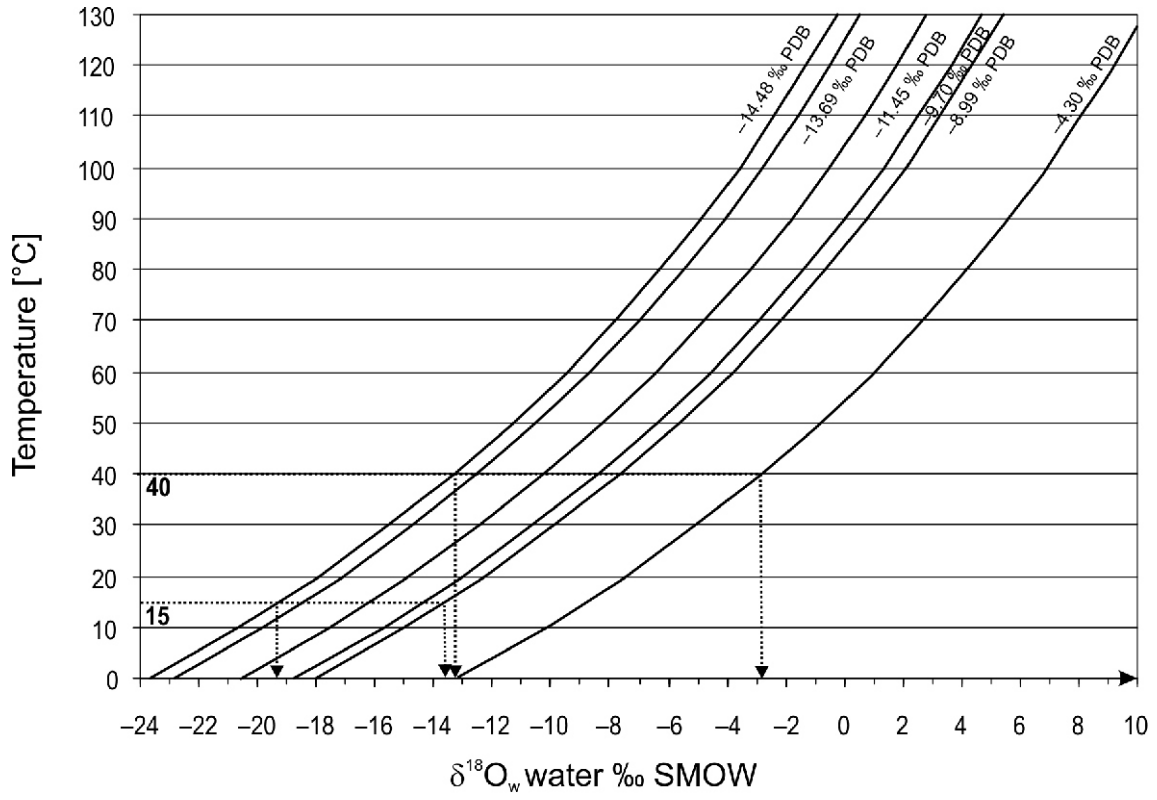

Fig. 19. Plot of ^{18}O pore water versus temperature for early siderite cement (Carothers et al., 1988)

and transformation of the organic matter, the pore waters were affected by acidification. Under such conditions, chlorite, siderite and sideroplesite, pyrite and glauconite precipitated.

Chlorites form rims on the mineral grains and the initial temperature of their formation is estimated at 20–40°C (Grigsby, 2001). Most probably Fe-chlorite precipitated as berthierine, which at the temperature of ~70°C is transformed into chamosite (Jahren and Aagaard, 1989). Locally Mg-chlorite occurs as rims or in pore spaces. The presence of Mg-chlorite whose origin is considered due to diagenetic chloritization of trioctahedral smectite preceded by an intermediate corrensite phase, is indicative of maximum palaeotemperatures >100°C (Środoń, 1996).

Early generations of sideroplesite and siderite have formed in such poorly oxidised environments as lakes and marshes on floodplains, at low concentrations of dissolved sulphates, in sediments rich in reactive minerals with a detectable iron content (Brown and Kingstone, 1993; Morad, 1998). The possible source of magnesium in the iron carbonates may have been detrital Mg-minerals such as biotite or some heavy minerals transformed due to infiltration of meteoric water into the pore space (i.a., Hawkins, 1978; Machemer and Hutcheon, 1988). On the other hand, the elevated Ca content in minerals can suggest a marine influence. Assuming the crystallization temperature of sideroplesite and siderite to be 15–40°C (Baker et al., 1995; Rezaee and Schulz-Rojahn, 1998) the ^{18}O value has been determined for the pore water from which this mineral had precipitated (Fig. 19). The obtained ^{18}O values fall into the range of ~–9.0 to –3.0‰SMOW. The majority of siderites and sideroplesites crystallized from pore water with a ^{18}O value <–10‰SMOW which indicates that the meteoritic water must have been strongly impoverished in ^{18}O.

Pyrite formed where the amount of H_2S produced by sulphate-reducing bacteria was higher than the amount of reduced iron (Postma, 1982; Pye et al., 1990). Its genesis can be related to sulphate ions derived from marine pore water (de Souza et al., 1995). The near-delta marine shelf provided conditions necessary for the formation of glauconite (Bolewski, 1982).

During the eodiagenesis, K-feldspar and mica grains were subjected to strong dissolution by meteoric water (Bjørlykke, 1989). Giles and de Boer (1990) consider this water to be slightly acid due to CO_2 dissolution and organic acids produced in the soil profile. Aluminum and silica ions released in these processes, in the acid environment, enabled crystallization of vermicular kaolinite (Osborne et al., 1994; Van Keer et al., 1998). The ^{18}O determinations for the vermicular kaolinite indicate that it crystallized from meteoric water impoverished in ^{18}O (Kozłowska, 2004, 2011).

At the end of eodiagenesis quartz overgrowths began to form. The principal sources providing silica for the quartz cement were both meteoritic pore waters containing silica and dissolution of feldspars and their transformation into kaolinite. The initial crystallization temperature of quartz is estimated at ~40°C (Kozłowska, 2004, 2009).

During mesodiagenesis, mechanical compaction and dissolution of K-feldspars continued along with the formation of authigenic quartz, which overgrew pore spaces and in places filled them completely, by the same token considerably reducing porosity. Examinations of homogenization temperatures of two-phase inclusions in the quartz cement point to crystallization within the 60–180°C range (Kozłowska, 2004; Kozłowska and Jarmołowicz-Szulc, 2009). An identical temperature range for quartz has been reported from many other depositional basins (Walderhaug, 1994). The source of silica for the quartz ce-

ment was the dissolution of detrital feldspar grains and their transformation into kaolinite, while at greater depths pressure dissolution of quartz grain contacts, illitization of kaolinite or replacement of quartz and feldspars by carbonates may have been key processes (Kozłowska, 2004).

The vermicular kaolinite was substituted by its blocky variety which originated during the dissolution-precipitation process (Ehrenberg et al., 1993; Beaufort et al., 1998; Hassouta et al., 1999). Moreover, part of the blocky kaolinite precipitated directly from pore solutions circulating in the sediment and containing aluminium and silica ions released during feldspar dissolution (McAulay et al., 1993). Macaulay et al. (1993) and Osborn et al. (1994) suggest that this mineral originated within the 50–80°C temperature range and isotopic results indicate that it crystallized from meteoritic water enriched in ^{18}O, as compared with the water from which the vermicular variety precipitated (Kozłowska, 2004, 2011).

The transformation of smectite into illite produced the illite/smectite mixed-layer mineral which is regarded as a paleothermometer. Dissolution and precipitation are responsible for the increase of illite content in the illite/smectite structure (Boles and Franks, 1979), particularly marked within the 60–80°C temperature range (Hartman et al., 1999). The mixed-layered illite/smectite has a >85% illite content and a highly ordered texture (R = 3 and R 3) which suggests that the temperature affecting the deposits examined was ~160°C (Środoń, 1996).

During mesodiagenesis, albitization of some plagioclases took place. Sodium necessary for the formation of authigenic albite was probably supplied by the dissolution of plagioclase (Strong and Milodowski, 1987; Morad et al., 1990) and transformation of smectite into illite (Aagaard et al., 1990). Albitization is the result of dissolution-replacement which occurred within the 75–100°C temperature range (Boles, 1982; Morad et al.,1990).

The very beginning of mesodiagenesis was accompanied by successive precipitation of carbonate cements: Fe-dolomite, ankerite, Fe-calcite and rhodochrosite. The crystallization temperature of Fe-dolomite and ankerite has been defined at 80–90°C (Kozłowska, 2004) on the basis of examinations of homogenization temperatures in fluid inclusions and of isotopic results. Assuming that the temperature of ankerite precipitation corresponds to the homogenization temperature of fluid inclusions in the 70–120°C range, the ^{18}O values for pore water have been estimated at –10 to –5‰SMOW. According to Boles and Franks (1979) the Mg^{2+}, Fe^{2+}, Mn^{2+} and Ca^{2+} cations for carbonates supplied during the late diagenetic stages could have come from transformation of detrital clay minerals (illite/smectite) caused by thermal alteration of clay sediments. De Souza et al. (1995) assume that the rhombohedral forms of dolomite and ankerite are indicative of crystallization from solution rather than replacement of an earlier carbonate cement e.g. calcite.

Fe-calcite crystallization succeeded that of authigenic quartz and ankerite cement and, as revealed by homogenization temperatures of fluid inclusions (Kozłowska, 2005; Kozłowska and Jarmołowicz-Szulc, 2009), occurred at 75–130°C. The dependence between the temperature of calcite formation and the ^{18}O value illustrated on the plot by Friedman and O'Neil (1977) shows that calcite precipitated from pore water with ^{18}O values falling in a wide range of –8 to 12‰SMOW (Fig. 20). Most probably, Ca needed for the formation of calcite was derived from solution and transformation of various kinds of plagioclases into albite or from local volcanoclastic components (Girard, 1998; Milliken, 1998; Morad, 1998). On the other hand, according to Boles and Frank (1979) and Hesse and Abid (1998) a potential source of calcium, and additionally of iron for calcite cementation in sandstones, can be the transformation of smectite into illite. Late generation calcite which crystallizes at 80–100°C has been described by Garcia et al. (1998), Girard (1998) and Schulz-Rojahn et al. (1998).

Isotopic oxygen analyses for ankerite and calcite revealed their crystallization from modified pore water of a composition corresponding to that of meteoritic water which, compared with early diagenetic siderite and sideroplesite, was enriched in ^{18}O. Such enrichment can result from water-sediment reactions during burial (Fisher and Land, 1986; Longstaffe and Ayalon, 1987). Locally, rhodochrosite precipitated and barite formed later or synchronously with carbonate cementation.

During mesodiagenesis mechanical compaction was replaced by chemical compaction and dissolution of carbonate cements commonly took place. The later generation of Fe-chlorite was formed in connection with kaolinite chloritization. This process can commence at temperatures between 90 and 100°C (Bjørlykke and Aagaard, 1992) and its intensity can depend on factors including the amount of iron and magnesium supplied by dissolution of carbonate cements (Hutcheon et al., 1980).

The last diagenetic stage consisted of transformation of kaolinite into dickite and of crystallization of fibrous illite. Dickite regarded as a potential palaeothermometer originated at a temperature of ~120°C (Ehrenberg et al.,1993). The formation of fibrous illite is connected mainly with the transformation of kaolinite and recrystallization of detrital clay minerals within the matrix (Amireh et al.,1994). Potassium needed for illite crystallization was released by dissolution of K-feldspars (Bjørlykke and Aagaard, 1992; Hassouta et al., 1999) and compaction of clay sediments (Burley and MacQuaker, 1992; Berger et al., 1997). With the progress of diagenesis the alkalinity of pore waters increased due to kaolinitization of K-feldspars and micas. Under conditions close to neutral, illitization of kaolinite took place (Kantorowicz, 1984; Van Keer et. al.,1998). Fibrous illite was the last mineral to crystallize in the Early Permian at a temperature which might have reached 160°C (Kozłowska, 2009, 2011).

During mesodiagenesis, migration of hydrocarbons might have been possible, as intense oil generation is known to take place at temperatures between 60 and 150°C (Hunt, 1979) and examinations of hydrocarbon inclusions from the NW part of the basin (the Stężyca area) have yielded the homogenization temperature to be ~60°C (Kozłowska, 2004). Such a conclusion is best corroborated by the presence of oil and gas fields in the Carboniferous found in the vicinity of Stężyca, Wilga, Minkowice and Świdnik (Fig. 1; Żywiecki et al., 1997; Helcel-Weil and Dzięgielowski, 2003; Helcel-Weil et al., 2007; Waksmundzka, 2008b, 2019).

Late Pennsylvanian–Jurassic/Createous uplift and erosion resulted in the telodiagenesis of Carboniferous deposits which were exposed to meteoric water. Feldspar dissolution and precipitation of vermiform kaolinite were the main telodiagenetic processes.

INFLUENCE OF DIAGENETIC PROCESSES ON SANDSTONE POROSITY

Compaction and cementation belong to those diagenetic processes which exerted the strongest influence on sandstone porosity, while dissolution, replacement and transformation played a less significant role.

Usually mechanical compaction markedly reduces primary porosity. The possible factors restricting its effect were the prevalence of hard grains over plastic ones and the formation of early rim cements (de Souza et al., 1995). Mechanical compaction accounts for a denser packing of the mineral framework,

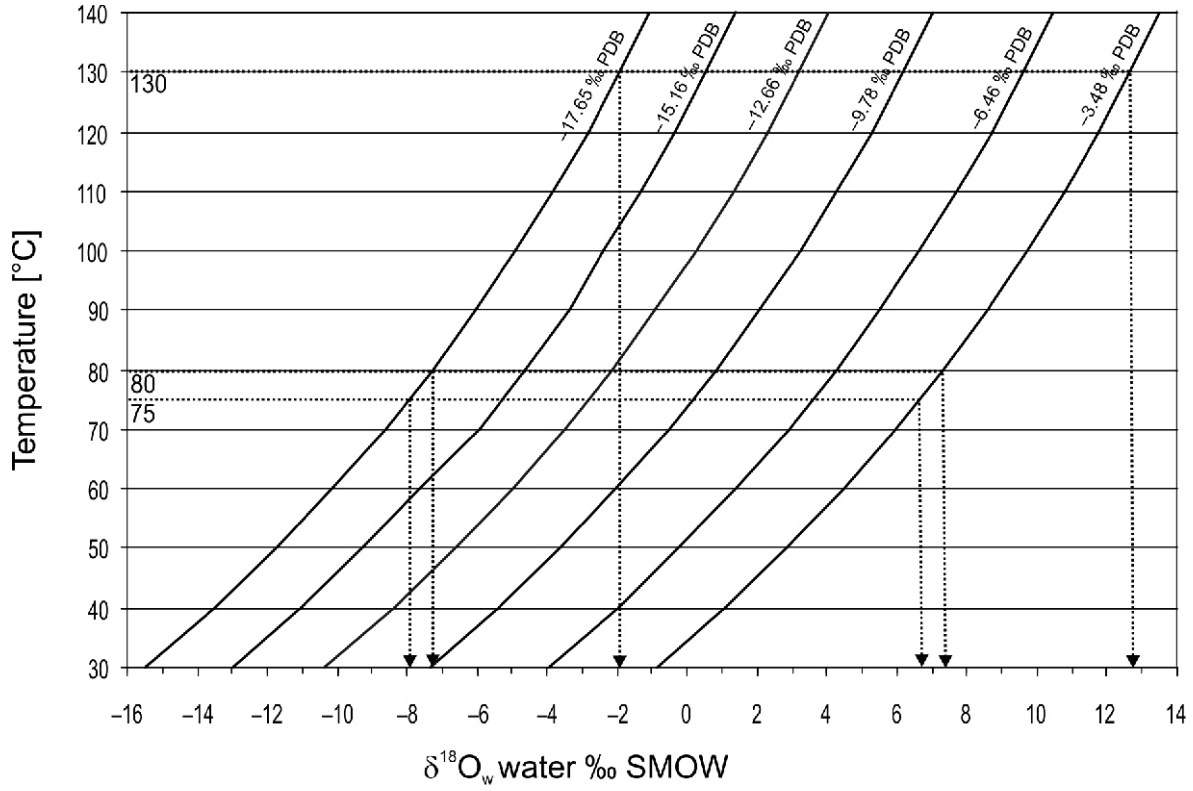

Fig. 20. Plot of ^{18}O pore water *versus* temperature for calcite cement (Friedman and O'Neil, 1977)

bending of micas and plastic rock fragments and fracturing of hard grains such as quartz and feldspars. Advanced mechanical compaction manifested by the rare presence of concave-convex contacts between the grains was of no notable significance in the lithification process, probably due mainly to early authigenic quartz cementation (Sommer, 1978). According to Ehrenberg (1989) primary porosity in the sandstones reduced compaction by ~55% on average (Fig. 21). In the Carboniferous sequences it varies from 35.7% (Marynin 1) to 67.7% (Terebin IG 4). A stronger compaction effect was noticed in the Bashkirian and Serpukhovian successions (~58%) and is much weaker (~41%) in the Tournaisian–Visean.

Cementation contributed to the reduced sandstone porosity. However, early cements forming rims on detrital grains such as Fe-chlorite, siderite, sideroplesite and quartz stiffened the sediment, thus impeding mechanical compaction (Kozłowska, 2004). As a result, part of the primary porosity in the Carboniferous sandstones may have been preserved (Fig. 14C). The later common development of cements, both in the form of growing quartz overgrowths or carbonates such as siderite, sideroplesite, ankerite and Fe-calcite filling pore spaces, had a negative effect on porosity. On the other hand, the kaolinite cement with visible microporosity between the grains may be only partly responsible for porosity reduction (Fig. 14B). Due to its local occurrence, the barite cement was of a negligible significance. Fibrous illite overgrowing inter- and intragranular as well as intracrystalline spaces (Fig. 15A) negatively influenced both porosity and permeability. It has been found that porosity decreases with an increase in carbonate cement amount, while most often the presence of authigenic quartz favourably affects porosity (Kozłowska, 2003). Occasionaly kaolinite cement, which precipitates in association with feldspar dissolution, can improve porosity.

The amount of primary porosity eliminated in the sandstone by cementation (Ehrenberg, 1989) is 38% on average (Fig. 21). Values obtained for these successions range from 18.4% (Terebin IG 4) to 57.8% (Marynin 1). More pronounced cementation resulting in ~56% porosity reduction has been observed

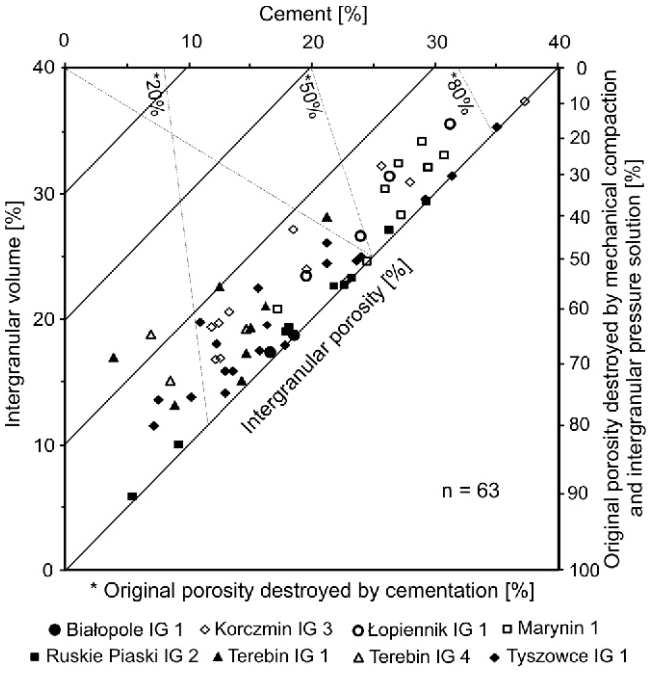

Fig. 21. Diagram modified from Houseknecht (1987) and Ehrenberg (1989) showing the effect of compaction and cementation on original porosity in the Carboniferous sandstones

in the Tournaisian–Visean, though is responsible for only 34% reduction in the Bashkirian and Serpukhovian.

The appearance of secondary porosity due to dissolution of grains and cements contributed to the growth of the total porosity in the sandstones. This process included both grains such as feldspars and lithoclasts (Fig. 14B) and cements, particularly ankerite and Fe-calcite. Dissolution is caused by acid meteoric waters, organic acids and CO_2 released during maturation of the organic matter (Meshri, 1986; Crossey et al., 1986; Bjørlykke, 1989).

Replacement could also have been responsible for the decrease in sandstone porosity. Most often feldspar and quartz grains, subordinately lithoclasts, though also the quartz (Fig. 14E) and kaolinite (Fig. 14H) cements have been replaced by carbonates. Locally the earlier carbonate is displaced by a younger one, while barite has only seldom replaced the carbonates.

Depending on the nature of its end product, transformation could either reduce or increase the porosity and permeability of the sandstones (Kozłowska, 2004). These processes included: kaolinization of micas and K-feldspars (Fig. 14B), chloritization of micas, K-feldspars and lithoclasts, as well as illitization of K-feldspars, lithoclasts and kaolinite. Locally plagioclases have been transformed into albite (Fig. 14A), kaolinite into illite, smectite into illite and kaolinite into dickite.

RESERVOIR QUALITY OF SANDSTONES

The sandstone reservoir quality is influenced by both depositional environment and diagenesis (i.a., Morad et al., 2000, 2012; Reed et al., 2005; Gaupp and Okkerman, 2011; Beyer et al., 2014).

The majority of the Carboniferous sandstones have been deposited in braided, meandering or anastomosing rivers, and by hyperconcentrated flows which filled incised valleys and belong to the LST. Several samples of sandstones deposited in deltaic mouth bars and distributary channels have been also examined.

Sandstones of river channels and hyperconcentrated flows represent a microlithofacies of quartz, subarkosic and sublithic from fine- to coarse-grained arenites. The main components of their cement are authigenic quartz together with a silty-clayey matrix. Additionally, kaolinite and carbonates (calcite, siderite, sideroplesite and ankerite) occur in varying amounts. Porosity ranges up to 15.1% (Terebin IG 1 – sequence 12) averaging ~8%. The highest porosity values have been found in Serpukhovian and Bashkirian sandstones from the following boreholes: Korczmin IG 3 – sequences 6, 9–11, Terebin IG 1 – sequences 9, 12, 13, Terebin IG 4 – sequence 12 and Tyszowce IG 1 – sequences 9–11, 14 (Tables 7 and 8; Fig. 2). Sandstones of sequences 9 and 11 have been deposited from hyperconcentrated flows, sequences 6, 10–13 in anastomosing, sequences 11–13 in meandering and sequence 10 in braided channels. But in the LST sequences 10–13 a vertical transition of environments is observed of higher- into lower energy ones e.g. of a braided or meandering river into an anastomosing fluvial system. Occasionally this phenomenon as preceded by the highest-energy hyperconcentrated flow.

In similar environments, reservoir sandstone lithosomes originated in the central and NW part of the Lublin Basin, where oil and gas fields as well as reservoir intervals are associated with sandstones of the following LST sequences: 6 (Świdnik field), 9 and 12 (Stężyca field), 12, 16, 17 (Wilga field; Fig. 1; Waksmundzka, 2008b, 2010a, 2019; Kombrink et al., 2010 see chapter 6.3.6). A possible hydrocarbon occurrence in the SE part of the Lublin Basin has been suggested by oil and gas shows (Żelichowski, 1969b; Miłaczewski, 1969; Łącka, 1987; Sieciarz, 2014) noted in sequences 3–7 (Visean–Serpukhovian) from the Komarów IG 1 borehole as well as in one or two sequences of this interval and also in sequence 8 (lowermost Bashkirian) in the Terebin IG 1, Terebin IG 4, Tyszowce IG 1 and Marynin 1 boreholes. Oil shows have been also described (Narecki, 1971) from sequences 12 and 16 (Bashkirian) from the Ruskie Piaski IG 2 section. Generally speaking, the amount of hydrocarbon shows increase from negligible in the

Table 8

Prospective reservoir quality of the Carboniferous succession in the southeastern Lublin Basin with reference to sequence stratigraphy and chronostratigraphy

Chronostratigraphy	Sequence stratigraphy	Prospectives of reservoir quality			
		Thickness =/> 10 m	Lateral continuation	Seal	Petrophysic Porosity >5% Permeability >1 mD
Bashkirian	16	+	+	+?	-
	15	+	+	+?	-
	14	+	+	+?	+
	13	+	+	+?	+
	12	+	+	+?	+
	11*	+	+	+	+
	10	+	–	+	+
	9	+	–	+	+
	8	–	–	–	–
Serpukhovian	7	+	–	+	–
	6	+	–	+	+
Visean	5	+	–	+	–
	4	+	–	+	–
Tournaisian–Visean	1–3	–	–	–	–

For explanation see Table 1; * for data regarding present thicknesses of the potential sandstone reservoir lithosomes of the LST and present summary thickness of the TST and HST of sequence 11 deposits see Figure 12

north to the most abundant in the south (Komarów IG 1 and Terebin IG 1).

Sandstones of the deltaic mouth bars and distributary channels belong to the microlithofacies of quartz-rich and subarkosic and local sublithic arenites from very fine-grained to medium-grained. These deposits are bound mainly by a silty-clayey matrix and by cements: carbonates (calcite, ankerite, siderite and sideroplesite), quartz, kaolinite and locally barite. Porosity can attain 9.1 vol.%, but is usually <3 vol.%. The highest porosity values have been found in sandstones of distributary channels of sequences 3 (Tyszowce IG 1) and 11 (Korczmin IG 3).

The reservoir qualities of sandstones are clearly controlled by the depositional environment, and their diagenetic history and burial. Fluvial sandstones show considerably better reservoir qualities than those deposited in the deltaic environment. A similar dependency has been recognized by Kozłowska (2009) in the Carboniferous sandstones of the central part of the basin (vicinity of Lublin). Pore space parameters were shaped during diagenesis. In the course of eodiagenesis, mechanical compaction has significantly reduced the porosity of the sandstones, but it had only a limited effect on those containing early cement rims (chlorite, quartz, siderite and sideroplesite) which stiffened the sediment leading to the partial preservation of primary porosity. It seems that during eodiagenesis, processes supporting primary porosity prevailed over those reducing porosity.

In the course of mesodiagenesis, however, processes reducing porosity predominated over those having a favourable effect. Also, secondary porosity in K-feldspar grains and in carbonate cement could have contributed to its growth. On the other hand a considerable reduction in porosity was caused by cementation with carbonates, mainly ankerite and Fe-calcite and crystallization of fibrous illite. Compared with cementation, compaction had a stronger effect on porosity reduction. Towards the base of the Carboniferous succession, there are clearly noticeable drops in mechanical compaction increases in cementation. In the Bashkirian and Serpukhovian sandstones, compaction usually prevailed over cementation, being 58 and 34%, respectively, while in the Tournaisian–Visean the situation is reversed. In the course of telodiagenesis, dissolution of feldspar may have enhanced the porosity that, however, may have been partially reduced due to precipitation of kaolinite.

The lowest porosity <5% occurs in the oldest lowermost buried part of the Carboniferous (Tournaisian–Visean).

CONCLUSIONS

1. In the SE part of the Lublin Basin the following depositional environments and processes have been reconstructed: shallow clayey and carbonate shelves, deltaic, fluvial and hyperconcentrated flow. The Carboniferous section is distinctive by its cyclic nature and the presence of various kinds of cyclothems such as fining-upward, coarsening-upward and non-gradational, each of them being equivalent to a respective parasequence.

2. 16 depositional sequences have been distinguished bounded by subaerial unconformities. The possible age of sequence 1 has been estimated at upper Tournaisian–middle Visean and of sequences 2 to the lower part of sequence 5 at upper Visean. Sequences 5–7 have been ascribed to the Serpukhovian, whereas 8–16 to the Bashkirian. As in other parts of the Lublin Basin, the presence of an intra-Carboniferous stratigraphic gap corresponding to the lower Bashkirian has been recognised. The Carboniferous top is, to a varying degree, affected by erosion.

3. Within the LST successions there are sandstone lithosomes laid down in braided and meandering rivers as well as anastomosing fluvial systems, with hyperconcentrated flows active in incised valleys. Sandstones are accompanied by claystones, mudstones, *Stigmaria* soils, and coals deposited on floodplains.

4. LST sequences 4–7 and 9–10 comprise channel sandstone lithosomes of promising thicknesses of 12–33 m but with small lateral and discontinuous extent, but in sequences 11–16 lithosomes of promising thicknesses of 15–40 m have a continuous lateral extent on the scale of km.

5. TST and HST sequences 1–3 originated in a marine-deltaic environment. Deposits of deltaic and shallow clayey and carbonate shelves predominate. In TST and HST sequences 4–16 deposits of deltaic provenance are most frequent, while above sequence 10 the growing share of delta plain deposits indicates a longer duration of continental deposition.

6. TST and HST sequences 4–11 represented by claystones and siltstones are distinctive by large thicknesses reaching up to 20–200 m and good sealing of sandstones of LST sequences 4–7 and 9–11 (excluding those from the Komarów IG 1 borehole). In sequences 12–16 the TST and HST deposits are thinner (~ten to several tens of metres) which locally can provide a sealing effect. Factors responsible for the deterioration of sealing quality are the proximity of the Carboniferous top being a major erosional surface and the wedging out of sandstone lithosomes under the Mesozoic overburden.

7. Three stages have been distinguished in the diagenetic history of the Carboniferous sandstones: eo-, meso- and telodiagenesis. The major eodiagenetic processes are as follows: mechanical compaction, dissolution of feldspar grains and mica flakes, the formation of early chlorite rims, siderite and sideroplesite, quartz overgrowths, and the precipitation of vermiform kaolinite. During mesodiagenesis the mechanical compaction transformed into chemical change where feldspar grains continued to be dissolved along with additional dissolution of cements. The most significant cements were found to be quartz, kaolinite, dickite, carbonates (ankerite and Fe-calcite) and fibrous illite. The effects of telodiagenetic precesses were feldspar dissolution and precipitation of kaolinite.

8. As indicated by the values of the reflectivity index for vitrinite, the presence of dickite and of fibrous illite coupled with homogenization temperatures of fluid inclusions in cements, the maximum temperature affecting the Carboniferous deposits during diagenesis was ~120°C.

9. Some Carboniferous sandstones have a good porosity attaining 15.1% and averaging ~8%. Primary and secondary porosity has been distinguished – the former of an intergranular nature, the latter formed due to dissolution of feldspar grains and cements. Compaction and cementation are the two major factors reducing porosity by ~55 and 38%, respectively. The effect of compaction on porosity decreases with depth, whereas cementation becomes more and more effective. One of the significant diagenetic processes is also dissolution responsible for the formation of secondary porosity.

10. The good porosity of the Carboniferous sandstones is due to: precipitation of early rim cements which hindered mechanical compaction and to the formation of secondary porosity. The major factors which contributed to the reduction of porosity of some sandstones are mechanical compaction, strong cementation with quartz and carbonates, predominantly with ankerite and Fe-calcite, but also crystallization of fibrous illite.

11. The Carboniferous sandstones are distinctive by their variable reservoir qualities. As compared with the delta deposits, the fluvial sandstones show better reservoir properties. The highest porosity values have been found in Serpukhovian and Bashkirian sandstones of sequences 6, 9–14 in boreholes situated farthest to the SE. Sandstones of sequences 9 and 11 have been deposited by hyperconcentrated flow, of sequences 6 and 10–13 in anastomosing channels, of sequences 11–13 in meandering and those of sequence 10 in braided rivers.

12. This integrated analysis has revealed that sandstone lithosomes of sequences 11 have a good reservoir potential, those of sequences 6, 9, 10, 12–14 a fair one, while the remaining sequences are poor. Factors reducing the reservoir potential are: a limited lateral extent, a smaller thickness of sealing intervals, the proximity of the Carboniferous top which is also a significant erosional surface and, finally, the wedging out of sandstone lithosomes under the Mesozoic overburden.

Acknowledgements. This paper is a part of the project No. N307 031 31/2521 financed by the Ministry of Science and Higher Education and No. 61.2901.0702.00.0 of the Polish Geological Institute-National Research Institute. The authors are grateful to the reviewers Prof. R. Gaupp and L. Leśniak for their suggestions and comments that improved this paper. The authors thank K. Jarmołowicz-Szulc for fluid inclusion studies. XRD analysis was performed by W. Narkiewicz and the SEM and EDS examination by L. Giro. IR analysis was made by the team of Prof. M. Michalik at the Jagiellonian University in Krakow. Isotope analyses were conducted by the team of Prof. S. Hałas at the Maria Curie-Skłodowska University in Lublin. The team of Prof. P. Such at the Oil and Gas Institute-National Research Institute in Krakow carried out the petrophysical studies. We are deeply indebted to W. Mizerski for encouraging us to write this paper.

REFERENCES

Aagaard, P., Egeberg, P.K., Saigal, G.C., Morad, S., Bjørlykke, K., 1990. Diagenetic albitization of detrital K-feldspars in Jurassic, Lower Cretaceous and Tertiary clastic reservoir rocks from offshore Norway, II. Formation water chemistry and kinetic considerations. Journal of Sedimentary Petrology, **60**: 575–581.

Al-Aasm, I.S., Taylor, B.E., South, B., 1990. Stable isotope analysis of multiple carbonate samples using selective acid extraction. Chemical Geology, **80**: 119–125.

Allen, J.R.L., 1963. Henry Clifton Sorby and the sedimentary structures of sands and sandstones in relation to flow conditions. Geologie en Mijnbouw, **42**: 223–228.

Allen, J.R.L., 1964. Studies in fluviatile sedimentation: six cyclothems from the Lower Old Red Sandstone, Anglo-Welsh Basin. Sedimentology, **3**: 163–198.

Allen, J.R.L., 1965. Finning-upwards cycles in alluvial successions. Liverpool and Manchester Geological Journal, **4**: 229–246.

Allen, J.R.L., 1970. Studies in fluvialite sedimentation: a comparision of fining-upwards cyclothems, with special reference to coarse-member composition and interpretation. Journal of Sedimentary Petrology, **40**: 298–323.

Amireh, B.S., Schneider, W., Abed, A.M., 1994. Diagenesis and burial history of the Cambrian-Cretaceous sandstone series in Jordan. Neues Jahrbuch für Geologie und Palaöntologie Abhandlungen, **192**: 151–181.

Arnott, R.W.C, Hand, B.M., 1989. Bedforms, primary structures and grain fabric in the presence of suspended sediment rain. Journal of Sedimentary Petrology, **59**: 1062–1069.

Baker, J.C., Kassan, J., Hamilton, P.J., 1995. Early diagenetic siderite as indicator of depositional environment in the Triassic Rewan Group, Southern Bowen basin, eastern Australia. Sedimentology, **43**: 77–88.

Baldwin, B., Butler, C.O., 1985. Compaction curves. AAPG Bulletin, **69**: 622–626.

Beaufort, D., Cassagrabere, A., Petit, S., Lanson, B., Berger, G., Lacharpagne J.C., Johansen, H., 1998. Kaolinite-to-dickite reaction in sandstone reservoirs. Clay Minerals, **33**: 237–316.

Berger, G., Lacharpagne, J.C., Velde, B., Beaufort, D., Lanson, B., 1997. Kinetic constrains on illitization reaction and the effect of organic diagenesis in sandstone/shale sequences. Applied Geochemistry, **12**: 23–35.

Beyer, D., Kunkel, C., Aehnelt, M., Pudlo, D., Voigt, T., Nover, G., Gaupp, R., 2014. Influence of depositional environment and diagenesis on petrophysical properties of clastic sediments (Buntsandstein of the Thuringian Syncline, Central Germany). Zeitschrift der deutschen Gesellschaft für Geowissenschaften, **165**: 345–365.

Bjørlykke, K., 1989. Sedimentology and Petroleum Geology. Springer, Berlin.

Bjørlykke, K., Aagaard, P., 1992. Clay minerals in North Sea sandstones. SEPM Special Publication, **47**: 65–80.

Blakey, R.C., Gubitosa, R., 1984. Controls of sandstone body geometry and architecture in the Chinle Formation (Upper Triassic), Colorado Plateau. Sedimentary Geology, **38**: 51–86.

Boles, J.R., 1982. Active albitization of plagioclase, Gulf Coast Tertiary. American Journal of Science, **282**: 165–180.

Boles, J.R., Franks, S.G., 1979. Clay diagenesis in Wilcox sandstones of Southwest Texas: implications of smectite diagenesis on sandstones cementation. Journal of Sedimentary Petrology, **49**: 55–70.

Bolewski, A., 1982. Mineralogia szczegółowa (in Polish). Wyd. Geol., Warszawa.

Briand, C., Izart, A., Vaslet, D., Vachard, D., Makhlina, M., Goreva, N., Isakova, T., Kossovaya, O., Jaroshenko, A., 1998. Stratigraphy and sequence stratigraphy of the Moscovian, Kasimovian and Gzhelian in the Moscow Basin. Bulletin de la Société Géologique de France, **169**: 35–52.

Bridge, J.S., Gordon, E.A., 1985. Quantitative interpretation of ancient river systems in the Oeonta Fm., Catskill Magnafaces. GSA Special Papers, **201**: 163–181.

Browne, G.H., Kingston, D.M., 1993. Early diagenetic spherulitic siderites from Pennsylvanian palaeosols in the Boss Point Formation, Maritime Canada. Sedimentology, **40**: 467–474.

Burley, S.D., MacQuaker, J.H.S., 1992. Authigenic clays, diagenetic sequences and conceptual diagenetic models in contrasting basin-margin and basin-center North Sea Jurassic sandstones and mudstones. SEPM Special Publication, **47**: 81–110.

Cant, D.J., Walker, R.G., 1978. Fluvial processes and facies sequences in the sandy braided South Saskatchewan River, Canada. Sedimentology, **25**: 625–648.

Carothers, W.W., Adami, L.H., Rosenbauer, R.J., 1988. Experimental oxygen isotope fractional between siderite-water and phosphoric acid liberated CO_2 – siderite. Geochimica et Cosmochimica Acta, **52**: 2445–2450.

Chabiera, A., 1997a. Analiza właściwości zbiornikowych utworów karbonu w obrębie struktury Stężycy (in Polish). Mat. Konf. XXX lat działalności geologicznej Oddziału Poszukiwania Nafty i Gazu w Wołominie, Pułtusk: 29–34.

Chabiera, A., 1997b. Wpływ środowiska depozycyjnego i procesów diagenetycznych na właściwości zbiornikowe utworów karbonu w obrębie struktury Stężyca (in Polish). Mat. Konfer. VI Krajowe Spotkanie Sedymentologów, Lewin Kłodzki: 1–3.

Coleman, J.M., 1988. Dynamic changes and processes in the Mississippi River delta. GSA Bulletin, **100**: 999–1015.

Coleman, J.M., Wright, L.D., 1975. Modern river deltas: variability of processes and sand bodies. In: Deltas, Models for Exploration (ed. M.L. Broussard): 99–150. Houston Geological Society.

Collinson, J.D., 1988. Controls on Namurian sedimentation in the Central Province basins of northern England. In: Sedimentation in a Synorogenic Basin Complex the Upper Carboniferous of North-west Europe (eds. B.M. Besly and G. Kelling): 85–101.

Crossey, L.J., Surdam, R.C., Lahann, R., 1986. Application of organic/inorganic diagenesis to porosity prediction. SEPM Special Publication, **38**: 147–156.

Davies, S.J., McLean, D., 1996. Spectral gamma-ray and palynological characteryzation of Kinderscoutian marine bands in the Namurian of the Pennine Basin. Proceedings of the Yorkshire Geological Society, **51**: 1–35.

Davydov, V.I., Korn, D., Schmitz, M.D., 2012. The Carbonifeous Period. In: The Geologic Time Scale (eds. F.M. Gradstein, J.G. Ogg, M.D. Schmitz and G.M. Ogg): 603–651. Elsevier, Amsterdam.

De Souza, R.S., De Ros, L.F., Morad, S., 1995. Dolomite diagenesis and porosity preservation in lithic reservoirs: Carmópolis Member, Sergipe – Alagoas Basin, Northeastern Brazil. AAPG Bulletin, **79**: 725–748.

Durakiewicz, T., Hałas, S., 1994. Triple collector system for isotope ratio mass spectrometer. IF UMCS Scientific Report 1994: 131–132.

Elliot, T., 1974. Interdistributary bay sequence and their genesis. Sedimentology, **21**: 611–622.

Elliot, T., 1975. The sedimentary history of a delta lobe from a Yoredale (Carboniferous) cyclothem. Proceedings of the Yorkshire Geological Society, **40**: 505–536.

Elliot, T., 1976a. Sedimentary sequences from the Upper Limestone Group of Northumberland. Scottish Journal of Geology, **12**: 115–124.

Elliot, T., 1976b. Upper Carboniferous sedimentary cycles produced by river-dominated, elongate deltas. Journal of the Geological Society, **132**: 199–208.

Elliot, T., 1978. Deltas. In: Sedimentary Environments and Facies (ed. H.G. Reading): 97–142. Oxford, Blackwell Scientific Publications.

Ehrenberg, S.N., 1989. Assessing the relative importance of compaction processes and cementation to reduction of porosity in sadndtones: discussion; Compaction and porosity evolution of Pliocene sandstones, Ventura Basin, California: discussion. AAPG Bulletin, **73**: 1274–1276.

Ehrenberg, S.N., Aagaard, P., Wilson, M.J., Fraser, A.R., Duthie, D.M.L., 1993. Depth-dependent transformation of kaolinite to dickite in sandstones of the Norwegian Continental Shelf. Clay Minerals, **28**: 325–352.

Fisher, R.S., Land, L.S., 1986. Diagenetic history of Eocene Wilcox sandstones, South-Central Texas. Geochimica et Cosmochimica Acta, **50**: 551–561.

Fisher, W.L., Brown, L.F., Jr., Scott, A.J., McGowen, J.H., 1969. Delta systems in the exploration for oil and gas. Texas Bureau of Economic Geology, **78**.

Flügel, E., 2004. Microfacies of Carbonate Rocks Analysis, Interpretation and Application. Springer.

Friedman I., O'Neil J., 1977. Compilation of stable isotope fractionation factors of geochemical interest. U. S. Geological Survey, Professional Paper, **440-K**: 1–12.

Garcia, A.J.V., Morad, S., De Ros, L.F., Al-Aasm, I.S., 1998. Palaeogeographical, palaeoclimatic and burial history controls on the diagenetic evolution of reservoir sandstones: evidence from the Lower Cretaceous Sevraria sandstones on the Sergipe – Alagoas basin, NE Brazil. IAS Special Publication, **26**: 107–140.

Gaupp, R., Okkerman, J.A., 2011. Diagenesis and reservoir quality of Rotliegend sandstones in the Northern Netherlands – a review. SEPM Special Publication, **98**: 193–226.

Giles, M.R., de Boer, R.B., 1990. Origin and significance of redistributional secondary porosity. Marine and Petroleum Geology, **7**: 378–397.

Girard, J.P., 1998. Carbonate cementation in the Middle Jurassic Oseberg reservoir sandstone Oseberg field, Norway: a case of deep burial – high temperature poikilotopic calcite. IAS Special Publication, **26**: 285–307.

Goldstein, R.H., Reynolds, T.J., 1994. Systematics of fluid inclusions in diagenetic minerals. SEPM Short Course, **31**.

Gradziński, R., 1973. Wyróżnianie i klasyfikacja kopalnych osadów rzecznych (in Polish). Postępy Nauk Geologicznych, **5**: 57–112.

Gradziński, R., Kostecka, A., Radomski, A, Unrug, R., 1986. Zarys sedymentologii (in Polish). Wyd. Geol., Warszawa.

Gradziński, R., Doktor, M., Słomka, T., 1995. Depositional environments of the coal-bearing Cracow Sandstone Series (upper Westphalian), Upper Silesia, Poland. Studia Geologica Polonica, **108**: 149–170.

Gradziński, R., Baryła, J., Danowski, W., Doktor, M., Gmur, D., Gradziński, M., Kędzior, A., Paszkowski, M., Soja, R., Zieliński, T., Żurek, S., 2000. Anastomosing system of the upper Narew River, NW Poland. Annales Societatis Geologorum Poloniae, **70**: 219–229.

Gradziński, R., Baryła, J., Doktor, M., Gmur, D., Gradziński, M., Kędzior, A., Paszkowski, M., Soja, R., Zieliński, T., Żurek, S., 2003. Vegetation-controlled modern anastomosing system of the upper Narew River (NW Poland) and its sediments. Sedimentary Geology, **157**: 253–276.

Grigsby, J.D., 2001. Origin and growth mechanism of authigenic chlorite in sandstones of the Lower Vickburg Formation, South Texas. Journal of Sedimentary Research, **71**: 27–36.

Grotek, I., 2005. Alteration of the coalification degree of the organic matter dispersed in the Carboniferous sediments along border of the East-European craton in Poland (in Polish with English summary). Biuletyn Państwowego Instytutu Geologicznego, **413**: 5–80.

Grotek, I., 2008. Charakterystyka petrologiczna oraz dojrzałość termiczna rozproszonej materii organicznej (in Polish with English summary). Profile Głębokich Otworów Wiertniczych Państwowego Instytutu Geologicznego, **123**: 176–185.

Hałas, S., 1979. An automatic inlet system with pneumatic changeover valves for isotope ratio mass spectrometer. Journal of Physics E: Scientific Instruments, **18**: 417–420.

Hampson, G., 1995. Discrimination of regionally extensive coals in the Upper Carboniferous of the Pennine Basin, UK using high resolution sequence stratigraphic concepts. Geological Society Special Publications, **82**: 79–97.

Hampson, G., Stollhofen, H., Flint, S., 1999. A sequence stratigraphic model for the Lower Coal Measures (Upper Carboniferous) of the Ruhr district, north-west Germany. Sedimentology, **46**: 1199–1231.

Hartmann, B.H., Juhász-Bodnár, K., Ramseyer, K., Matter, A., 1999. Effect of Permo-Carboniferous climate on illite-smectite, Haushi Group, Sultanate of Oman. Clays and Clay Minerals, **47**: 131–143.

Hassouta, L., Bautier, M.D., Potolevin, J.L., Liewig, N., 1999. Clay diagenesis in the sandstone reservoir of the Ellon Field (Alwyn) North Sea. Clays and Clay Minerals, **47**: 269–585.

Hawkins, P.J., 1978. Relationship between diagenesis, porosity reduction, and oil emplacement in late Carboniferous sandstones reservoirs, Bothamsall Oilfield, E Midlands. Journal of the Geological Society, **135**: 7–24.

Helcel-Weil, M., Dzięgielowski, J., 2003. Lublin Basin – petroleum prospecting results and their importance for future exploration (in Polish with English summary). Przegląd Geologiczny, **51**: 764–770.

Helcel-Weil, M., Dzięgielowski, J., Florek, R., Maksym, A., Słyś, M., 2007. The Lublin Basin: petroleum exploration results and their importance for future prospects (in Polish with English

summary). Biuletyn Państwowego Instytutu Geologicznego, **422**: 51–62.

Hesse, R., Abid, I. A., 1998. Carbonate cementation – the key to reservoir properties of four sandstone levels (Cretaceous) in the Hiberian Oilfield Jeanne d'Arc Basin, Newfoundland, Canada. IAS Special Publication, **26**: 363–393.

Houseknecht, D.W., 1987. Assessing the relative importance of compaction processes and cementation to reduction of porosity in sandstones. AAPG Bulletin, **71**: 633–642.

Hunt, J.M., 1979. Petroleum Geochemistry and Geology. W.H. Freeman and Company, San Francisco.

Hutcheon, I., Oldershaw, A., Ghent, E.D., 1980. Diagenesis of Cretaceous sandstones of the Kootenay Formation at Elk Valley (southestern British Columbia) and Mt Allan (southwestern Alberta). Geochimica et Cosmochimica Acta, **44**: 1425–1435.

Izart, A., Le Nindre, Y., Stephenson, R., Vaslet, D., Stovba, S., 2003a. Quantification of the control of sequences by tectonics and eustacy in the Donets Basin and on the Russian Platform during Carboniferous and Permian. Bulletin de la Société Géologique de France, **174**: 93–100.

Izart, A., Stephenson, R., Vai, G.B., Vachard, D., Le Nindre, Y., Vaslet, D., Fauvel, P.J., Süss, P., Kossovaya, O., Chen, Z., Maslo, A., Stovba, S., 2003b. Sequence stratigraphy and Correlation of the Late Carboniferous and Permian in CIS, Europe, Tethyan area, North Africa, China, Gondwanaland and USA. Palaeogeography, Palaeoclimatology, Palaeoecology, **196**: 59–84.

Jahren, J.S., Aagaard, P., 1989. Compositional variations in diagenetic chlorites and illites and relationships with formation-water chemistry. Clay Minerals, **24**: 157–170.

Jackson, R.G. II, 1978. Preliminary evaluation of lithofacies models for meandering alluvial streams. Canadian Society of Petroleum Geologists Memoir, **5**: 543–576.

Jaworowski, K., 1987. Kanon petrograficzny najczęstszych skał osadowych (in Polish). Przegląd Geologiczny, **35**: 205–209.

Jaworowski, K., Juskowiak, M., 1973. Metoda punktowa analizy geometrycznej na tle podstawowych zagadnień opisu skał (in Polish). Instrukcje i metody badań geologicznych, **22**. Wyd. Geol., Warszawa.

Jenyon, M.K., 1990. Oil and Gas Traps. Aspects of their seismostratigraphy, morphology and development. John Wiley and Sons.

Kaczyński,J. 1984. Perspectives of search for oil and gas in the Lublin region (in Polish with English summary). Przegląd Geologiczny, **32**: 330–333.

Kantorowicz, J.D., 1984. The nature, origin and distribution of authigenic clay minerals from Middle Jurassic Ravenscar and Brent Group sandstones. Clay Minerals, **19**: 359–375.

Kombrink, H., Besly, B.M., Collinson, J.D., den Hartog Jager, D.G., Drozdzewski, G., Dusar, M., Hoth, P., Pagnier, H.J.M., Stemmerik, L., Waksmundzka, M.I., Wrede, V., 2010. Carboniferous. In: Petroleum Geological Atlas of the Southern Permian Basin Area (eds. J.C. Doornenbal and A.G. Stevenson): 81–99. EAGE Publications, Houten.

Kozłowska, A., 1997. Carbonate cements of the Carboniferous sandstones in NW part of the Lublin Graben (eastern Poland) (in Polish with English summary). Przegląd Geologiczny, **45**: 301–304.

Kozłowska, A., 2001. Syderyty magnezowe w piaskowcach górnokarbońskich środkowej Polski (in Polish). Przegląd Geologiczny, **49**: 343–344.

Kozłowska A., 2003. The influence of diagenesis on the reservoir quality of the Upper Carboniferous sandstones in the region between Warsaw and Dęblin (central Poland) (in Polish with English summary). Przegląd Geologiczny, **51**: 777–782.

Kozłowska, A., 2004. Diagenesis of the Upper Carboniferous sandstones occurring at the border of the Lublin Trough and the Warsaw Block (in Polish with English summary). Biuletyn Państwowego Instytutu Geologicznego, **411**: 5–70.

Kozłowska, A., 2005. Charakterystyka petrologiczna a ewolucja właściwości zbiornikowych utworów karbonu (in Polish). In: Budowa geologiczna i system naftowy rowu lubelskiego (ed. M. Narkiewicz). PIG, NAG, Nr. 856/2006, Warszawa.

Kozłowska, A., 2007. Wyniki badań petrograficznych (in Polish with English summary). Profile Głębokich Otworów Wiertniczych Państwowego Instytutu Geologicznego, **119**: 126–134.

Kozłowska, A., 2009. Diagenetic processes affecting pore space in Carboniferous sandstones of the Lublin region (in Polish with English summary). Przegląd Geologiczny, **57**: 335–342.

Kozłowska, A., 2011. Clay minerals in the Carboniferous sandstones of the southeastern part of the Lublin Basin as paleotemperature indicators of diagenesis (in Polish with English summary). Biuletyn Państwowego Instytutu Geologicznego, **444**: 99–112.

Kozłowska, A., Jarmołowicz-Szulc, K., 2009. Geochemical and mineralogical exploration of sandstones in the Lublin Carboniferous Basin, SE Poland. Proceedings of the 24th IAGS, Fredericton, Kanada, **1**: 365–368.

Kozłowska, A., Such, P., Kobyłecka, A., 1998. Evolution of pore space in the Carboniferous deposits of the Radom-Lublin area basing on selected boreholes (in Polish with English summary). Prace Państwowego Instytutu Geologicznego, **165**: 167–176.

Krzywiec, P., 2009. Devonian-Cretaceous repeated subsidence and uplift along the Teisseyre-Tornquist zone in the SE Poland-Insight from seismic data interpretation. Tectonophysics, **475**: 142–159.

Krzywiec, P., Mazur, S., Gągała, Ł., Kufrasa, M., Lewandowski, M., Malinowski, M., Buffenmyer, V., 2017. Late Carboniferous thin-skinned compressional deformation above the SW Edge of the East European craton as revealed by seismic reflection and potential field data – correlation with the Variscides and the Appalachians. GSA Memoir, **213**: 353–372.

Kufrasa, M., Stypa, A., Krzywiec, P., Słonka, Ł., 2019. Late Carboniferous thin-skinned deformation in the Lublin Basin, SE Poland: results of combined seismic data interpretation, structural restoration and subsidence analysis. Annales Societatis Geologorum Poloniae, **89**: 175–194.

Leeder, M.R., Strudwick, A.E., 1987. Delta-marine interactions: a discussion of sedimentary models for Yoredale-type cyclicity in the Dinantian of Northern England. In: European Dinantian Environments (eds. J. Miller, A.E. Adams and V.P. Wright): 115–130.

Levorsen, A.I., 1967. Geology of Petroleum. Freeman and Comp., San Francisco.

Longstaffe, F.J., Ayalon, A., 1987. Oxygen-isotope studies of clastic diagenesis in the Lower Cretaceous Viking Formation, Alberta: implications for the role of meteoric water. Geological Society Special Publications, **36**: 277–296.

London, D., 1992. Phosphorous in S-type magma: the P_2O_5 content of feldspar from peraluminous granites, pegmatites, and rhyolites. American Mineralogist, **77**: 1–2.

Łącka, M., 1987. Dokumentacja wynikowa odwiertu poszukiwawczego: Marynin 1. PIG, NAG, Nr. 130291, Warszawa.

Macaulay, C.I., Fallick, A.E., Haszeldine, R.S., 1993. Textural and isotopic variations in diagenetic kaolinite from the Magnus Oilfield sandstones. Clay Minerals, **28**: 625–639.

Machemer, S.D., Hutcheon, J., 1988. Geochemistry of early cements in the Cardium formation, Central Alberta. Journal of Sedimentary Petrology, **58**: 136–147.

Makaske, B., 2001. Anastomosing rivers: a review of their classification, origin and sedimentary products. Earth-Science Reviews, **53**: 149–196.

Martinsen, O.J., 1994. Evolution of an incised-valley fill, the Pine Ridge Sandstone of Southeastern Wyoming, U. S. A.: systematic sedimentary response to relative sea-level change. SEPM Special Publication, **51**: 109–128.

Martinsen, O.J., Collinson, J.D., Holdsworth, B.K., 1995. Millstone Grit cyclicity revisited, II: Sequence stratigraphy and sedimentary responses to changes of relative sea-level. IAS Special Publication, **22**: 305–327.

Maynard, J.R., Leeder, M.R., 1992. On the periodicity and magnitude of Late Carboniferous glacio-eustatic sea-level changes. Journal of the Geological Society, **149**: 303–311.

McAulay, G.E., Burley, S.D., Johnes, L.H., 1993. Silicate mineral authigenesis in the Hutton and NW Hutton fields: implications for sub-surface porosity development. In: Petroleum Geology of North-west Europe: Proceeding of the 4th Conference (ed J.R. Parker): 1377–1394. Geological Society, London.

McCrea, J.M., 1950. On the isotopic geochemistry of carbonates and a paleotemperature scale. Journal of Chemical Physics, **18**: 849–857.

Meshri, I.D., 1986. On the reactivity of carbonic and organic acids and generation of secondary porosity. SEPM Special Publication, **38**: 123–128.

Miall, A.D., 1977. A review of the braided-river depositional environment. Earth-Science Reviews, **13**: 1–62.

Miall, A.D., 1978. Lithofacies types and vertical profile models in braided river deposits: a summary. Canadian Society of Petroleum Geologists Memoir, **5**: 597–604.

Miall, A.D., 1985. Architectural-element analysis: a new method of facies analysis applied to fluvial deposits. Earth-Science Reviews, **22**: 261–308.

Miall, A.D., 1988. Architectural elements and bounding surfaces in fluvial deposits: anatomy of the Kayenta Formation (Lower Jurassic), south-west Colorado. Sedimentary Geology, **55**: 233–262.

Miall, A.D., 1996. The Geology of Fluvial Deposits Sedimentary Facies, Basin Analysis, and Petroleum Geology. Springer-Verlag.

Michum, Jr. R.M., 1977. Seismic stratigraphy and global changes of sea level, Part 1: Glossary of terms used in seismic stratigraphy. AAPG Memoir, **26**: 205–212.

Milliken, K.L., 1998. Carbonate diagenesis in non-marine foreland sandstones at the western edge of the Alleghanian overthrust belt, Southern Appalachians. IAS Special Publication, **26**: 87–105.

Miłaczewski, L., 1969. Dokumentacja wynikowa otworu wiertniczego Terebin IG 4. PIG, NAG, Nr. 93595, Warszawa.

Moody-Stuart, M., 1966. High- and low-sinuosity stream deposits, with examples from the Devonian of Spitsbergen. Journal of Sedimentary Petrology, **36**: 1102–1117.

Moore, D.M., Reynolds, R.C. Jr., 1989. X-Ray Diffraction and Identification and Analysis of Clay Minerals. Oxford University Press.

Morad, S., 1990. Mica alteration reactions in Jurassic reservoir sandstones from the Haltenbanken area, offshore Norway. Clay and Clays Minerals, **38**: 584–590.

Morad, S., 1998. Carbonate cementation in sandstones: distribution patterns and geochemical evolution. IAS Special Publication, **26**: 1–26.

Morad, S., Bergan, M., Knarud, R., Nystuen, J.P., 1990. Albitization of detrital plagioclase in Triassic reservoir sandstones from the Snorre Field, Norwegian North Sea. Journal of Sedimentary Petrology, **60**: 411–425.

Morad, S., Ketzer, J.M., De Ros, L.F., 2000. Spatial and temporal distribution of diagenetic alterations in siliciclastic rocks: implications for mass transfer in sedimentary basins. Sedimentology, **47**: 95–120.

Morad, S., Ketzer, J.M., De Ros, L.F., 2012. Linking diagenesis to sequence stratigraphy: an integrated tool for understanding and predicting reservoir quality distribution. IAS Special Publication, **45**: 1–36.

Musiał, Ł., Tabor, M., 1979. Stratygrafia karbonu Lubelskiego Zagłębia Węglowego na podstawie makrofauny (in Polish). In: Stratygrafia Węglonośnej Formacji Karbońskiej w Polsce (ed. T. Migier). II Sympozjum Sosnowiec, 4–5 maja 1977: 35–43.

Musiał, Ł., Tabor, M., 1988. Stratygrafia karbonu na podstawie makrofauny (in Polish with English summary). Prace Instytutu Geologicznego, **122**: 88–122, 232–233.

Mücke, A., 1994. Postdiagenetic ferruginization of rocks (sandstones, oolitic ironstones, kaolins and bauxites) – including a comparative study of the reddening of red beds. Developments in Sedimentology, **51**: 361–423.

Nadon, G.C., 1994. The genesis and recognition of anastomosed fluvial deposits: data from the St. Mary River Formation, southwestern Alberta, Canada. Journal of Sedimentary Research, **B 64**: 451–463.

Narecki, Z., 1971. Dokumentacja wstępna otworu Ruskie Piaski IG 2. PIG, NAR, Nr. 111948, Warszawa.

Narkiewicz, M., Jarosiński, M., Krzywiec, P., Waksmundzka M.I., 2007. Regional controls on the Lublin Basin development and inversion in the Devonian and Carboniferous (in Polish with English summary). Biuletyn Państwowego Instytutu Geologicznego, **422:** 19–34.

Nemec, W., 1984. Wałbrzych Beds (Lower Namurian, Wałbrzych Coal Measures): analysis of alluvial sedimentation in a coal basin (in Polish with English summary). Geologia Sudetica, **19**: 7–73.

Osborne, M., Haszeldine, R.S., Fallick, A.E., 1994. Variation in kaolinite morphology with growth temperature in isotopically mixed pore - fluids, Brent Group, UK North Sea. Clay Minerals, **29**: 591–608.

Pańczyk, M., Nawrocki, J., 2015. Tournaisian $^{40}Ar/^{39}Ar$ age from alkaline basalts from the Lublin Basin (SE Poland). Geological Quarterly, **59** (3): 473–478.

Pettijohn, F.J., Potter, P.E., Siever, R., 1972. Sand and Sandstone. Springer, New York.

Pierson, T.C., Costa, J.E., 1987. A rheologic classification of subaerial sediment – water flows. GSA Reviews in Engeneering Geology, **7**: 1–12.

Pirson, S.J., 1950. Elements of Oil Reservoir Engineering. McGraw – Hill Book Comp., New York.

Plint, A.G., 1988. Sharp-based shoreface sequences and „offshore bars" in the Cardium Formation of Alberta: their relationship to relative changes in sea level. SEPM Special Publication, **42**: 357–370.

Postma, D., 1982. Pyrite and siderite formation in brackish and freshwater swamp sediments. American Journal of Science, **282**: 1151–1183.

Postma, G., 1990. An analysis of the variation in delta architecture. Terra Nova, **2**: 124–130.

Postma, G., 1995. Causes of architectural variation in deltas. In: Geology of Deltas: 3–16. Brookfield, A.A. Balkema, Rotterdam.

Porębski, S.J., Steel, R.J., 2003. Shelf-margin deltas: their stratigraphic significance and relation to deepwater sands. Earth-Science Reviews, **62**: 283–326.

Porzycki, J., 1979. Litostratygrafia osadów karbonu Lubelskiego Zagłębia Węglowego (in Polish). In: Stratygrafia Węglonośnej Formacji Karbońskiej w Polsce (ed. T. Migier): 19–27. II Sympozjum, Sosnowiec. Wyd. Geol., Warszawa.

Porzycki, J., Zdanowski, A., 1995. Southeastern Poland (Lublin Carboniferous Basin). Prace Państwowego Instytutu Geologicznego, **168**: 102–109.

Pye, K., Dickson, J.A.D., Schiavon, N., Coleman, M.L., Cox, M., 1990. Formation of siderite–Mg-calcite–iron sulphide concretions in intertidal marsh and sandflat sediments, north Norfolk, England. Sedimentology, **37**: 325–343.

Radke, B.M., Mathis, R.L., 1980. On the formation and occurrence of saddle dolomite. Journal of Sedimentary Petrology, **50**: 1149–1168.

Radomski, A., Gradziński, R., 1981. Facies sequences in the Upper Carboniferous alluvial coal-bearing deposits, Upper Silesia, Poland. Studia Geologica Polonica, **68**: 29–41.

Ramsbottom, W.H.C., 1977. Major cycles of transgression and regression (mesothems) in the Namurian. Proceedings of the Yorkshire Geological Society, **41**: 261–291.

Ramsbottom, W.H.C., 1978. Namurian mesothems in South Wales and northern France. Journal of the Geological Society, **135**: 307–312.

Read, W.A., Dean, J.M., 1976. Cycles and subsidence: their relationship in different sedimentary and tectonic environments in the Scottish Carboniferous. Sedimentology, **23**: 107–120.

Reading, H.G., 1978. Facies. In: Sedimentary Environments and Facies (ed. H.G. Reading): 4–14. Blackwell Science.

Reed, J.S., Eriksson, K.A., Kowalewski, M., 2005. Climatic, depositional and burial controls on diagenesis of Appalachian Carboniferous sandstones: qualitative and quantitative method. Sedimentary Geology, **176**: 225–246.

Rezaee, M.R., Schulz-Rojahn, J.P., 1998. Application of quantitative back-scattered electron image analysis in isotope interpretation of siderite cement: Tirrawarra sandstone, Cooper Basin, Australia. IAS Special Publication, **26**: 461–481.

Rust, B.R., 1978. A classification of alluvial channel systems. Canadian Society of Petroleum Geologists Memoir, **5**: 187–198.

Rust, B.R., 1984. Proximal braidplain deposits in the Middle Devonian Malbaie Formation of eastern Gaspé, Quebec, Canada. Sedimentology, **31**: 675–695.

Rust, B.R., Gibling, M.R., 1990. Braidplain evolution in the Pennsylvanian South Bar Fm., Sydney Basin, Nova Scotia, Canada. Journal of Sedimentary Petrology, **60**: 59–72.

Schulz-Rojahn, J., Ryan-Grigor, S., Anderson, A., 1998. Structural controls on seismic-scale carbonate cementation in hydrocarbon-bearing Jurassic fluvial and marine sandstones from Australia: a comparison. IAS Special Publication, **26**: 327–362.

Scruton, P.C., 1960. Delta building and the deltaic sequence. In: Recent Sediments, Northwest Gulf of Mexico (eds. F.P. Shepard, F.B. Phleger and T.H. van Andel): 82–102. AAPG Tulsa.

Sieciarz, K., 2014. Objawy węglowodorów (in Polish with English summary). Profile Głębokich Otworów Wiertniczych Państwowego Instytutu Geologicznego, **139**: 134.

Skompski, S., 1988. Limestone microfacies and facies position of Upper Visean sediments in north-eastern part of the Lublin Coal basin (in Polish with English summary). Przegląd Geologiczny, **36**: 25–30.

Skompski, S., 1995a. Tectonic framework and development of sedimentation at the margin of the East European Platform. XIII Inter. Congr. Carbon.-Permian, Kraków, Exc. Guide A-2: 5–9.

Skompski, S., 1995b. Succession of limestone microfacies as a key to the origin of the Yoredale-type cyclicity (Viséan/Namurian, Lublin Basin, Poland). XIII Inter. Congr. Carbon.-Permian, Kraków, Abstr.: 133.

Skompski, S., 1996. Stratigraphic position and facies significance of the limestone bands in the subsurface Carboniferous succession of the Lublin Upland. Acta Geologica Polonica, **46**: 171–268.

Skompski, S., 1998. Regional and global chronostratigraphic correlation levels in the late Viséan to Westphalian succession of the Lublin Basin (SE Poland). Geological Quarterly, **42** (2): 121–130.

Smith, D.G., 1983. Anastomosed fluvial deposits: modern examples from Western Canada. IAS Special Publications, **6**: 155–168.

Smith, L.B. Jr., Read, J.F., 1999. Application of high-resolution sequence stratigraphy to tidally influenced Upper Mississippian carbonates, Illinois Basin. SEPM Special Publication, **63**: 107–126.

Smith, L.B. Jr., Read, J.F., 2001. Discrimination of local and global effects on Upper Mississippian stratigraphy, Illinois Basin, U. S. A. Journal of Sedimentary Research, **71**: 985–1002.

Sommer, F., 1978. Diagenesis of Jurassic sandstones in the Viking Graben. Journal of the Geological Society, **135**: 63–67.

Spötl, C., Pitman, J.K., 1998. Saddle (baroque) dolomite in carbonates and sandstones: a reappraisal of burial – diagenetic concept. IAS Special Publication, **26**: 437–460.

Strong, G.E., Milodowski, A.E., 1987. Aspects of the diagenesis of the Sherwood sandstones of the Wessex Basin and their influence on reservoir characteristics. Geological Society Special Publications, **36**: 325–337.

Süss, M.P., Schäfer, A., Drozdzewski, G., 2001. A sequence stratigraphic model for the Lower Coal Measure (Upper Carboniferous) of the Ruhr district, North West Germany. Sedimentology, **48**: 1171–1179.

Svendsen, J., Stollhofen, H., Krapf, C.B.E, Stanistreet, I.G., 2003. Mass and hyperconcentrated flow deposits record dune damming and catastrophic breakthrough of ephemeral rivers, Skeleton Coast Erg, Namibia. Sedimentary Geology, **160**: 7–31.

Środoń, J., 1996. Clay minerals in diagenetic processes (in Polish with English summary). Przegląd Geologiczny, **44**: 604–607.

Tomaszczyk, M., Jarosiński, M., 2017. The Kock Fault Zone as an indicator of tectonic stress regime changes at the margin of the East European Craton (Poland). Geological Quarterly, **61** (4): 908–925.

Tucker, M.E., 1991. An Introduction to the Origin of Sedimentary Rocks . Sedimentary Petrology, **2**.

Tucker, M.E., 2003. Mixed clastic-carbonate and sequences: Quaternary of Egypt and Carboniferous of England. Geologia Croatica, **56**: 19–37.

Vail, P.R., Todd, R.G., 1981. Northern North Sea Jurassic unconformities, chronostratigraphy and sea-level changes from seismic stratigraphy. In: Petroleum Geology of the Continental Shelf of North West Europe (eds. L.V. Illing and G.D. Hobson): 216–235. John Wiley and Sons/Institute of Petroleum.

Van Wagoner, J.C., 1985. Reservoir facies distribution as controlled by sea-level change. SEPM Mid-Year Meeting Abstracts, Golden, Colorado: 91–92.

Van Keer, I., Muchez, P.H., Viaene, W., 1998. Clay mineralogical variations and evolutions in sandstones sequences near a coal seam and shales in the Westphalian of the Campine Basin (NE Belgium). Clay Minerals, **33**: 159–169.

Waksmundzka, M.I., 1998. Depositional architecture of the Carboniferous Lublin Basin (in Polish with English summary). Prace Państwowego Instytutu Geologicznego, **165**: 89–100.

Waksmundzka, M.I., 2005. Karbon (in Polish). In: Budowa geologiczna i system naftowy rowu lubelskiego (ed. M. Narkiewicz). PIG, NAG, Nr. 856/2006, Warszawa.

Waksmundzka, M.I., 2007a. Karbon. Litologia, stratygrafia i sedymentologia (in Polish with English summary). Profile Głębokich Otworów Wiertniczych Państwowego Instytutu Geologicznego, **118**: 124–130.

Waksmundzka, M.I., 2007b. Karbon. Litologia, stratygrafia i sedymentologia (in Polish with English summary). Profile Głębokich Otworów Wiertniczych Państwowego Instytutu Geologicznego, **119**: 112–116.

Waksmundzka, M.I., 2008a. Karbon. Litologia, sedymentologia i stratygrafia (in Polish with English summary). Profile Głębokich Otworów Wiertniczych Państwowego Instytutu Geologicznego, **123**: 161–166.

Waksmundzka, M.I., 2008b. Correlation and origin of the Carboniferous sandstones in the light of sequence stratigraphy and their hydrocarbon potential in the NW and Central parts of the Lublin Basin (in Polish with English summary). Biuletyn Państwowego Instytutu Geologicznego, **429**: 215–224.

Waksmundzka, M.I., 2010a. Sequence stratigraphy of Carboniferous paralic deposits in the Lublin Basin (SE Poland). Acta Geologica Polonica, **60**: 557–597.

Waksmundzka, M.I., 2010b. Lithofacies-paleothickness and worm's eye maps of Carboniferous. Plates 21–24, 33–35 (in Polish with English summary). In: Paleogeological Atlas of the sub-Permian Paleozoic of the East-European Craton in Poland and neighbouring areas (ed. Z. Modliński). PIG-PIB, Warszawa.

Waksmundzka, M.I., 2012a. Karbon – litologia, sedymentologia i stratygrafia (in Polish with English summary). Profile Głębokich Otworów Wiertniczych Państwowego Instytutu Geologicznego, **134**: 90–98.

Waksmundzka, M.I., 2012b. Braided-river and hyperconcentrated-flow deposits from the Carboniferous of the Lublin Basin (SE Poland) – a sedimentological study of core data. Geologos, **18**: 135–161.

Waksmundzka, M.I., 2012c. Charakterystyka formacji geologicznych odpowiednich do składowania CO_2 (karbon) (in Polish). In: Rozpoznanie formacji i struktur do bezpiecznego geologicznego składowania CO_2 wraz z ich programem monitorowania (ed. A. Wójcicki). https://skladowanie.pgi.gov.pl/twiki/bin/view/CO2/WynikiPrac/I-1.

Waksmundzka, M.I., 2013. Carboniferous coarsening-upward and non-gradational cyclothems in the Lublin Basin (SE Poland):

palaeoclimatic implications. Geological Society Special Publications, **376**: 141–175.

Waksmundzka, M.I., 2014. Karbon – litologia, sedymentologia i stratygrafia (in Polish with English summary). Profile Głębokich Otworów Wiertniczych Państwowego Instytutu Geologicznego, **139**: 77–82.

Waksmundzka, M.I., 2018. Karbon – litologia, sedymentologia i stratygrafia (in Polish with English summary). Profile Głębokich Otworów Wiertniczych Państwowego Instytutu Geologicznego, **149**: 53–59.

Waksmundzka, M.I., 2019. Karbon – litologia, sedymentologia i stratygrafia (in Polish with English summary). Profile Głębokich Otworów Wiertniczych Państwowego Instytutu Geologicznego, **157**: 92–99.

Waksmundzka, M.I., Buła, Z., 2017. Mapa geologiczna Polski bez utworów kenozoiku, mezozoiku i permu. In: Atlas Geologiczny Polski (eds. J. Nawrocki and A. Becker). PIG-PIB, Warszawa: 28–29.

Walderhaug, O., 1994. Temperatures of quartz cementation in Jurassic sandstones from the Norwegian Continental Shelf - evidence from fluid inclusions. Journal of Sedimentary Research, **A 64**: 324–333.

Walker, R.G., 1992. Facies, facies models, and modern stratigraphic concepts. In: Facies Models: Response to Sea Level Change (eds. R.G. Walker and N.P. James). Geological Association of Canada, St. Johns: 1–14.

Zieliński, T., 1992a. Marginal moraines of NE Poland – sediments and depositional conditions (in Polish with English summary). Prace Naukowe Uniwersytetu Śląskiego, **1325**: 7–95.

Zieliński, T., 1992b. Proglacial valleys facies of the Silesian Upland – genetic factors and their sedimentological effects. Geologia Sudetica, **26**: 83–118.

Zieliński, T., 1995. Kod litofacjalny i litogenetyczny – konstrukcja i zastosowanie (in Polish). In: Badania osadów czwartorzędowych, wybrane metody i interpretacja wyników (eds. E. Mycielska-Dowgiałło and J. Rutkowski): 220–235.

Zieliński, T., 1997. Cykliczność w osadach rzek roztokowych (in Polish). Geologia (Prace Naukowe Uniwersytetu Śląskiego), **14**: 68–119.

Żelichowski, A.M., 1969a. Karbon (in Polish). In: Ropo- i gazonośność obszaru lubelskiego na tle budowy geologicznej – część I: Budowa geologiczna obszaru lubelskiego (ed. S. Depowski). Prace Geostrukturalne IG: 70–85.

Żelichowski, A.M., 1969b. Dokumentacja wynikowa otworu wiertniczego Terebin IG 1 (in Polish). PIG, NAG, Nr 93593, Warszawa.

Żelichowski, A.M., 1972. Evolution of the geological structure of the area between the Góry Świętokrzyskie and the River Bug (in Polish with English summary). Biuletyn Instytutu Geologicznego, **263**: 7–97.

Żelichowski, A.M., Porzycki, J., 1983. Mapa strukturalno-geologiczna bez utworów młodszych od karbonu (in Polish). In: Atlas geologiczno-surowcowy obszaru lubelskiego (eds. A.M. Żelichowski and S. Kozłowski). Instytut Geologiczny, Warszawa.

Żywiecki, M., Kopczyński, R., Rochewicz, A., 1997. Rozwój i dystrybucja porowatości w osadach klastycznych – przykłady ze złóż karbonu Lubelszczyzny (in Polish). Mat. Konfer. XXX lat działalności geologicznej Oddziału Poszukiwania Nafty i Gazu w Wołominie, Pułtusk: 53–58.